Hadronic structure on the light front. VII. Pions and kaons and their partonic distributions

Wei-Yang Liu,[*] Edward Shuryak,[†] and Ismail Zahed[‡]

Center for Nuclear Theory, Department of Physics and Astronomy, Stony Brook University, Stony Brook, New York 11794–3800, USA

(Received 25 February 2023; accepted 25 April 2023; published 22 May 2023)

This work is a continuation in our series of papers that addresses quark models of hadronic structure on the light front, motivated by the QCD vacuum structure and lattice results. The spontaneous breaking of chiral symmetry on the light front is shown to parallel that in the rest frame, where the nonlocal instanton induced 't Hooft interaction plays a central role. By rewriting this interaction solely in terms of the good component of the fermionic field, a scalar chiral condensate emerges in the mean-field approximation, which is identical to the one obtained in the rest frame. The pions and kaons emerge as deeply bound Goldstone modes in the chiral limit, with the scalar-isoscalar sigma meson mode as a threshold state with zero binding. We explicitly derive the light front distribution amplitudes (DAs) and parton distribution functions (PDFs) for these mesons. The DAs and PDFs are in good agreement with those extracted from the QCD instanton vacuum in the rest frame, using the large momentum effective theory (LaMET). The QCD evolved DAs and PDFs compare well with available measurements, as well as recent lattice results.

DOI: 10.1103/PhysRevD.107.094024

I. INTRODUCTION

Parton distribution functions (PDFs) are important for the description of hadrons at high energy. They are currently central for the description of high energy cross sections at the Large Hadron Collider (LHC). The PDFs describe unidimensional distribution of the quark and gluons in the infinite momentum frame, and are inherently nonperturbative. In the leading twist approximation, they can be gleaned from experiments [1], or more recently from first principle lattice simulations [2] using the large momentum effective theory (LaMET) as suggested in [3], and some variants [4,5]. The generalized PDFs offer a multidimensional description of the quarks and gluons, but their extraction from current or future experiments, as well as numerical lattice simulations, is more challenging.

A physical understanding of the quark and gluon distributions in hadrons at low resolution requires an understanding of the QCD vacuum. Cooled lattice simulations whereby the gauge configurations are iteratively pruned of quantum fluctuations [6] suggest a semiclassical landscape dominated by tunneling instanton and anti-instanton configurations, with large actions and finite topological charge. Their inclusion in the determination of the PDFs for the light pseudoscalar mesons is one of the essential thrusts of this work.

The QCD instanton liquid model (ILM) is a comprehensive model of QCD at low resolution that is currently supported in its details by current lattice cooling simulations. It unequivocally captures the essentials of the spontaneous breaking of chiral symmetry, with the emergence of the quark zero mode zone. It provides a semiclassical description of the QCD ground state at low resolution, hence a well-defined organizational principle that enforces chiral and gauge Ward identities [7–11].

However, the QCD instanton liquid model is inherently spacelike, making the ensuing physics less transparent timelike. This is particularly acute for the PDFs which capture the nonperturbative timelike structure the partonic constituents of hadrons, as probed by deep inelastic scattering. Recently, two of us in a series of papers [12–16] have put forth a program on how to export the successes of the QCD instanton liquid model, spacelike. The program is based on the idea of deriving the essential of the central and spin forces on the light front by analytically continuing in (Euclidean) rapidity pertinent correlators spacelike. In a way, this construction is similar in spirit to the one put forth by Ji [3].

This paper is a continuation of this series [17], whereby we show in detail how chiral symmetry is spontaneously broken on the light front, using solely the emergent

[*]wei-yang.liu@stonybrook.edu
[†]edward.shuryak@stonybrook.edu
[‡]ismail.zahed@stonybrook.edu

't Hooft effective interactions from the QCD instanton liquid model. It fufills for the schematic argument we put forth in [13]. The light front formulation of the QCD vacuum supports a scalar chiral condensate, which is identical to the one derived in the rest frame, as expected. The ensuing light front (LF) pion and kaon wave functions are characterized by the same masses and decay constants as in the rest frame. In addition, they provide a detailed description of the partonic content of these mesons for the leading twist-2 operators. For the latter, a number of models has been also used [5,18–38].

The organization of the paper is as follows. In Sec. II we briefly review the emergent 't Hooft multiflavor and nonlocal fermionic interactions in the QCD ILM vacuum. In Sec. III we address the role of these effective interactions on the light front. The central new element on the light front is the decomposition of the fermionic fields into good plus bad components along the light cone directions. The bad component is a constraint, as it does not propagate in the light front direction. The elimination of the constraint in the mean-field approximation yields a constituent quark mass much like in the rest frame, and renormalized 't Hooft multiflavor interactions, as initially proposed in [39–41] for local interactions of the Nambu-Jona-Lasinio (NJL) type. In Sec. IV we derive the corresponding light front Hamiltonian solely in terms of the good fermionic component. In Sec. V we show that the emergent constituent quark mass and chiral condensate on the light front are identical to the ones in the rest frame. As expected, the spontaneous breaking of chiral symmetry is driven by the induced multiflavor instanton and anti-instanton interactions in the ILM. It is universal and frame independent.

In Sec. VI we diagonalize the light front Hamiltonian in the two-body sector for light u, d quarks, with a strongly bound pion as a Goldstone mode. All other scalar and pseudoscalar modes are unbound on the light front, in the mean-field approximation, and away from the chiral limit. The pion distribution amplitude (DA) stemming from the diagonalization is also discussed. In Sec. VII we derive the pion PDF. The result is QCD evolved with a detailed comparison to existing measurements, lattice results, and models. In Sec. VIII we extend our analysis to include strangeness, and derive the pertinent gap equations and chiral condensates. In Sec. IX the light front wave functions and masses for the kaons using U and V spin are discussed. The kaon DA and PDF are derived. The results are also evolved and compared with available empirical data, recent lattice results, and models. Our conclusions are in Sec. X. A number of appendices are included to complement some of the derivations.

II. FLAVOR INTERACTIONS IN ILM

In the ILM, the QCD vacuum is composed of instanton and anti-instanton gauge fields, tunneling and topologically active gauge configurations, surrounded by swaths of empty space-time free of perturbative fields [42–44]. These configurations are self-dual and strong, with a typical size of $\frac{1}{3}$ fm, and a mean tunneling density of $1/R^4 \approx 1\ \text{fm}^{-4}$ [45]. As a result, the starting and complex gauge dynamics can be reduced to the dynamics of a dilute ensemble of pseudoparticles on their pertinent moduli, and organized using the packing fraction

$$\kappa_{I+\bar{I}} = \frac{2\pi^2\rho^4}{R^4} \approx 0.1. \tag{1}$$

The remarkable thing about the self-dual instantons (anti-self-dual anti-instantons) is their ability to trap quark states as zero modes with fixed helicity (left for instantons and right for anti-instantons). The collectivization of these zero modes gives rise to a zero mode zone in a narrow band of virtualities

$$|\Delta\lambda| \sim \frac{\rho^2}{R^3} \sim 20\ \text{MeV} \tag{2}$$

with a mean density $\varrho(0)$ of near-zero Dirac eigenvalues. As noted initially by Banks and Casher [46], this mean density gives rise to a finite quark condensate

$$\langle\bar{\psi}\psi\rangle = -\pi\varrho(0). \tag{3}$$

Equation (2) is also characterized by universal fluctuations of the chiral condensate in the microscopic limit, which are captured by chiral random matrix theory [47]. In many ways, the spontaneous breaking of chiral symmetry in the ILM is tantamount of the onset of conductivity in dirty metals.

The delocalization of the quark zero modes and the emergence of (2) is a direct proof of the importance of the gauge topology in the spontaneous breaking of chiral symmetry. It provides for a microscopic origin of the spontaneous breaking of chirality in QCD, as noted originally by 't Hooft [48]. It generates four-dimensional fermionic zero modes, which lead to multifermion flavor mixing interactions,

$$\bar{u}u \leftrightarrow \bar{d}d \leftrightarrow \bar{s}s,$$

which are quasilocal.

For $N_f = 3$ and in the instanton zero size approximation, the interactions between the u, d, s quarks in the current mass limit is [49]

$$\mathcal{V}^{L+R}_{qqq} = \frac{G_{\text{Hooft}}}{N_c(N_c^2-1)}\left[\left(\frac{2N_c+1}{2(N_c+2)}\right)\det(UDS) + \frac{1}{2(N_c+1)}(\det(U_{\mu\nu}D_{\mu\nu}S) + \text{cyclic})\right] + (L \leftrightarrow R) \tag{4}$$

with $U = \bar{u}_R u_L$ and $U_{\mu\nu} = \bar{u}_R \sigma_{\mu\nu} u_L$, and similarly for D, S. The strength of the 6-quark operators is related to the instanton plus anti-instanton density

$$G_{\text{Hooft}} = \frac{n_{I+\bar{I}}}{2}(4\pi^2\rho^3)^3\left(\frac{1}{m_u^*\rho}\right)\left(\frac{1}{m_d^*\rho}\right)\left(\frac{1}{m_s^*\rho}\right) \tag{5}$$

with the effective quark masses m_q^*. For most of the analyses to follow in this work, we will specialize to $N_f = 2$ with u, d species with almost degenerate quark masses. Strangeness will be addressed also in the same spirit, using U and V spin. With this in mind, (4) reduces to

$$\mathcal{V}_{qq}^{L+R} = \kappa_2 \frac{(2N_c-1)}{2N_c(N_c^2-1)}\left(\det(UD) + \frac{1}{4(2N_c-1)}\det(U_{\mu\nu}D_{\mu\nu})\right) + (L \leftrightarrow R) \tag{6}$$

with $\kappa_2 = 3G_{\text{Hooft}}\langle\bar{s}s\rangle < 0$ and attractive. Equation (6) breaks explicitly $U_A(1)$ axial symmetry, but otherwise preserves flavor left-right symmetry. This can be made explicit through Fierzing, with the full Lagrangian now of the form

$$\mathcal{L} \propto \bar{\Psi}(i\partial\!\!\!/ - m)\Psi + \frac{G}{8(N_c^2-1)}\left\{\frac{2N_c-1}{2N_c}[(\bar{\Psi}\Psi)^2 - (\bar{\Psi}\tau^a\Psi)^2 - (\bar{\Psi}i\gamma^5\Psi)^2 + (\bar{\Psi}i\gamma^5\tau^a\Psi)^2] - \frac{1}{4N_c}[(\bar{\Psi}\sigma_{\mu\nu}\Psi)^2 - (\bar{\Psi}\sigma_{\mu\nu}\tau^a\Psi)^2]\right\}. \tag{7}$$

It is strongly attractive in the sigma and pion channel, and repulsive in the η' channel thereby solving the $U_A(1)$ problem. Equation (7) in QCD is a replacement to the posited Nambu-Jona-Lasinio model [50] of pre-QCD.

For the small size mesons such as pions and kaons (and also Upsilons), the quasilocal approximation is not reliable, and the full nonlocality of the instanton zero modes need to be retained. This amounts to the shift

$$\psi(x) \to \sqrt{\mathcal{F}(i\partial)}\psi(x) \tag{8}$$

in (7). The explicit form of $\mathcal{F}(k)$ in momentum space is

$$\mathcal{F}(k) = [(zF'(z))^2]\Big|_{z=\frac{k\rho}{2}}, \tag{9}$$

where

$$F(z) = I_0(z)K_0(z) - I_1(z)K_1(z)$$

and $k = \sqrt{k^2}$ is the Euclidean 4-momentum.

III. 'T HOOFT EFFECTIVE LAGRANGIAN ON THE LIGHT FRONT

On the light front, the old lore was that the QCD vacuum is trivial owing to the vanishing of the backward diagrams in perturbation theory [51]. However, more careful analyses reveal that the vacuum physics is encoded in the longitudinal zero modes of the fields [52], which is rather manifest in two-dimensional QCD [53] (and references therein). In effective models of QCD such as the NJL model, the nontrivial aspects of the vacuum on the light front are explicitly tied to the tadpole contributions, generated by the constrained part of the fermion field [39–41]. Most of the analysis to follow in the ILM will make use of this observation.

More specifically, the projection of the fermion field along the light front splits the field into a good plus bad component, with the latter nonpropagating or constraint. The elimination of the constraint induces multifermion interactions in terms of the good component. In the mean-field approximation, using $\frac{1}{N_c}$ counting rules, these interactions account for the spontaneous breaking of chiral symmetry on the light front through tadpoles [39–41]. In this section, we will show that this approach can be applied to the emergent multiflavor interactions in the ILM, with finite size form factors from the quark zero modes.

For simplicity and clarity of the analysis, we consider first the local form of (7) in the large N_c approximation. The modifications for the finite instanton sizes will be quoted at the end. More specifically, we have

$$\mathcal{L} \propto \bar{\Psi}(i\partial\!\!\!/ - m)\Psi + \frac{G_S}{2}[(\bar{\Psi}\Psi)^2 - (\bar{\Psi}\tau^a\Psi)^2 - (\bar{\Psi}i\gamma^5\Psi)^2 + (\bar{\Psi}i\gamma^5\tau^a\Psi)^2] \tag{10}$$

with $G_S = \frac{G}{4N_c^2}$. In the mean field or $\frac{1}{N_c}$ approximation, it is customary to use the semibosonized form of (10), through the use of the auxillary fields σ, σ^a, π, and π^a

$$\mathcal{L} \propto \bar{\Psi}(i\partial\!\!\!/ - m)\Psi + G_S\bar{\Psi}(\sigma - \sigma^a\tau^a - i\pi\gamma^5 + i\pi^a\tau^a\gamma^5)\Psi - \frac{G_S}{2}[\sigma^2 - (\sigma^a)^2 - \pi^2 + (\pi^a)^2], \tag{11}$$

where $m = m_u = m_d$ represents the current mass of the u, d quarks. Note that the combination

$$\sigma^2 - (\sigma^a)^2 - \pi^2 + (\pi^a)^2$$

is flavor $U_A(1)$ violating. The extension to s quarks with larger mass will be discussed below, by reduction to U and V spin.

To proceed, we now split the fermionic field Ψ into a good component Ψ_+ and a bad component Ψ_-

$$\Psi = \Psi_+ + \Psi_- \equiv \frac{1}{2}\gamma^-\gamma^+\Psi + \frac{1}{2}\gamma^+\gamma^-\Psi. \tag{12}$$

The bad component does not propagate along the light front x^+ direction, and therefore can be eliminated from (10) using the equation of motion. The latter is readily solved in terms of the good component Ψ_+

$$\Psi_- = \frac{\gamma^+}{2}\frac{-i}{\partial_-}(-i\gamma^i_\perp\partial_i + \hat{M})\Psi_+, \tag{13}$$

where $\hat{M}$ denotes

$$\hat{M} = m - G_S(\sigma - \sigma^a\tau^a - i\pi\gamma^5 + i\pi^a\tau^a\gamma^5), \tag{14}$$

$\frac{-i}{\partial_-}$ is equal to the Green's function $G(x^-, y^-)$ for $i\partial_-$ where the Green's function can be defined as

$$G(x^-, y^-) = \int_{-\infty}^{\infty}\frac{dk^+}{2\pi}\frac{1}{k^+}e^{-ik^+(x-y)^-} = \frac{-i}{2}\epsilon(x^- - y^-). \tag{15}$$

In terms of (12), the semibosonized Lagrangian (11) can be solely rewritten in terms of the good component

$$\mathcal{L} \propto \bar{\Psi}_+ i\gamma^+\partial_+\Psi_+ - \frac{G_S}{2}[\sigma^2 - (\sigma^a)^2 - \pi^2 + (\pi^a)^2] - \bar{\Psi}_+(i\gamma^i_\perp\partial_i - \hat{M})\frac{\gamma^+}{2}\frac{-i}{\partial_-}(i\gamma^i_\perp\partial_i - \hat{M})\Psi_+. \tag{16}$$

It is now clear that the elimination of the Gaussian mesonic fields from (16) generates strings of multifermion interactions, of increasing complexity on the light front. Fortunately, they are tractable in $1/N_c$, with the leading order referred to as the mean-field approximation. For that, we shift the scalar field by $\sigma = N_c\sigma_0 + \delta\sigma$ in (16) with a finite vev $\sigma_0 \sim N_c^0$, as all other vevs are excluded by isospin symmetry and parity. We can now use the counting rules

$$\sigma^a, \quad \pi, \quad \pi^a, \quad \delta\sigma \sim \mathcal{O}(\sqrt{N_c})$$

with $g_S = N_c G_S \sim N_c^0$, in the semibosonized Lagrangian (16) to resum all of the leading tadpole diagrams, by setting the coefficient of $\delta\sigma$ to zero,

$$\langle\bar{\psi}\psi\rangle - N_c\sigma_0 = 0 \tag{17}$$

with now the effective fermionic field

$$\psi = \Psi_+ + \frac{\gamma^+}{2}\frac{-i}{\partial_-}(i\gamma^i_\perp\partial_i - M)\Psi_+. \tag{18}$$

As a result, the good component of the quark field acquires a constituent mass of order N_c^0

$$M = m - G_S\langle\bar{\psi}\psi\rangle. \tag{19}$$

Equations (17) and (19) reflect on the spontaneous breaking of chiral symmetry. Equation (19) is a gap equation as we detail below.

As the remnant fluctuation of the bosonic fields σ^a, π, π^a, and $\delta\sigma = \sigma - N_c\sigma_0$ are of order $\mathcal{O}(\sqrt{N_c})$, these fields compensate the $\mathcal{O}(1/N_c)$ contribution from the 't Hooft coupling $G_S = g_S/N_c$, leaving the semibosonized Lagrangian at the leading order of large N_c of the form

$$\mathcal{L} = \bar{\psi}(i\partial\!\!\!/ - M)\psi - \frac{1}{2}G_S[\delta\sigma\hat{D}_+\delta\sigma - \sigma^a\hat{D}_-\sigma^a - \pi\hat{D}_-\pi + \pi^a\hat{D}_+\pi^a] + G_S[\bar{\psi}\psi\hat{\sigma} - \bar{\psi}\tau^a\psi\sigma^a - \bar{\psi}i\gamma^5\psi\pi + \bar{\psi}i\gamma^5\tau^a\psi\pi^a]. \tag{20}$$

Higher order contributions have not been retained. The factors $\hat{D}_\pm$ inside the quadratic bosonic potential are defined as

$$\hat{D}_\pm = 1 \pm G_S\left\langle\bar{\psi}\gamma^+\frac{-i}{\overleftrightarrow{\partial_-}}\psi\right\rangle, \tag{21}$$

where $-i/\overleftrightarrow{\partial_-}$ in (25), is defined such that for any fields $\chi(x)$ and $\psi(x)$,

$$\chi(x)\frac{-i}{\overleftrightarrow{\partial_-}}\psi(x) = \frac{i}{\partial_-}[\chi(x)]\psi(x) + \chi(x)\frac{-i}{\partial_-}[\psi(x)]. \tag{22}$$

$\hat{D}_\pm$ follows from the resummation of the tadpole diagrams in the mean field, or leading order in $1/N_c$. Indeed, each virtual quark tadpole is of order $\mathcal{O}(N_c)$, thereby compensating the 't Hooft coupling $G_S \sim \mathcal{O}(1/N_c)$, with a net factor of $\mathcal{O}(N_c^0)$. Note that the fermionic contributions $\bar{\psi}\psi$, $\bar{\psi}\tau^a\psi$, $\bar{\psi}i\gamma^5\psi$, and $\bar{\psi}i\gamma^5\tau^a\psi$ in (20) are all of the same order as the remnant quantum fluctuations or $\mathcal{O}(\sqrt{N_c})$. With this in mind, we can now eliminate the auxillary bosonic fields, to obtain the light front Lagrangian,

$$\mathcal{L} = \bar{\psi}(i\partial\!\!\!/ - M)\psi + \frac{G_S}{2}[\bar{\psi}\psi\hat{D}_+^{-1}\bar{\psi}\psi - \bar{\psi}\tau^a\psi\hat{D}_-^{-1}\bar{\psi}\tau^a\psi - \bar{\psi}i\gamma^5\psi\hat{D}_+^{-1}\bar{\psi}i\gamma^5\psi + \bar{\psi}i\gamma^5\tau^a\psi\hat{D}_+^{-1}\bar{\psi}i\gamma^5\tau^a\psi]. \tag{23}$$

In the mean field or leading order in $1/N_c$ approximation, the light front Lagrangian can be solely written in terms of the good fermionic component. The elimination of the bad component generates a constituent mass, introduces an effective quark field (18), and renormalizes by $\hat{D}_\pm^{-1}$ (tadpole resummation) each of the original multifermion interaction in the ILM in the zero size limit.

Most of the arguments presented above carry for the nonlocal effective Lagrangian in the ILM. More specifically, the mean-field version of (20) is now

$$\begin{aligned}\mathcal{L} = {} & \bar{\psi}(i\partial\!\!\!/ - M)\psi - \frac{1}{2}G_S[\delta\sigma\hat{D}_+\delta\sigma - \sigma^a\hat{D}_-\sigma^a - \pi\hat{D}_-\pi + \pi^a\hat{D}_+\pi^a] \\ & + G_S\Big(\bar{\psi}\sqrt{\mathcal{F}(i\partial)}\,\delta\sigma\sqrt{\mathcal{F}(i\partial)}\psi - \bar{\psi}\sqrt{\mathcal{F}(i\partial)}\,\sigma^a\tau^a\sqrt{\mathcal{F}(i\partial)}\psi - \bar{\psi}\sqrt{\mathcal{F}(i\partial)}\,i\gamma^5\pi\sqrt{\mathcal{F}(i\partial)}\psi + \bar{\psi}\sqrt{\mathcal{F}(i\partial)}\,i\gamma^5\tau^a\pi^a\sqrt{\mathcal{F}(i\partial)}\psi\Big).\end{aligned} \tag{24}$$

Here $\sqrt{\mathcal{F}}(i\partial)$ is a derivative operator acting on all of the fields on its right-hand side. In momentum space, it generates the pertinent form factors inherited from the underlying quark zero modes. Also,

$$\hat{D}_\pm \to 1 \pm G_S\left\langle \bar{\psi}\gamma^+\mathcal{F}(i\partial)\frac{-i}{\overleftrightarrow{\partial_-}}[\mathcal{F}(i\partial)\psi]\right\rangle \tag{25}$$

following from the mean-field resummation of the leading tadpoles. The auxillary bosonic fields can be eliminated by carrying explicitly the Gaussian integration, as in the zero size limit. The astute reader may object that (24) may suffer from abnormal characteristics and light propagation. However, since $\sqrt{\mathcal{F}(i\partial)}$ vanishes rapidly at large $|\rho\partial|$, this is not the case.

IV. LIGHT FRONT HAMILTONIAN

The effective light front Hamiltonian associated with the mean-field Lagrangian (20) in the zero size limit, or (24) in the finite size limit, can be derived using the canonical rules. The light front Hamiltonian allows for the explicit derivation of the boost-invariant meson spectra and their corresponding light-cone wave function. We now detail the canonical Legendre transformation from (20) to the Hamiltonian, and quote the results for (24) at the end.

Given a fermionic field theory in Lagrangian form, the corresponding symmetric energy-momentum tensor is

$$T^{\mu\nu} = \frac{1}{2}[\bar{\psi}i\gamma^\mu\partial^\nu\psi + \bar{\psi}i\gamma^\nu\partial^\mu\psi] - g^{\mu\nu}\mathcal{L}. \tag{26}$$

The light front Hamiltonian is then

$$\begin{aligned}P^- &= \int dx^- d^2x_\perp T^{+-} \\ &= \int dx^- d^2x_\perp \frac{1}{2}[\bar{\psi}i\gamma^+\partial_+\psi + \bar{\psi}i\gamma^-\partial_-\psi] - \mathcal{L}.\end{aligned} \tag{27}$$

Applying this to (20) gives

$$\begin{aligned}P^- = {} & \int dx^- d^2x_\perp \bar{\psi}\frac{(-\partial_\perp^2 + M^2)}{2i\partial_-}\gamma^+\psi \\ & - \frac{G_S}{2}\int dx^- d^2x_\perp[\bar{\psi}\psi\hat{D}_+^{-1}\bar{\psi}\psi - \bar{\psi}\tau^a\psi\hat{D}_-^{-1}\bar{\psi}\tau^a\psi - \bar{\psi}i\gamma^5\psi\hat{D}_+^{-1}\bar{\psi}i\gamma^5\psi + \bar{\psi}i\gamma^5\tau^a\psi\hat{D}_+^{-1}\bar{\psi}i\gamma^5\tau^a\psi]\end{aligned} \tag{28}$$

or in momentum space

$$\begin{aligned}P^- = {} & \int [d^3k]_+ \int [d^3q]_+ \frac{k_\perp^2 + M^2}{2k^+}\bar{\psi}(k)\gamma^+\psi(q)(2\pi)^3\delta_+^3(k-q) \\ & + \int [d^3k]_+ \int [d^3q]_+ \int [d^3p]_+ \int [d^3l]_+ (2\pi)^3\delta_+^3(p+k-q-l)V(k,q,p,l).\end{aligned} \tag{29}$$

The first term in the light front Hamiltonian corresponds to the kinetic term. The second term is the two-body interaction relevant to two-particle bound states where the interaction kernel in the scalar and pseudoscakar channels can be defined as

$$\begin{aligned}
V(k,q,p,l) = &-\frac{G_S}{2}\alpha_+(k^+-q^+)\bar{\psi}_+(k)\left(\frac{\vec{\gamma}_\perp\cdot\vec{k}+M}{2k^+}\gamma^+ + \gamma^+\frac{\vec{\gamma}_\perp\cdot\vec{q}+M}{2q^+}\right)\psi_+(q)\\
&\times\bar{\psi}_+(p)\left(\frac{\vec{\gamma}_\perp\cdot\vec{p}+M}{2p^+}\gamma^+ + \gamma^+\frac{\vec{\gamma}_\perp\cdot\vec{l}+M}{2l^+}\right)\psi_+(l)\\
&+\frac{G_S}{2}\alpha_-(k^+-q^+)\bar{\psi}_+(k)\left(\frac{\vec{\gamma}_\perp\cdot\vec{k}+M}{2k^+}i\gamma^+\gamma^5 + i\gamma^5\gamma^+\frac{\vec{\gamma}_\perp\cdot\vec{q}+M}{2q^+}\right)\psi_+(q)\\
&\times\bar{\psi}_+(p)\left(\frac{\vec{\gamma}_\perp\cdot\vec{p}+M}{2p^+}i\gamma^+\gamma^5 + i\gamma^5\gamma^+\frac{\vec{\gamma}_\perp\cdot\vec{l}+M}{2l^+}\right)\psi_+(l)\\
&+\frac{G_S}{2}\alpha_-(k^+-q^+)\bar{\psi}_+(k)\left(\frac{\vec{\gamma}_\perp\cdot\vec{k}+M}{2k^+}\gamma^+\tau^a + \tau^a\gamma^+\frac{\vec{\gamma}_\perp\cdot\vec{q}+M}{2q^+}\right)\psi_+(q)\\
&\times\bar{\psi}_+(p)\left(\frac{\vec{\gamma}_\perp\cdot\vec{p}+M}{2p^+}\gamma^+\tau^a + \gamma^+\tau^a\frac{\vec{\gamma}_\perp\cdot\vec{l}+M}{2l^+}\right)\psi_+(l)\\
&-\frac{G_S}{2}\alpha_+(k^+-q^+)\bar{\psi}_+(k)\left(\frac{\vec{\gamma}_\perp\cdot\vec{k}+M}{2k^+}i\gamma^+\gamma^5\tau^a + \tau^a i\gamma^5\gamma^+\frac{\vec{\gamma}_\perp\cdot\vec{q}+M}{2q^+}\right)\psi_+(q)\\
&\times\bar{\psi}_+(p)\left(\frac{\vec{\gamma}_\perp\cdot\vec{p}+M}{2p^+}i\gamma^+\gamma^5\tau^a + i\gamma^5\gamma^+\tau^a\frac{\vec{\gamma}_\perp\cdot\vec{l}+M}{2l^+}\right)\psi_+(l).
\end{aligned} \tag{30}$$

Here

$$\alpha_\pm(P^+) = \left[1 \pm 2g_S\int\frac{dl^+d^2l_\perp}{(2\pi)^3}\frac{\epsilon(l^+)}{P^+-l^+}\right]^{-1}. \tag{31}$$

The fermionic field in momentum space is defined as

$$\psi(x^-,x_\perp) = \int[d^3k]_+\psi(k)e^{-ik^+x^- + ik_\perp\cdot x_\perp}. \tag{32}$$

It annihilates a particle in a $u_s(k)$ mode, or creates an antiparticle in a $v_s(k)$ mode, i.e.

$$\psi(k) = \sum_s u_s(k)b_s(k)\theta(k^+) + v_s(-k)c_s^\dagger(-k)\theta(-k^+). \tag{33}$$

The measure in momentum space is

$$[d^3k]_+ = \frac{dk^+d^2k_\perp}{(2\pi)^3 2k^+}\epsilon(k^+) \tag{34}$$

which sums over the positive k^+ region for particle modes and over the negative k^+ region for antiparticle modes. For the 't Hooft interaction in the zero size limit, the interaction is generically of the form

$$\begin{aligned}
&V(k,q,p,l)\\
&= \sum_{s_1,s_1',s_2,s_2'}\mathcal{V}_{s_1,s_2,s_1',s_2'}(k,q,p,l)b_{s_1}^\dagger(k)c_{s_2}^\dagger(q)c_{s_2'}(p)b_{s_1'}(l)
\end{aligned} \tag{35}$$

with

$$\begin{aligned}
\mathcal{V}_{s_1,s_2,s_1',s_2'}(k,q,p,l) = &-g_S\alpha_+(k^++q^+)\bar{u}_{s_1}(k)v_{s_2}(q)\bar{v}_{s_2'}(p)u_{s_1'}(l) + g_S\alpha_-(k^++q^+)\bar{u}_{s_1}(k)i\gamma^5 v_{s_2}(q)\bar{v}_{s_2'}(p)i\gamma^5 u_{s_1'}(l)\\
&+ g_S\alpha_-(k^++q^+)\bar{u}_{s_1}(k)\tau^a i\gamma^5 v_{s_2}(q)\bar{v}_{s_2'}(p)\tau^a i\gamma^5 u_{s_1'}(l)\\
&- g_S\alpha_+(k^++q^+)\bar{u}_{s_1}(k)\tau^a i\gamma^5 v_{s_2}(q)\bar{v}_{s_2'}(p)\tau^a i\gamma^5 u_{s_1'}(l).
\end{aligned} \tag{36}$$

In the large N_c limit, only the s-channel contribution of the 't Hooft interaction dominates. Further details regarding the interplay of the s- and t-channel exchanges can be found in Appendix B.

These arguments carry to the mean-field Lagrangian (24) through the substitutions

$$V(k,q,p,l) \to \sqrt{\mathcal{F}(k)\mathcal{F}(k)\mathcal{F}(k)\mathcal{F}(l)}V(k,q,p,l) \tag{36}$$

and

$$\alpha_\pm(P^+) \to \left[1 \pm 2g_S \int \frac{dl^+ d^2l_\perp}{(2\pi)^3}\frac{\epsilon(l^+)}{P^+ - l^+}\mathcal{F}(l)\mathcal{F}(P-l)\right]^{-1} \tag{37}$$

so that

$$\begin{aligned} P^- = &\int [d^3k]_+ \int [d^3q]_+ \frac{k_\perp^2 + M^2}{2k^+}\bar\psi(k)\gamma^+\psi(q)(2\pi)^3\delta_+^3(k-q) \\ &+ \int [d^3k]_+ \int [d^3q]_+ \int [d^3p]_+ \int [d^3l]_+ (2\pi)^3\delta_+^3(p+k-q-l)\sqrt{\mathcal{F}(k)\mathcal{F}(q)\mathcal{F}(p)\mathcal{F}(l)}V(k,q,p,l). \end{aligned} \tag{38}$$

The interaction kernel is now

$$\begin{aligned} V(k,q,p,l) = -\frac{G_S}{2}[&\alpha_+(k^+-q^+)\bar\psi(k)\psi(q)\bar\psi(p)\psi(l) - \alpha^-(k^+-q^+)\bar\psi(k)i\gamma^5\psi(q)\bar\psi(p)i\gamma^5\psi(l) \\ &- \alpha^-(k^+-q^+)\bar\psi(k)\tau^a\psi(q)\bar\psi(p)\tau^a\psi(l) + \alpha^+(k^+-q^+)\bar\psi(k)i\tau^a\gamma^5\psi(q)\bar\psi(p)i\tau^a\gamma^5\psi(l)], \end{aligned} \tag{39}$$

where the tadpole resummed vertices read as

$$\alpha_\pm(P^+) = \left[1 \pm 2g_S \int \frac{dl^+ d^2l_\perp}{(2\pi)^3}\frac{\epsilon(l^+)}{P^+ - l^+}\mathcal{F}(l)\mathcal{F}(P-l)\right]^{-1}.$$

Again, the astute reader may have noticed that for the Lagrangian (24) in nonlocal form, the symmetric form of the energy-momentum tensor may require further amendment in the presence of the nonlocal form factors. This is not the case, as we now explain. Indeed, boost invariance and parity suggests the substitution

$$\lim_{P^+\to\infty}\sqrt{\mathcal{F}(k)\mathcal{F}(P-k)} \to \mathcal{F}\left(\frac{2P^+P^-}{\lambda_S^2} = \frac{k_\perp^2 + M^2}{\lambda_S^2 x\bar x}\right). \tag{40}$$

The same substitution was developed in the analysis of the ILM using the large momentum effective theory (LaMET) [54,55]. The substitution (40) guarantees the consistency of the two approaches. λ_S is a parameter of order 1. Remarkably, the same boost-invariant substitution with $\lambda_S = 1$ was argued long ago by Lepage and Brodsky in [51] in their analysis of two-body bound states on the light front using Bethe-Salpeter vertices. Note that the substitution (40) eliminates the metric component g_{-+} from the nonlocal form factors, with consequently no change in the symmetric energy-momentum tensor component T^{+-}.

Finally, we note that it is straightforward to generalize the Hamiltonian formalism to consider meson bound states in the U-spin or V-spin sectors relevant for kaons. In the case of kaons, the coupling constant will be replaced by $g_K = N_c G_K$, with a constituent mass matrix $M = \mathrm{diag}(M_u, M_d)$ in the flavor basis, as the s quark is significantly heavier than u, d quarks. This construction will be detailed below.

V. CONSTITUENT MASS AND CHIRAL CONDENSATE

The emergent chiral condensate (17) and constituent quark mass (19) are frame-invariant scalars. Whether evaluated in the rest frame or on the light front, they should give the same results. We now show that this is the case for the resummed tadpoles provided careful considerations are given to the form factor arising from the zero mode in the ILM.

A. Rest frame

The emergent constituent quark mass in the rest frame follows readily from (19) supplemented by (8) in the mean-field approximation. In Euclidean signature, we have

$$M(k) = m + 2g_S\mathcal{F}(k)\int \frac{d^4q}{(2\pi)^4}\frac{4M(q)}{q^2 + M^2(q)}\mathcal{F}(q), \tag{41}$$

where $g_S = G_S/N_c$ is the coupling strength for the 't Hooft interaction. At low momenta $k\rho \ll 1$, the dynamical mass $M(k)$ is about constant $M = M(0)$. This is consistent with the 't Hooft interaction in the zero instanton size limit.

At high momenta, the dynamical constituent mass asymptotes the current mass m.

The formal solution to (41) is

$$M(k) = m[1 - \mathcal{F}(k)] + M\mathcal{F}(k) \sim M\mathcal{F}(k) \tag{42}$$

for which (41) turns to a gap equation for the constant part M,

$$\frac{m}{M} = 1 - 8g_S \int \frac{d^4k}{(2\pi)^4} \frac{\mathcal{F}^2(k)}{k^2 + M^2}. \tag{43}$$

Solutions for M only exist for a critical g_S, which in ILM is fixed by the mean instanton-anti-instanton density. Following the arguments in [55], we have dropped the k dependence of the running mass in the denominator of (43), thanks to the smallness of the packing fraction (1).

The chiral condensate follows similarly,

$$\begin{aligned}\langle\bar{\psi}\psi\rangle &= -\int \frac{d^4k}{(2\pi)^4} \mathrm{Tr}S(k) \\ &= -8N_c M \int \frac{d^4k}{(2\pi)^4} \frac{1}{k^2 + M^2} \mathcal{F}(k).\end{aligned} \tag{44}$$

It reduces the scalar mean-field expectation $\langle\sigma\rangle = \langle\bar{\psi}\psi\rangle/N_c$ only in the zero instanton size limit. In the latter, 43)) and (44) are seen to diverge logarithmically, both in the IR and UV limits. So the quark zero mode induced form factor $\mathcal{F}(k)$ is key for a finite result.

In Fig. 1(a) we show the dependence of the constituent mass M on the current mass, for different multifermion couplings g_S in the ILM of the QCD vacuum. In Fig. 1(b) we show the scalar quark condensate dependence on these parameters.

B. Light front frame

On the light front only the physical modes of the good fermionic component ψ_+ are present after removal of the bad component in the mean-field approximation. The running quark mass on the light front is $M(k^-) \sim M\mathcal{F}(k^-)$ with the on-shell condition $2k^-k^+ = k_\perp^2 + M^2$, where M is fixed by the scalar gap equation (43). In terms of the physical modes for ψ_+, (43) can be rewritten as

$$\frac{m}{M} = 1 - 2g_S \int \frac{dk^+ d^2k_\perp}{(2\pi)^3} \frac{\epsilon(k^+)}{k^+} \mathcal{F}^2(k)\Big|_{k^- = \frac{k_\perp^2 + M^2}{2k^+}} \tag{45}$$

assuming that $\mathcal{F}(k^2)$ is free of physical poles. This is the case of (9) after analytical continuation, except for spurious branch points, which contributions can be disregarded in leading order in the diluteness factor (1) as detailed in [55].

For the chiral condensate on the light front, the quark propagator for the effective light front effective field (18), with the bad component fully reexpressed in terms of the good component, reads as

$$S(k) \to \left[\frac{i[\not{k} + M(k^2)]}{k^2 - M(k^2)^2} - \frac{i\gamma^+}{2k^+}\right] \to \left[\frac{i[\not{k} + M(k^2)]}{k^2 - M^2} - \frac{i\gamma^+}{2k^+}\right]. \tag{46}$$

The quark condensate in the light front signature is then

$$\langle\bar{\psi}\psi\rangle = -2N_c M \int \frac{dk^+ d^2k_\perp}{(2\pi)^3} \frac{\epsilon(k^+)}{k^+} \mathcal{F}(k^-). \tag{47}$$

More specifically, the gap equation with the ILM induced form factor is

$$\begin{aligned}\frac{m}{M} = 1 - \frac{4g_S}{\pi^2\rho^2} \int_0^\infty dzz \frac{z^3}{z^2 + \frac{\rho^2 M^2}{4}} \\ \times |z(I_0(z)K_0(z) - I_1(z)K_1(z))'|^4.\end{aligned} \tag{48}$$

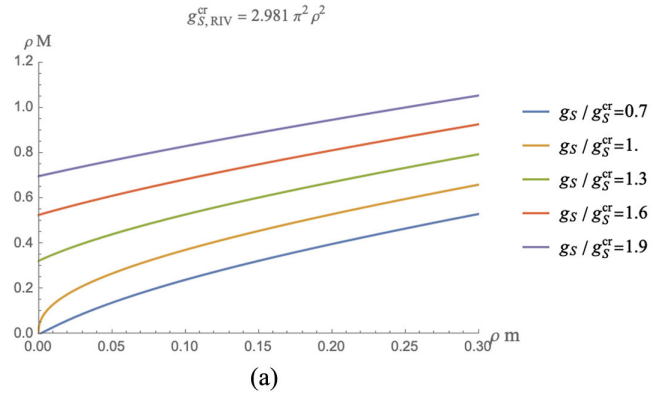

(a)

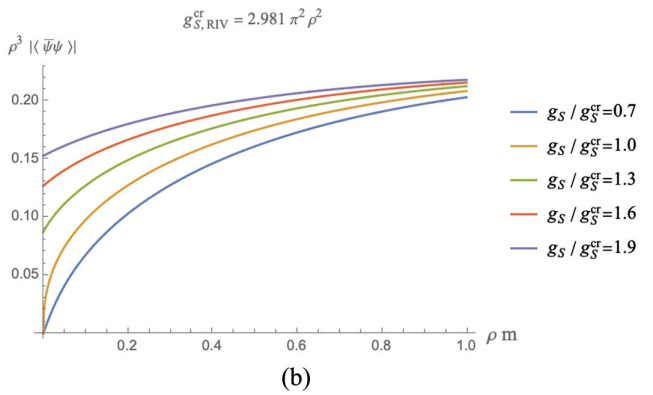

(b)

FIG. 1. (a) Quark constituent mass M versus the current quark mass m in the ILM for increasing strength of the 't Hooft coupling g_S (from bottom to top), with the critical coupling $g^{cr}_{S,\mathrm{RIV}} = 2.981\pi^2\rho^2$ and fixed instanton size ρ. (b) Quark condensate $\langle\bar{\psi}\psi\rangle$ versus the current quark mass in the ILM.

In the chiral limit, the constituent mass is nonzero only when the 't Hooft coupling is stronger than the critical coupling $g^{\rm cr}_{S,\rm RIV}$, which is defined as

$$g^{\rm cr}_{S,\rm RIV} = 2\pi^2\rho^2\left[8\int_0^\infty dz z|z(I_0(z)K_0(z) - I_1(z)K_1(z))'|^4\right]^{-1} \approx 2.981\pi^2\rho^2. \tag{49}$$

Similarly, the quark condensate is explicitly given by

$$\rho^3\langle\bar\psi\psi\rangle = -\frac{4N_c}{\pi^2}\rho M\int_0^\infty dz\frac{z^3}{z^2+\frac{\rho^2M^2}{4}}|z(I_0(z)K_0(z) - I_1(z)K_1(z))'|^2. \tag{50}$$

In the small size expansion, apart from the quadratic dependence of ρ in leading order, the next-to-leading-order dependence in ρM is dominated by polynomials. In the ILM, a slightly stronger coupling $g^{\rm cr}_{S,\rm RIV} = 2.981\pi^2\rho^2$ (instanton density) is required to produce a quark condensate that breaks chiral symmetry spontaneously.

For comparison, we will also quote the results in the zero instanton size limit for which $\mathcal{F}\to 1$. This case necessitates the introduction of a sharp cutoff. For vacuum loops in the zero-body sector, we will always enforce the on-shell condition $k^2 = 2k^+k^- - k_\perp^2$ and use the boost-invariant and parity-even cutoffs,

$$|\sqrt{2}k^\pm| \le \Lambda \sim 1/\rho.$$

More discussions on this point can be found in Appendix E. In the two-body sector and higher, boost invariance requires a different cutoff as we detail in Appendix F.

VI. LIGHT FRONT SPECTRUM

Now, we can use the light front Hamiltonian (38) to solve the eigenvalue equation for the meson wave functions,

$$P^-|X,P\rangle = \frac{m_X^2}{2P^+}|X,P\rangle. \tag{51}$$

In the valence approximation, which is compatible with the mean-field analysis in leading order in $1/N_c$, the meson's state is dominated by valence constituent quark dynamics,

$$|\text{meson } X,P\rangle = \frac{1}{\sqrt{N_c}}\int_0^1\frac{dx}{\sqrt{2x\bar x}}\int\frac{d^2k_\perp}{(2\pi)^3} \times\sum_{s_1,s_2}\Phi_X(x,k_\perp,s_1,s_2)b^\dagger_{s_1}(k)c^\dagger_{s_2}(P-k)|0\rangle. \tag{52}$$

The wave function is normalized by $\langle P|P'\rangle = (2\pi)^3 2P^+\delta^3(P-P')$,

$$\int_0^1 dx\int\frac{d^2k_\perp}{(2\pi)^3}\sum_{s_1,s_2}|\Phi_X(x,k_\perp,s_1,s_2)|^2 = 1. \tag{53}$$

A. Boost-invariant bound state equations

For two light flavors (u,d) with equal current masses, we expect light scalar and pseudoscalar mesons σ, σ_5, $\pi^{\pm,0}$, and $\pi_5^{\pm,0}$. A heavy scalar σ meson is commensurate with the order parameter of the spontaneous breaking of $SU(2)_V\times SU(2)_A$ to $SU(2)_V$. The broken $SU(2)_A$ symmetry generates near massless Goldstone modes $\pi^{\pm,0}$ with the valence quark assignments

$$\sigma = \frac{1}{\sqrt{2}}(u\bar u + d\bar d),\quad \pi^{\pm,0} = u\bar d,\quad d\bar u,\quad \frac{1}{\sqrt{2}}(u\bar u - d\bar d). \tag{54}$$

Both of these channels are strongly attractive in the ILM. In contrast, the ILM interaction in the pseudoscalar meson σ_5 (η') and flavor nonsinglet scalar partners $\pi_5^{\pm,0}$ is strongly repulsive. They are unbound both in the rest frame and on the light front. Irrespective of binding, the generic light front vertices Φ_X in (52) for all these mesonic channels are

$$\begin{aligned}
\Phi_\sigma(x,k_\perp,s_1,s_2) &= \phi_\sigma(x,k_\perp)\bar u_{s_1}(k)\frac{1}{\sqrt{2}}v_{s_2}(P-k),\\
\Phi_{\sigma_5}(x,k_\perp,s_1,s_2) &= \phi_{\sigma_5}(x,k_\perp)\bar u_{s_1}(k)\frac{1}{\sqrt{2}}i\gamma^5 v_{s_2}(P-k),\\
\Phi^a_\pi(x,k_\perp,s_1,s_2) &= \phi_\pi(x,k_\perp)\bar u_{s_1}(k)\frac{\tau^a}{\sqrt{2}}i\gamma^5 v_{s_2}(P-k),\\
\Phi^a_{\pi_5}(x,k_\perp,s_1,s_2) &= \phi_{\pi_5}(x,k_\perp)\bar u_{s_1}(k)\frac{\tau^a}{\sqrt{2}}v_{s_2}(P-k).
\end{aligned} \tag{55}$$

For convenience the spin-flavor part is made explicit using the light front spinors $u_s(k)$ for a particle spinor, and $v_s(k)$ for an anitparticle spinor, with the remaining ϕ_X a scalar-isoscalar wave function. The spinors are explicitly given in Appendix A.

Inserting (55) in (52) and then in (51), and unwinding the various contractions from the 4-Fermi interaction terms, yields the boost-invariant eigenvalue equation

$$m_X^2\Phi_X(x,k_\perp,s_1,s_2)=\frac{k_\perp^2+M^2}{x\bar{x}}\Phi_X(x,k_\perp,s_1,s_2)+\frac{1}{\sqrt{2x\bar{x}}}\sqrt{\mathcal{F}(k)\mathcal{F}(P-k)}\int_0^1\frac{dy}{\sqrt{2y\bar{y}}}\int\frac{d^2q_\perp}{(2\pi)^3}\times\sum_{s,s'}\mathcal{V}_{s_1,s_2,s,s'}(k,P-k,q,P-q)\Phi_X(y,q_\perp,s,s')\sqrt{\mathcal{F}(q)\mathcal{F}(P-q)} \tag{56}$$

with the ILM interaction kernel $\mathcal{V}_{s_1,s_2,s_1',s_2'}$

$$\mathcal{V}_{s,s',s_1,s_2}(q,q',k,k')=-G_S[\alpha_+(P^+)\bar{u}_{s_1}(k)v_{s_2}(k')\bar{v}_{s'}(q')u_s(q)-\alpha_-(P^+)\bar{u}_{s_1}(k)i\gamma^5v_{s_2}(k')\bar{v}_{s'}(q')i\gamma^5u_s(q)+\alpha_+(P^+)\bar{u}_{s_1}(k)\tau^ai\gamma^5v_{s_2}(k')\bar{v}_{s'}(q')\tau^ai\gamma^5u_s(q)-\alpha_-(P^+)\bar{u}_{s_1}(k)\tau^av_{s_2}(k')\bar{v}_{s'}(q')\tau^au_s(q)]. \tag{57}$$

Channel by channel, the explicit form of the kernel is

$$\sum_{s,s'}\mathcal{V}_{s,s',s_1,s_2}(q,q',k,k')\Phi_\sigma(y,q_\perp,s,s')=-g_S\alpha_+(P^+)\mathrm{Tr}[(\not{q}+M)(\not{q}'-M)]\phi_\sigma(y,q_\perp)\bar{u}_{s_1}(k)\mathbf{1}\mathrm{tr}(\mathbf{1})v_{s_2}(k')$$
$$=-4g_S\alpha_+(P^+)\left(\frac{q_\perp^2+(y-\bar{y})^2M^2}{y\bar{y}}\right)\phi_\sigma(y,q_\perp)\bar{u}_{s_1}(k)v_{s_2}(k'), \tag{58}$$

$$\sum_{s,s'}\mathcal{V}_{s,s',s_1,s_2}(q,q',k,k')\Phi_{\sigma_5}(y,q_\perp,s,s')=g_S\alpha_-(P^+)\mathrm{Tr}[(\not{q}+M)(\not{q}'+M)]\phi_{\sigma_5}(y,q_\perp)\bar{u}_{s_1}(k)i\gamma^5\mathbf{1}\mathrm{tr}(\mathbf{1})v_{s_2}(k')$$
$$=4g_S\alpha_-(P^+)\left(\frac{q_\perp^2+M^2}{y\bar{y}}\right)\phi_{\sigma_5}(y,q_\perp)\bar{u}_{s_1}(k)i\gamma^5v_{s_2}(k'), \tag{59}$$

$$\sum_{s,s'}\mathcal{V}_{s,s',s_1,s_2}(q,q',k,k')\Phi^a_{\pi_5}(y,q_\perp,s,s')=g_S\alpha_-(P^+)\mathrm{Tr}[(\not{q}+M)(\not{q}'-M)]\phi_{\pi_5}(y,q_\perp)\bar{u}_{s_1}(k)\tau^b\mathrm{tr}(\tau^a\tau^b)v_{s_2}(k')$$
$$=4g_S\alpha_-(P^+)\left(\frac{q_\perp^2+(y-\bar{y})^2M^2}{y\bar{y}}\right)\phi_{\pi_5}(y,q_\perp)\bar{u}_{s_1}(k)\tau^av_{s_2}(k'), \tag{60}$$

$$\sum_{s,s'}\mathcal{V}_{s,s',s_1,s_2}(q,q',k,k')\Phi^a_{\pi}(y,q_\perp,s,s')=-g_S\alpha_+(P^+)\mathrm{Tr}[(\not{q}+M)(\not{q}'+M)]\phi_{\pi}(y,q_\perp)\bar{u}_{s_1}(k)i\gamma^5\tau^b\mathrm{tr}(\tau^a\tau^b)v_{s_2}(k')$$
$$=-4g_S\alpha_+(P^+)\left(\frac{q_\perp^2+M^2}{y\bar{y}}\right)\phi_{\pi}(y,q_\perp)\bar{u}_{s_1}(k)i\gamma^5\tau^av_{s_2}(k'). \tag{61}$$

The corresponding eigenvalue equations for the scalar-isoscalar wave functions ϕ_X are

$$m_\sigma^2\phi_\sigma(x,k_\perp)=\frac{k_\perp^2+M^2}{x\bar{x}}\phi_\sigma(x,k_\perp)-\frac{2g_S\alpha_+(P^+)}{\sqrt{x\bar{x}}}\sqrt{\mathcal{F}(k)\mathcal{F}(P-k)}\int\frac{dy}{\sqrt{y\bar{y}}}\int\frac{d^2q_\perp}{(2\pi)^3}\left(\frac{q_\perp^2+(y-\bar{y})^2M^2}{y\bar{y}}\right)\phi_\sigma(y,q_\perp)\sqrt{\mathcal{F}(q)\mathcal{F}(P-q)} \tag{62}$$

$$m_{\sigma_5}^2\phi_{\sigma_5}(x,k_\perp)=\frac{k_\perp^2+M^2}{x\bar{x}}\phi_{\sigma_5}(x,k_\perp)+\frac{2g_S\alpha_-(P^+)}{\sqrt{x\bar{x}}}\sqrt{\mathcal{F}(k)\mathcal{F}(P-k)}\int\frac{dy}{\sqrt{y\bar{y}}}\int\frac{d^2q_\perp}{(2\pi)^3}\left(\frac{q_\perp^2+M^2}{y\bar{y}}\right)\phi_{\sigma_5}(y,q_\perp)\sqrt{\mathcal{F}(q)\mathcal{F}(P-q)}, \tag{63}$$

$$m_{\pi_5}^2\phi_{\pi_5}(x,k_\perp)=\frac{k_\perp^2+M^2}{x\bar{x}}\phi_{\pi_5}(x,k_\perp) + \frac{2g_S\alpha_-(P^+)}{\sqrt{x\bar{x}}}\sqrt{\mathcal{F}(k)\mathcal{F}(P-k)}\int\frac{dy}{\sqrt{y\bar{y}}}\int\frac{d^2q_\perp}{(2\pi)^3}\left(\frac{q_\perp^2+(y-\bar{y})^2M^2}{y\bar{y}}\right)\phi_{\pi_5}(y,q_\perp)\sqrt{\mathcal{F}(q)\mathcal{F}(P-q)}, \quad (64)$$

$$m_\pi^2\phi_\pi(x,k_\perp)=\frac{k_\perp^2+M^2}{x\bar{x}}\phi_\pi(x,k_\perp) - \frac{2g_S\alpha_+(P^+)}{\sqrt{x\bar{x}}}\sqrt{\mathcal{F}(k)\mathcal{F}(P-k)}\int\frac{dy}{\sqrt{y\bar{y}}}\int\frac{d^2q_\perp}{(2\pi)^3}\left(\frac{q_\perp^2+M^2}{y\bar{y}}\right)\phi_\pi(y,q_\perp)\sqrt{\mathcal{F}(q)\mathcal{F}(P-q)}. \quad (65)$$

B. Meson masses

The generic solution to the boost-invariant equations (62)–(65) is

$$1=\int_0^1 dy\int d^2q_\perp\frac{V_X(y,q_\perp)}{y\bar{y}m_X^2-(q_\perp^2+M^2)}\mathcal{F}(q)\mathcal{F}(P-q), \quad (66)$$

where for each of the mesonic channels we have for V_X in the numerator

$$V_X=\begin{cases}\mp\frac{2g_S}{(2\pi)^3}\alpha_\pm(P^+)\left(\frac{q_\perp^2+(y-\bar{y})^2M^2}{y\bar{y}}\right), & \text{scalars } \sigma,\pi_5\\ \mp\frac{2g_S}{(2\pi)^3}\alpha_\pm(P^+)\left(\frac{q_\perp^2+M^2}{y\bar{y}}\right), & \text{pseudo scalars } \pi,\sigma_5\end{cases}. \quad (67)$$

For the scalar σ and pseudoscalar π channel, the potential is negative and a bound solution exists, while for σ_5 and π_5, the potential is positive and a solution is ruled out in the mean-field approximation.

To deal with the coupling renormalization $\alpha(P^+)$ induced by the bad component through the constraint equation, we separate the k^+ integral into an integral in the physical range $0<k^+<P^+$ where the quark momentum can be associated with the momentum fraction x in the bound state, plus an integral outside the physical range $k^+<0$ or $k^+>P^+$. The latter contribution can be identified with a similar contribution in the mass gap equation

$$\begin{aligned}\alpha_\pm(P^+)^{-1}&=1\pm2g_S\int\frac{dk^+d^2k_\perp}{(2\pi)^3}\frac{\epsilon(k^+)}{P^+-k^+}\mathcal{F}(k)\mathcal{F}(P-k)\\&=1\pm\frac{2g_S}{(2\pi)^3}\int d^2k_\perp\left[\int_0^\infty dk^+\frac{1}{P^+-k^+}\mathcal{F}(k)\mathcal{F}(P-k)-\int_{-\infty}^0 dk^+\frac{1}{P^+-k^+}\mathcal{F}(k)\mathcal{F}(P-k)\right]\\&=1\pm\frac{2g_S}{(2\pi)^3}\int d^2k_\perp\left(\int_0^{P^+}dk^+\frac{2}{k^+}\mathcal{F}(k)\mathcal{F}(P-k)-\int_{-\infty}^\infty dk^+\frac{\epsilon(k^+)}{k^+}\mathcal{F}^2(k)\right).\end{aligned} \quad (68)$$

When the integration runs outside of the physical range of the two-body bound state, the virtual quark momentum will overtake the two-body bound light front momentum P^+ logarithmically. For fixed P^+ but large, the difference between $\mathcal{F}(k)$ and $\mathcal{F}(P-k)$ is then negligible. Hence, in the second part of the integral in (68) where k^+ runs outside $0<k^+<P^+$, we have replaced $\mathcal{F}(k)\mathcal{F}(P-k)$ by $\mathcal{F}^2(k)$, which gives a contribution identical to that in the mass gap equation (45). With this in mind, (68) simplifies to

$$\alpha_\pm(P^+)^{-1}=\begin{cases}\frac{m}{M}+\frac{4g_S}{(2\pi)^3}\int d^2k_\perp\int_0^1 dx\frac{1}{x}\mathcal{F}(k)\mathcal{F}(P-k)\\ 2-\frac{m}{M}-\frac{4g_S}{(2\pi)^3}\int d^2k_\perp\int_0^1 dx\frac{1}{x}\mathcal{F}(k)\mathcal{F}(P-k)\end{cases}, \quad (69)$$

where $x=k^+/P^+$ is the momentum fraction of the quark inside the bound state.

1. Scalars

For the scalar type particle σ and π_5^a, the mass eigenvalue equations are

$$\begin{aligned}0&=\alpha_\pm(P^+)^{-1}\pm\frac{2g_S}{(2\pi)^3}\int dy\int d^2q_\perp\frac{(q_\perp^2+(y-\bar y)^2M^2)/y\bar y}{y\bar y m_X^2-(q_\perp^2+M^2)}\mathcal{F}(q)\mathcal{F}(P-q)\\&=\begin{cases}\frac{m}{M}+\frac{2g_S}{(2\pi)^3}\int_0^1 dy\int d^2q_\perp\left[\frac{2}{y}-\frac{1}{y\bar y}+\frac{m_\sigma^2-(1-(y-\bar y)^2)M^2/y\bar y}{y\bar y m_X^2-(q_\perp^2+M^2)}\right]\mathcal{F}(q)\mathcal{F}(P-q)\\2-\frac{m}{M}-\frac{2g_S}{(2\pi)^3}\int_0^1 dy\int d^2q_\perp\left[\frac{2}{y}-\frac{1}{y\bar y}+\frac{m_{\pi_5}^2-(1-(y-\bar y)^2)M^2/y\bar y}{y\bar y m_X^2-(q_\perp^2+M^2)}\right]\mathcal{F}(q)\mathcal{F}(P-q)\end{cases}\\&=\begin{cases}\frac{m}{M}+\frac{2g_S}{(2\pi)^3}\int_0^1 dy\int d^2q_\perp\left[\frac{m_\sigma^2-4M^2}{y\bar y m_X^2-(q_\perp^2+M^2)}\right]\mathcal{F}(q)\mathcal{F}(P-q), & \sigma\text{ meson}\\2-\frac{m}{M}-\frac{2g_S}{(2\pi)^3}\int_0^1 dy\int d^2q_\perp\left[\frac{m_{\pi_5}^2-4M^2}{y\bar y m_X^2-(q_\perp^2+M^2)}\right]\mathcal{F}(q)\mathcal{F}(P-q), & \pi_5\text{ meson.}\end{cases}\end{aligned}\tag{70}$$

The boost-invariant property of the form factor guarantees the cancellation between the integral $\int_0^1 dy\frac{2}{y}$ and $\int_0^1 dy\frac{1}{y\bar y}$.

2. Pseudoscalars

For the pseudoscalar type particle σ_5 and π^a, the mass eigenvalue equations are

$$\begin{aligned}0&=\alpha_\pm(P^+)^{-1}\pm\frac{2g_S}{(2\pi)^3}\int_0^1 dy\int d^2q_\perp\frac{(q_\perp^2+M^2)/y\bar y}{y\bar y m_X^2-(q_\perp^2+M^2)}\mathcal{F}(q)\mathcal{F}(P-q)\\&=\begin{cases}2-\frac{m}{M}-\frac{2g_S}{(2\pi)^3}\int_0^1 dy\int d^2q_\perp\left[\frac{2}{y}-\frac{1}{y\bar y}+\frac{m_{\sigma_5}^2}{y\bar y m_{\sigma_5}^2-(q_\perp^2+M^2)}\right]\mathcal{F}(q)\mathcal{F}(P-q)\\\frac{m}{M}+\frac{2g_S}{(2\pi)^3}\int_0^1 dy\int d^2q_\perp\left[\frac{2}{y}-\frac{1}{y\bar y}+\frac{m_\pi^2}{y\bar y m_\pi^2-(q_\perp^2+M^2)}\right]\mathcal{F}(q)\mathcal{F}(P-q)\end{cases}\\&=\begin{cases}2-\frac{m}{M}-\frac{2g_S}{(2\pi)^3}\int_0^1 dy\int d^2q_\perp\left[\frac{m_{\sigma_5}^2}{y\bar y m_{\sigma_5}^2-(q_\perp^2+M^2)}\right]\mathcal{F}(q)\mathcal{F}(P-q), & \sigma_5\text{ meson}\\\frac{m}{M}+\frac{2g_S}{(2\pi)^3}\int_0^1 dy\int d^2q_\perp\left[\frac{m_\pi^2}{y\bar y m_\pi^2-(q_\perp^2+M^2)}\right]\mathcal{F}(q)\mathcal{F}(P-q), & \pi\text{ meson.}\end{cases}\end{aligned}\tag{71}$$

3. σ meson

With the transverse cutoff regularization from the ILM, the mass eigenvalue of the σ meson is

$$\begin{aligned}\frac{m}{M}&=-\frac{g_S}{4\pi^2}\int_0^1 dy\int_0^\infty dq_\perp^2\left[\frac{m_\sigma^2-4M^2}{y\bar y m_\sigma^2-(q_\perp^2+M^2)}\right][(zF'(z))^4]\Big|_{z=\frac{\rho\sqrt{q_\perp^2+M^2}}{2\lambda_S\sqrt{y\bar y}}}\\&=-\frac{g_S}{2\pi^2}(4M^2-m_\sigma^2)\int_0^1 dy\int_{\frac{\rho M}{2\lambda_S\sqrt{y\bar y}}}^\infty dz\frac{z}{z^2-\frac{\rho^2m_\sigma^2}{4\lambda_S^2}}[zF'(z)]^4,\qquad m_\sigma^2<4M^2.\end{aligned}\tag{72}$$

In the chiral limit $m=0$ of the scalar-isoscalar σ meson is a threshold state, with mass $m_\sigma=2M$. The same threshold mass has been observed for the standard ILM in the rest frame, as it should be. For $m\neq 0$, since the integration in the second line of (72) is always positive, the σ meson unbinds in the ILM. In the mean-field approximation and away from the chiral limit, the 't Hooft interaction in the ILM is not strong enough to bind $\sigma=\bar uu+\bar dd$.

4. σ_5 and π_5 mesons

The same observation applies to the scalar-isovector π_5 and the pseudoscalar-isoscalar σ_5 channels. The eigenvalue equation for π_5 is

$$2-\frac{m}{M}=\frac{g_S}{4\pi^2}\int_0^1 dy\int_0^\infty dq_\perp^2\left[\frac{m_{\pi_5}^2-4M^2}{y\bar{y}m_{\pi_5}^2-(q_\perp^2+M^2)}\right][(zF'(z))^4]\Big|_{z=\frac{\rho\sqrt{q_\perp^2+M^2}}{2\lambda_S\sqrt{y\bar{y}}}}$$
$$=\frac{g_S}{2\pi^2}(4M^2-m_{\pi_5}^2)\int_0^1 dy\int_{\frac{\rho M}{2\lambda_S\sqrt{y\bar{y}}}}^\infty dz\frac{z}{z^2-\frac{\rho^2 m_{\pi_5}^2}{4\lambda_S^2}}[zF'(z)]^4,\qquad m_{\pi_5}^2<4M^2 \tag{73}$$

and the eigenvalue equation for π_5 is

$$2-\frac{m}{M}=\frac{g_S}{4\pi^2}\int_0^1 dy\int_0^\infty dq_\perp^2\left[\frac{m_{\sigma_5}^2}{y\bar{y}m_{\sigma_5}^2-(q_\perp^2+M^2)}\right][(zF'(z))^4]\Big|_{z=\frac{\rho\sqrt{q_\perp^2+M^2}}{2\lambda_S\sqrt{y\bar{y}}}}$$
$$=-\frac{g_S}{2\pi^2}m_{\sigma_5}^2\int_0^1 dy\int_{\frac{\rho M}{2\lambda_S\sqrt{y\bar{y}}}}^\infty dz\frac{z}{z^2-\frac{\rho^2 m_{\sigma_5}^2}{4\lambda_S^2}}[zF'(z)]^4 \tag{74}$$

Regardless of the chiral limit, π_5 and σ_5 cannot be bound in the mean-field approximation of the ILM on the light front.

5. π meson

The interaction induced by the ILM in the pion channel is very strong and attractive, leading to a triplet of massless Nambu-Goldstone modes $\pi^{\pm,0}$. The pion decay constant in the chiral limit is solely given by the zero mode form factor on the light front

$$f_\pi=\frac{\sqrt{N_c}M}{\sqrt{2}\pi}\times\left[\int_0^1 dx\int_0^\infty dk_\perp^2\left(\frac{1}{k_\perp^2+M^2}\right)\mathcal{F}(k)\mathcal{F}(P-k)\right]^{1/2}$$
$$=\frac{\sqrt{N_c}M}{\pi}\left[\int_0^1 dx\int_{\frac{\rho M}{2\lambda_S\sqrt{x\bar{x}}}}^\infty dz z^3(F'(z))^4\right]^{1/2}\approx\frac{\sqrt{N_c}M}{\sqrt{2}\pi}\sqrt{\ln\frac{C}{\rho^2M^2}}+\mathcal{O}(\rho). \tag{75}$$

In the small ρ expansion, it can be defined as

$$f_\pi^2=\frac{1}{2\pi^2}M^2N_c\ln\left(\frac{C}{\rho^2M^2}\right),$$

where $C\approx 0.361$ is the constant determined numerically with the input parameter $\lambda_S=3.285$, in total agreement with the result obtained also in the ILM using the large momentum effective theory [54]. The pion mass is a solution to the eigenvalue equation

$$\frac{m}{M}=-\frac{g_S}{4\pi^2}\int_0^1 dy\int_0^\infty dq_\perp^2\left[\frac{m_\pi^2}{y\bar{y}m_\pi^2-(q_\perp^2+M^2)}\right][(zF'(z))^4]\Big|_{z=\frac{\rho}{2\lambda_S}\sqrt{\frac{q_\perp^2+M^2}{y\bar{y}}}}$$
$$=\frac{g_S}{2\pi^2}m_\pi^2\int_0^1 dy\int_{\frac{\rho M}{2\lambda_S\sqrt{y\bar{y}}}}^\infty dz\frac{z}{z^2-\frac{\rho^2 m_\pi^2}{4\lambda_S^2}}[zF'(z)]^4,\qquad m_\pi^2<4M^2 \tag{76}$$

with clearly a massless pion in the chiral limit. Away from the chiral limit and with a nonvanishing constituent quark mass M, the pion mass following from (76) can be assessed in perturbation theory, with the result

$$m_\pi^2=\frac{2m}{f_\pi^2}|\langle\bar{\psi}\psi\rangle|+\mathcal{O}(m^2), \tag{77}$$

where the quark condensate

$$|\langle\bar{\psi}\psi\rangle|=|\langle\bar{u}u\rangle+\langle\bar{d}d\rangle|=\frac{N_c}{g_S}(M-m)$$

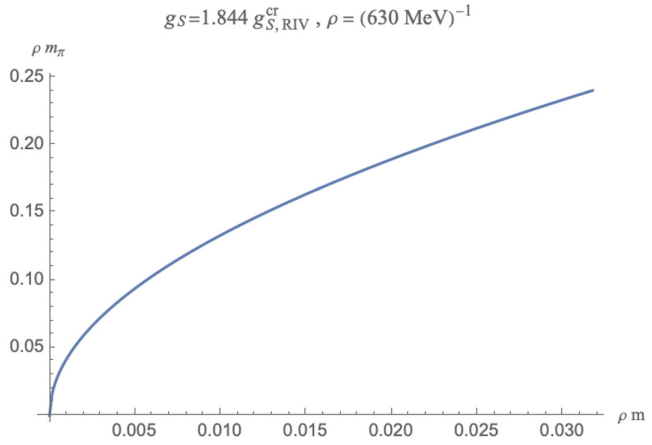

FIG. 2. Change of the pion mass with the current quark mass m, for a fixed fermionic coupling $g_S = 1.844 g^{cr}_{S,\mathrm{RIV}}$ and instanton size $\rho = (630\ \mathrm{MeV})^{-1}$.

is given by the gap equation. Equation (77) is the expected Gell-Mann-Oakes-Renner relation for Nambu-Goldstone modes. In Fig. 2 we show the pion mass solution to (76) in the ILM on the light front, as a function of the current quark mass m, for the fermionic coupling $g_S = 1.844 g^{cr}_{S,\mathrm{RIV}}$ and a fixed instanton size $\rho = (630\ \mathrm{MeV})^{-1}$.

The parameters ρ, m, g_S, λ_S in the mean-field approximation of the ILM are fixed as follows: the instanton size is set at its mean canonical value $\rho = 0.313$ fm; the light current quark mass is set to $m = 16.0$ MeV; the multifermion coupling is set to $g_S = 1.844 g^{cr}_{S,\mathrm{RIV}}$ to give a constituent quark mass of $M = 444.8$ MeV and a chiral condensate $|\langle\bar{\psi}\psi\rangle|^{1/3} = 337.9$ MeV; the cutoff parameter is set to $\lambda_S = 3.285$ to give a pion decay constant $f^{\mathrm{RIV}}_\pi = 130.3$ MeV and pion mass $m^{\mathrm{RIV}}_\pi = 135$ MeV, very close to the empirical results. In Fig. 2 we show the change of the pion mass with the current quark mass. We note the rapid vanishing of the mass in the chiral limit, for a nonvanishing constituent quark mass M and a chiral condensate, as expected for a Goldstone mode.

C. Pion DA from LFWF

In the mean-field approximation to the ILM, the generic solution for the valence light front wave functions (LFWFs) is generically of the form

$$\phi_X(x,k_\perp) = \frac{1}{\sqrt{2x\bar{x}}}\frac{C_X}{m_X^2 - \frac{k_\perp^2+M^2}{x\bar{x}}}\sqrt{\mathcal{F}(k)\mathcal{F}(P-k)} \tag{78}$$

with the constant C_X fixed by the normalization (53). Alternatively, the LFWFs can also be deduced from the quark-meson interaction amplitude (by integration over k^-) in which case C_X corresponds to the effective quark-meson coupling g_X in the interaction, i.e. $C_X = -\sqrt{N_c} g_X$. The minus sign is chosen to ensure a positive-definite LFWF.

Since of all the light scalars and pseudoscalars made out of u, d light quarks, only the pion is strongly bound in the mean-field approximation (the sigma meson is a threshold state), we now construct the pion DA using the pion LFWF. More specifically, using the pion DA as defined through the forward matrix element of the twist-2 operator on the light cone,

$$\phi_\pi(x) = -i\int\frac{d\xi^-}{2\pi}e^{ixP^+\xi^-}\langle 0|\bar{\psi}(0)\gamma^+\gamma^5\frac{\tau^a}{\sqrt{2}}W(0,\xi^-)\psi(\xi^-)|\pi^a(P)\rangle \tag{79}$$

with the normalization fixed by the pion weak decay constant

$$\langle 0|\bar{\psi}\gamma^+\gamma^5\frac{\tau^a}{\sqrt{2}}\psi|\pi^a(P)\rangle = if_\pi P^+, \tag{80}$$

we obtain

$$\phi_\pi(x) = \frac{\sqrt{N_c}M}{2\sqrt{2}\pi^2}\int_0^\infty dk_\perp^2\frac{C_\pi}{x\bar{x}m_\pi^2 - (k_\perp^2+M^2)}\mathcal{F}(k)\mathcal{F}(P-k). \tag{81}$$

The on-shell normalization (80) fixes the dependence of the pion weak decay constant $f_\pi(m_\pi)$ on the pion mass m_π,

$$f_\pi(m_\pi) = f_\pi\frac{\int_0^1 dx\int_0^\infty dk_\perp^2\left(\frac{1}{k_\perp^2+M^2-x\bar{x}m_\pi^2}\right)\mathcal{F}(k)\mathcal{F}(P-k)}{\left[\int_0^1 dx\int_0^\infty dk_\perp^2\frac{k_\perp^2+M^2}{(k_\perp^2+M^2-x\bar{x}m_\pi^2)^2}\mathcal{F}(k)\mathcal{F}(P-k)\right]^{1/2}\left[\int_0^1 dx\int_0^\infty dk_\perp^2\left(\frac{1}{k_\perp^2+M^2}\right)\mathcal{F}(k)\mathcal{F}(P-k)\right]^{1/2}} \tag{82}$$

with f_π given in (75).

In the zero instanton size approximation with a fixed transverse momentum cutoff $|k_\perp| < \Lambda$, the pion DA amplitude is a step function

$$\phi_\pi(x) = -\frac{\sqrt{N_c}MC_\pi}{2\sqrt{2}\pi^2}\theta(x\bar{x})\ln\left(1+\frac{\Lambda^2}{M^2-x\bar{x}m_\pi^2}\right)\overset{m_\pi\to 0}{\longrightarrow}\frac{\sqrt{N_c}M}{\sqrt{2}\pi}\left[\ln\left(1+\frac{\Lambda^2}{M^2}\right)\right]^{1/2}\theta(x\bar{x}) \tag{83}$$

in agreement with a result established first in the local NJL model [23]. The pion weak decay constant is

$$f_\pi = -\frac{\sqrt{N_c}MC_\pi}{\sqrt{2}\pi^2}\left[\frac{1}{2}\ln\left(1+\frac{\Lambda^2}{M^2}\right)-\sqrt{\frac{4M^2-m_\pi^2}{m_\pi^2}}\tan^{-1}\frac{1}{\sqrt{\frac{4M^2-m_\pi^2}{m_\pi^2}}}\right. \tag{84}$$

$$\left.+\sqrt{\frac{4(M^2+\Lambda^2)-m_\pi^2}{m_\pi^2}}\tan^{-1}\frac{1}{\sqrt{\frac{4(M^2+\Lambda^2)-m_\pi^2}{m_\pi^2}}}\right]\overset{m_\pi\to 0}{\longrightarrow}\frac{\sqrt{N_c}M}{\sqrt{2}\pi}\left[\ln\left(1+\frac{\Lambda^2}{M^2}\right)\right]^{1/2}. \tag{85}$$

In the ILM with a finite instanton size, the pion DA is

$$\phi_\pi(x) = \frac{\sqrt{N_c}M}{\sqrt{2}\pi^2}C_\pi\int_{\frac{\rho M}{2\lambda\sqrt{x\bar{x}}}}^{\infty}dz\,\frac{z^5}{\frac{\rho^2 m_\pi^2}{4\lambda^2}-z^2}(F'(z))^4 \tag{86}$$

which simplifies in the chiral limit to

$$\phi_\pi(x) = -\frac{\sqrt{N_c}M}{\sqrt{2}\pi^2}C_\pi\int_{\frac{\rho M}{2\sqrt{x\bar{x}}}}^{\infty}dz z^3(F'(z))^4. \tag{87}$$

In general, we note that the induced form factors $\sqrt{\mathcal{F}(i\partial)}$ give rise to extra contributions to the Noether axial vector current, and possibly the axial source current in (79). Indeed, the semibosonized Lagrangian $\mathcal{L}$ in (24) with the minimal substitution

$$i\partial_\mu \to i\partial_\mu + \gamma^5\tau^a A_\mu^a,$$

where A_μ^a is a local external flavor gauge field, yields the conserved $SU(2)_A$ current in the chiral limit,

$$\left.\frac{\partial\mathcal{L}}{\partial A^a}\right|_{\substack{A,\pi=0\\ \sigma=\bar{\sigma}}} = \bar{\psi}\gamma^\mu\tau^a\psi + \bar{\sigma}\bar{\psi}\sqrt{\mathcal{F}(i\partial)}'\tau^a\sqrt{\mathcal{F}(i\partial)}\psi + \bar{\sigma}\bar{\psi}\sqrt{\mathcal{F}(i\partial)}\tau^a\sqrt{\mathcal{F}(i\partial)}'\psi \tag{88}$$

with $\sqrt{\mathcal{F}(x)}' = \frac{d}{dx}\sqrt{\mathcal{F}(x)}$. From (40) it follows that the extra contributions in Sec. VI C are absent for the leading twist-2 operator on the light front. Therefore, the Gell-mann-Oakes-Renner (GOR) relation and the normalization of the pion DA are unchanged. The results (86) and (87) are in agreement with those derived from the ILM using the large momentum effective theory, in the dilute approximation [54].

D. ERBL evolution of the pion DA

The evolution of the pion DA is governed by ERBL equation

$$\phi(x,Q) = 6x\bar{x}\sum_{n=0}^{\infty}a_n(Q_0)\left(\frac{\alpha_s(Q^2)}{\alpha_s(Q_0^2)}\right)^{\gamma_n/\beta_0}C_n^{3/2}(x-\bar{x}) \tag{89}$$

which is an expansion in Gegenbauer polynomials $C_n^m(z)$ of increasing powers, with anomalous dimension

$$\gamma_n = C_F\left[-3+4\sum_{j=1}^{n+1}\frac{1}{j}-\frac{2}{(n+1)(n+2)}\right], \tag{90}$$

where $C_F = \frac{N_c^2-1}{2N_c}$,

$$\alpha_s(Q) = \frac{4\pi}{\beta_0\ln\left(\frac{Q^2}{\Lambda_{\rm QCD}^2}\right)},$$

$\beta_0 = \frac{11}{3}N_c - \frac{2}{3}n_f$, and $\Lambda_{\rm QCD} = 226$ MeV. Due to the orthogonality of the Gegenbauer polynomials, the initial coefficients can be evaluated by

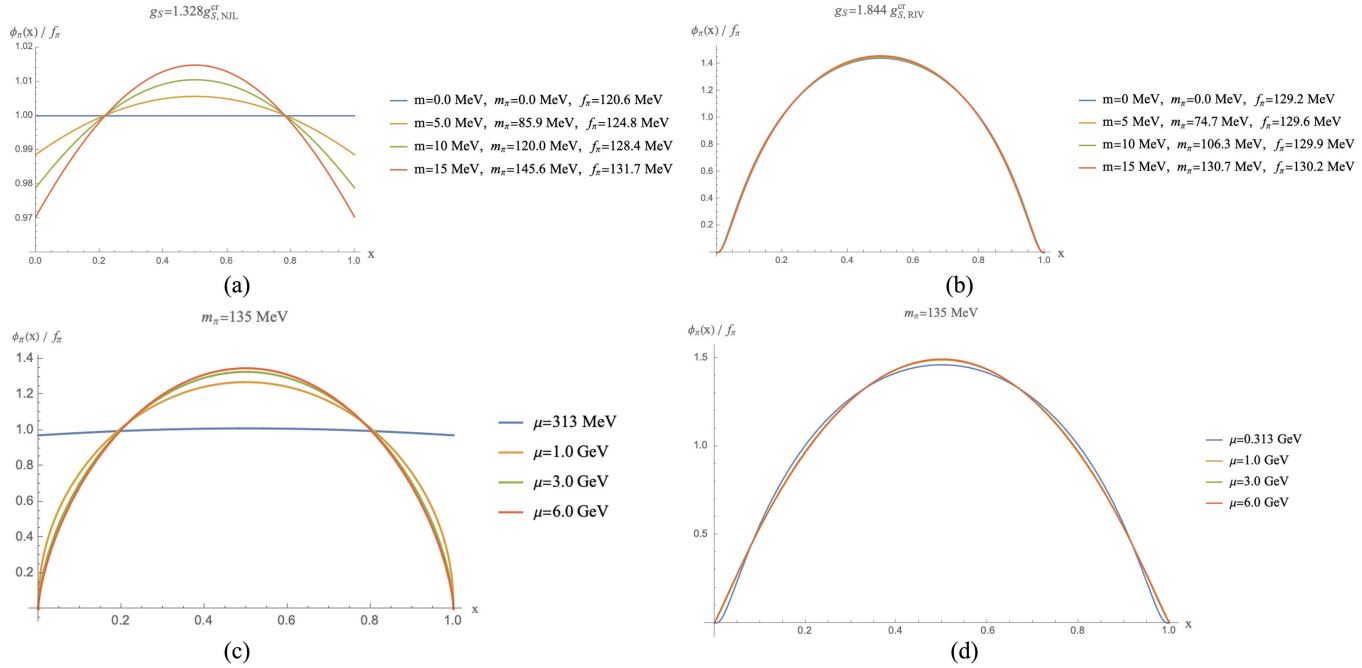

FIG. 3. (a) The pion DA with different pion mass m_π in the zero instanton size limit. (b) The pion DA with different pion mass m_π in the ILM with finite instanton size $\rho = (630\ \mathrm{MeV})^{-1}$. (c) The Efremov-Radyushkin-Brodsky-Lepage (ERBL) evolution of pion DA in zero instanton size limit. (d) The ERBL evolution of pion DA in RIV with finite instanton size $\rho = (630\ \mathrm{MeV})^{-1}$.

$$a_n(Q_0) = \frac{2(2n+3)}{3(n+1)(n+2)} \int_0^1 dy C_n^{3/2}(y-\bar{y})\phi(y,Q_0). \tag{91}$$

In Fig. 3(a) we show the pion DA versus x in the zero instanton size limit for fixed fermionic coupling $g_S = 1.32 g^{cr}_{S,\mathrm{NJL}}$ and different current quark masses. In Fig. 3(b) we show the same pion DA versus x in the ILM for a similar fermionic coupling $g_S = 1.844 g^{cr}_{S,\mathrm{RIV}}$ and different current quark masses. There is a dramatic change at the endpoints following the emergence of the instanton induced form factors from the quark zero modes. In Fig. 3(c) we show the ERBL evolved pion DA in the zero instanton size limit and in Fig. 3(d) the same evolution in the ILM. The initial scale used is $\mu_0 = 0.313$ GeV to $\mu = 6$ GeV. The pion mass is $m_\pi = 135$ MeV.

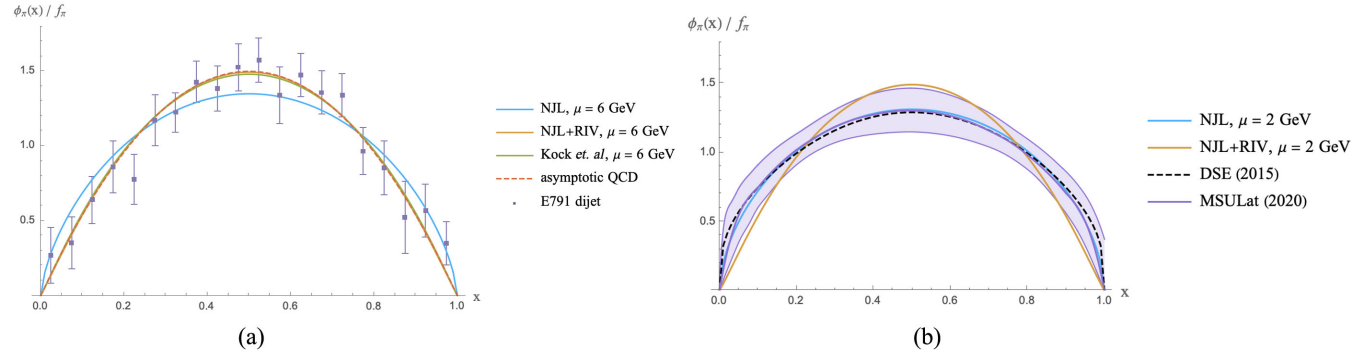

FIG. 4. (a) Pion DA in the ILM with zero instanton size (NJL-like) as given in (99) (solid blue curve), in the ILM with finite instanton size as given in (103) (solid orange curve), after ERBL evolution from $\mu_0 = 0.313$ GeV to $\mu = 6$ GeV. The pion mass is $m_\pi = 135$ MeV. The results are compared to the DAs obtained in [54,55] (green solid curve) by applying the LaMET in the ILM, also evolved to $\mu = 6$ GeV. We also show the asymptotic pQCD result of $6x\bar{x}$ from [56] (dashed red curve). The measured DA (purple) is from π^- into dijets via diffractive dissociation, with invariant dijet mass of 6 GeV [57], as extracted and normalized in [58]. (b) The same evolved pion DAs from (99) (solid blue curve) and from (103) (solid orange curve) now evolved to only $\mu = 2$ GeV are compared to recent lattice results using LaMET (purple band) from [60]. The DSE curve (dashed black curve) follows from Dyson-Schwinger equations with Bethe-Salpeter wave functions [59].

In Fig. 4(a) we compare the ERBL evolved pion DAs to $\mu = 6$ GeV with the QCD asymptotic result of $6x\bar{x}$ [56] (dashed red curve) and the measured pion DA by the E791 dijet collaboration [57] (purple points). The data are from π^- into dijets via diffractive dissociation with invariant dijet mass 6 GeV [57], as compiled in [58]. The evolved DAs are for zero size insantons (blue solid curve), the current light front analysis of the ILM (orange solid curve), and the LaMET analysis of the ILM in [54,55]. In Fig. 4(b) we compare our pion DA to the Dyson-Schwinger result [59] (dashed black curve) and the more recent lattice result done by the lattice group in Michigan State University (MSULAT) using the LaMET procedure [60] (filled purple band). The evolution is now from $\mu_0 = 0.313$ GeV to $\mu = 2$ GeV. Our evolved results are for zero size instantons (solid blue curve), and the ILM (solid orange curve).

VII. PARTON DISTRIBUTION FUNCTIONS

In general, the partonic structures in a hadron are related to pertinent leading twist matrix elements, following factorization of various observables. The PDFs are Fourier transforms of fermionic (gluonic) correlators at fixed separation on the light cone. They follow from the LFWFs. More specifically, the quark twist-2 PDF in a bound meson state, is given by

$$q_X(x) = \int_{-\infty}^{\infty} \frac{d\xi^-}{4\pi} e^{ixP^+\xi^-} \langle P|\bar{\psi}(0)\gamma^+ W(0,\xi^-)\psi(\xi^-)|P\rangle = \int \frac{d^2k_\perp}{(2\pi)^3} |\Phi_X(x,k_,s,s')|^2 \tag{92}$$

while the antiquark PDF is given by

$$\bar{q}_X(x) = \int_{-\infty}^{\infty} \frac{d\xi^-}{4\pi} e^{-ixP^+\xi^-} \langle P|\bar{\psi}(0)\gamma^+ W(0,\xi^-)\psi(\xi^-)|P\rangle = \int \frac{d^2k_\perp}{(2\pi)^3} |\Phi_X(\bar{x},k_,s,s')|^2. \tag{93}$$

Here

$$W(\xi^-,0) = \exp\left[-ig\int_0^{\xi^-} d\eta^- A^+(\eta^-)\right] \to 1$$

is a gauge link, which will be set to 1 throughout. For the meson PDFs, the quark and antiquark distributions are related by charge symmetry

$$\bar{q}_X(x) = q_{\bar{X}}(x) = q_X(1-x) = \bar{q}_{\bar{X}}(1-x).$$

Also, the PDFs are normalized to 1 by charge conservation

$$\langle X(P)|\bar{\psi}\frac{1}{2}\gamma^+\psi|X(P)\rangle = 1. \tag{94}$$

A. σ and pion PDFs

The σ PDF is

$$q_\sigma(x) = \frac{1}{4\pi^2}\int_0^\infty dk_\perp^2 \frac{1}{x\bar{x}} \left|\frac{C_\sigma}{m_\sigma^2 - \frac{k_\perp^2+M^2}{x\bar{x}}}\right|^2 \frac{k_\perp^2 + (x-\bar{x})^2M^2}{x\bar{x}} \mathcal{F}(k)\mathcal{F}(P-k). \tag{95}$$

Also, the pion PDF is

$$q_\pi(x) = \frac{1}{4\pi^2}\int_0^\infty dk_\perp^2 \frac{1}{x\bar{x}} \left|\frac{C_\pi}{m_\pi^2 - \frac{k_\perp^2+M^2}{x\bar{x}}}\right|^2 \frac{k_\perp^2 + M^2}{x\bar{x}} \mathcal{F}(k)\mathcal{F}(P-k). \tag{96}$$

In the chiral limit, the normalization constant can be determined by the cutoff function induced by the nonlocal quark form factor as well. Thus, the normalization constant can be related to the pion decay constant f_π and the constituent mass M,

$$C_\pi = -2\pi \int_0^\infty dk_\perp^2 \frac{1}{k_\perp^2 + M^2} \mathcal{F}(k)\mathcal{F}(P-k) = -\frac{\sqrt{2N_c}M}{f_\pi}. \tag{97}$$

Again, the minus sign is chosen to make the wave function positive-definite for convenience.

In the zero instanton size limit, we can use the same hard cutoff described in Appendix E, with the result for the sigma PDF as

$$q_\sigma(x) = \frac{C_\sigma^2}{4\pi^2}\theta(x\bar{x}) \ln\left(1 + \frac{\Lambda^2}{(x-\bar{x})^2 M^2}\right), \tag{98}$$

where

$$-C_\sigma = 2\pi\left[\ln\left(1+\frac{\Lambda^2}{M^2}\right) + 2\frac{\Lambda}{M}\tan^{-1}\frac{M}{\Lambda}\right]^{-1/2}.$$

Recall that the sigma meson is only bound in the chiral limit with $m_\sigma = 2M$. For comparison, we note that in the same approximation of zero instanton size, the pion PDF is

$$q_\pi(x) = \frac{C_\pi^2}{4\pi^2}\theta(x\bar{x})\left[\frac{x\bar{x}m_\pi^2\Lambda^2}{(M^2 - x\bar{x}m_\pi^2)(M^2+\Lambda^2 - x\bar{x}m_\pi^2)} - \ln\left(\frac{M^2 - x\bar{x}m_\pi^2}{M^2+\Lambda^2 - x\bar{x}m_\pi^2}\right)\right] \xrightarrow{m_\pi \to 0} \frac{C_\pi^2}{4\pi^2}\theta(x\bar{x}) \ln\left(1+\frac{\Lambda^2}{M^2}\right), \tag{99}$$

where in the chiral limit

$$C_\pi = -2\pi\left[\ln\left(1+\frac{\Lambda^2}{M^2}\right)\right]^{-1/2}.$$

This result agrees with the result in the zero instanton size limit $\rho \to 0$ in [54,55] using the large momentum effective theory. It was first established in the NJL model in [21]. However, it is at variance with the endpoint expectation $f_{q/\pi}(x \to 1, Q^2) \sim (1-x)$ at $Q^2 \to \infty$, from the Drell-Yan-West result [61,62]. The discrepancy is expected to wane out with QCD evolution, which depletes the large-x part of the PDF as we show below.

For a finite instanton size, all integrations are tamed by the induced zero mode form factor $\sqrt{\mathcal{F}(i\partial)}$ discussed earlier. The ensuing nonlocal interactions are expected to contribute to the currents, hence to the twist-2 part of the PDFs in general [63,64], as we noted earlier for the axial-vector current in Sec. VI C. For the vector current, the extra contributions follow from minimal substitution,

$$i\partial_\mu \to i\partial_\mu + V_\mu, \tag{100}$$

where V_μ is the external $U(1)$ flavor gauge field. The vector current for the nonlocal semibosonized Lagrangian (24) follows from the Noether construction in the form

$$\left.\frac{\partial \mathcal{L}}{\partial V}\right|_{\substack{V,\pi=0\\ \sigma=\bar{\sigma}}} = \bar{\psi}\gamma^\mu\psi + \bar{\sigma}\,\bar{\psi}\,\sqrt{\mathcal{F}(i\partial)}'\sqrt{\mathcal{F}(i\partial)}\psi + \bar{\sigma}\,\bar{\psi}\,\sqrt{\mathcal{F}(i\partial)}\,\sqrt{\mathcal{F}(i\partial)}'\psi, \tag{101}$$

where again, the derivative on the functional form of the form factor is defined as $\sqrt{\mathcal{F}(x)}' = \frac{d}{dx}\sqrt{\mathcal{F}(x)}$. Now we recall that in the two-body channel, the boost-invariant substitution (40) is only dependent on the relative transverse momentum of the pair. From (101), it follows that the leading twist-2 light front current is not modified, leaving the chiral relation and normalization of the twist-2 meson PDF and DA unchanged.

With this in mind, the sigma PDF in the ILM in the chiral limit is

$$q_\sigma(x) = \frac{1}{4\pi^2}\int_0^\infty dk_\perp^2 C_\sigma^2 \frac{1}{k_\perp^2 - (4x\bar{x}-1)M^2}\mathcal{F}(k)\mathcal{F}(P-k) = \frac{C_\sigma^2}{2\pi^2}\int_{\frac{\rho M}{2\lambda_S\sqrt{x\bar{x}}}}^\infty dz \frac{z^5}{z^2 - \rho^2 M^2/\lambda_S^2}(F'(z))^4 \tag{102}$$

while the pion PDF, in general, is

$$q_\pi(x) = \frac{1}{4\pi^2}\int_0^\infty dk_\perp^2 \frac{C_\pi^2(k_\perp^2+M^2)}{(x\bar{x}m_\pi^2 - k_\perp^2 - M^2)^2}\mathcal{F}(k)\mathcal{F}(P-k)$$
$$= \frac{C_\pi^2}{2\pi^2}\int_{\frac{\rho M}{2\lambda_S\sqrt{x\bar{x}}}}^\infty dz \frac{z^3}{\left(\frac{\rho^2 m_\pi^2}{4\lambda_S^2} - z^2\right)^2}[zF'(z)]^4.$$

In the chiral limit,

$$q_\pi(x) \xrightarrow{m_\pi\to 0} \frac{C_\pi^2}{2\pi^2}\int_{\frac{\rho M}{2\lambda_S\sqrt{x\bar{x}}}}^\infty dz z^3 (F'(z))^4, \tag{103}$$

with the normalization constant

$$C_\pi = -\sqrt{2}\pi\left[\int_0^1 dx \int_{\frac{\rho M}{2\lambda_S\sqrt{x\bar{x}}}}^\infty dz z^3 (F'(z))^4\right]^{-1/2}$$
$$= -\sqrt{2N_c}M/f_\pi \approx -7.993 \tag{104}$$

with $M = 421.5$ MeV, $\rho = 0.313$ fm, and $f_\pi = 130.3$ MeV. At the endpoint $x, \bar{x} = 0$, the asymptotic form of $F(z) \sim 1/4z^3$ dominates the integral. The endpoint behavior of the pion PDF in the ILM at a resolution of $Q^2 \sim 1/\rho^2$ is softer than the one expected from the Drell-Yan-West relation at much larger resolution [61,62] with

$$q_\pi(x) \sim \frac{C_\pi^2}{2\pi^2}\frac{108\lambda_S^{12}}{\rho^{12}M^{12}}(x\bar{x})^6. \tag{105}$$

In Fig. 5(a) we show the sigma PDF in the chiral limit, with a threshold sigma mass $2M = 418.3$ MeV, in the instanton zero size approximation. The PDF is sharply picked at $x = \frac{1}{2}$ and does not vanish at the endpoints $x = 0, 1$. In Fig. 5(b) we show the pion PDF for different current quark masses, also in the zero instanton size approximation. In Fig. 5(c) we show the sigma PDF in the ILM, with a much sharper distribution at $x = \frac{1}{2}$ that reflects on the threshold state, in the zero instanton size limit. In Fig. 5(d) the pion PDF in the ILM is shown for different current quark masses. The instanton induced form factors cause it to vanish at the endpoints, with little sensitivity to the current quark masses.

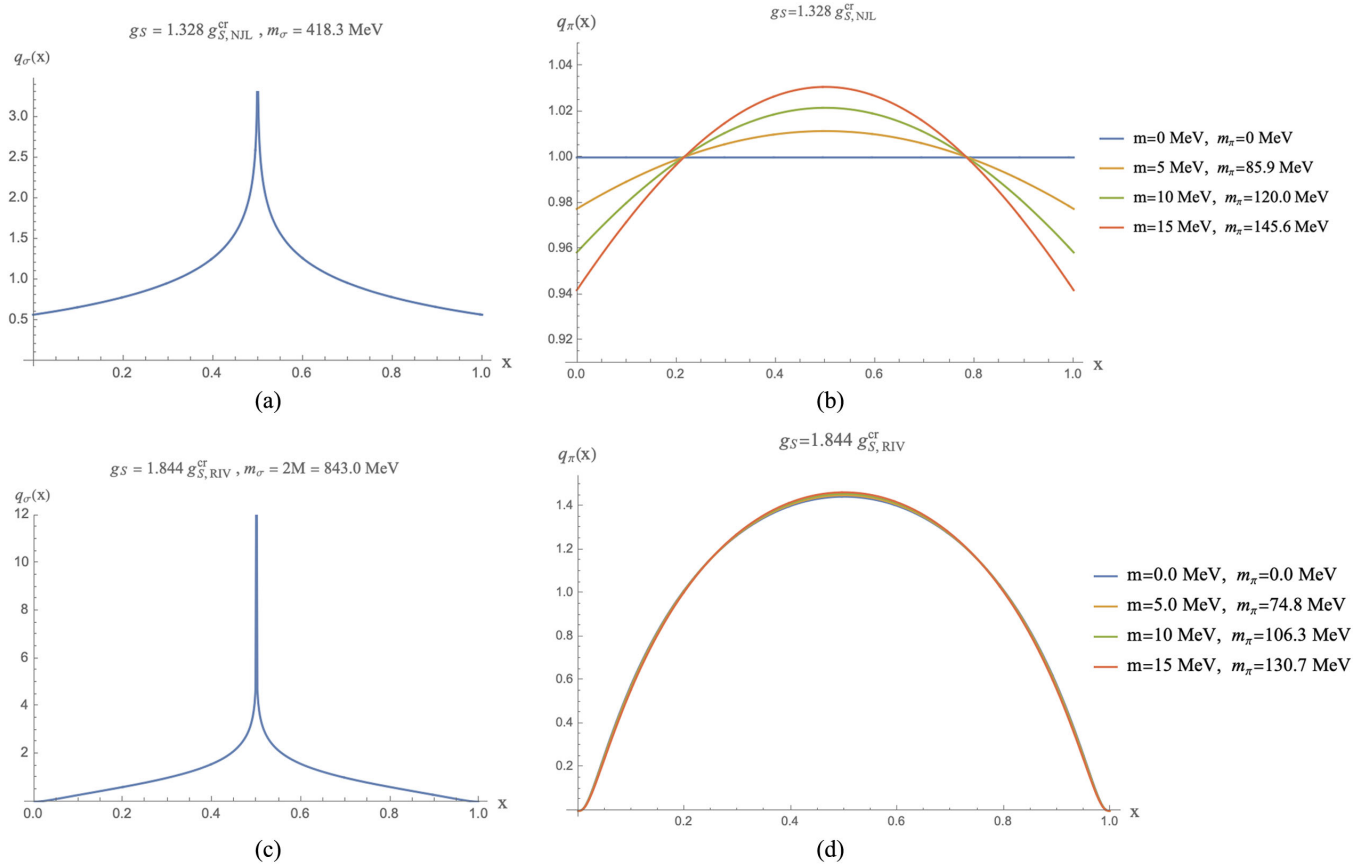

FIG. 5. (a) The σ PDF in zero instanton size and in the chiral limit, with a threshold σ mass $2M = 418.9$ MeV. (b) The pion PDF with zero instanton size, but with different pion masses varying with quark current masses. (c) The σ PDF with the finite instanton size $1/\rho = 630$ MeV, with a threshold σ mass $2M = 418.9$ MeV in the chiral limit. (d) The pion PDF with the finite instanton size $\rho = 0.313$ fm with different pion masses.

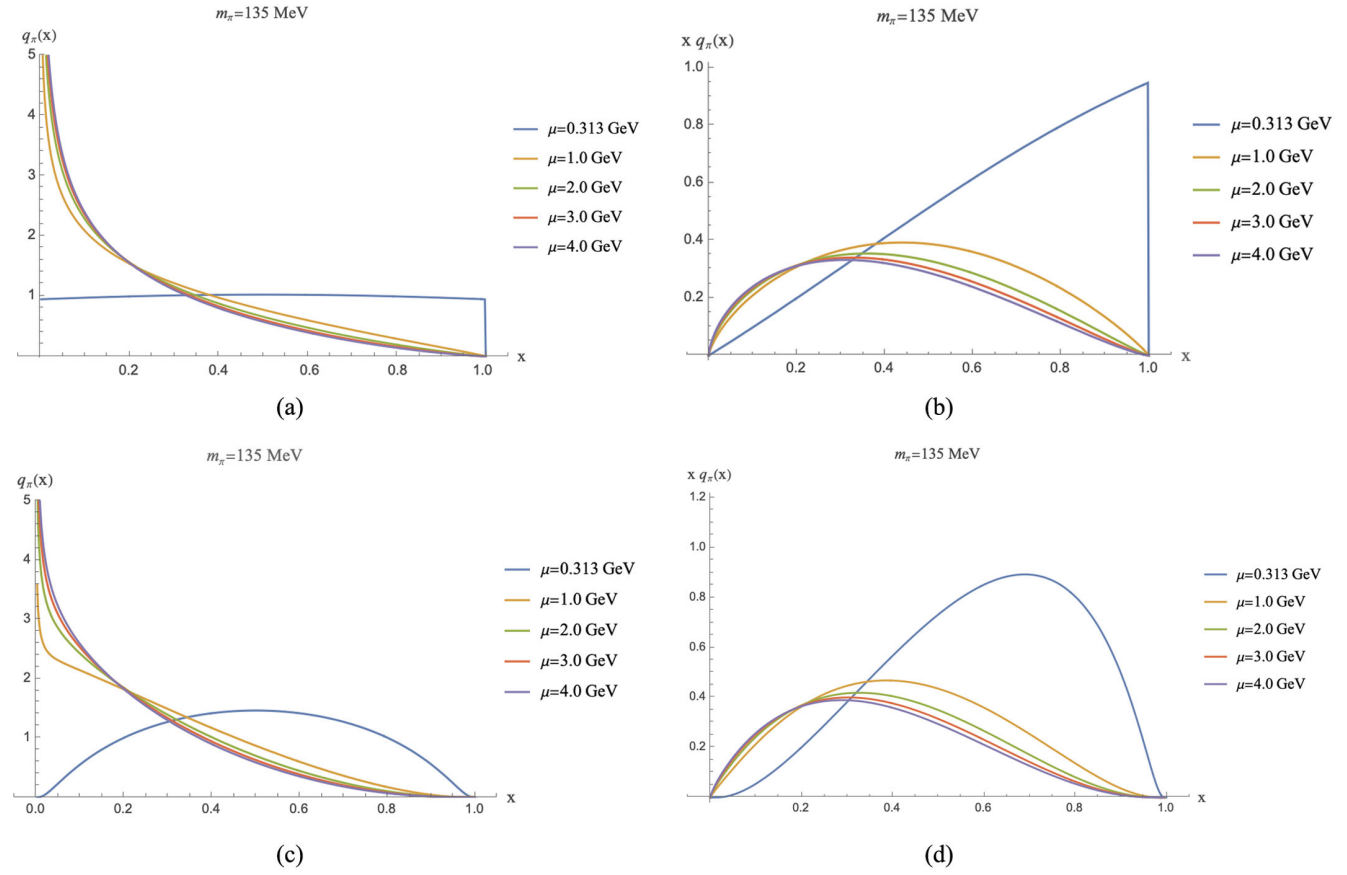

FIG. 6. (a) DGLAP evolution of pion PDF for zero instanton size and in the chiral limit. (b) DGLAP evolution of the pion valence quark momentum distribution for zero instanton size and in the chiral limit. (c) DGLAP evolution for the pion PDF with a finite instanton size $\rho = 0.313$ fm. (d) DGLAP evolution of the pion valence quark momentum distribution with a finite instanton size $\rho = 0.313$ fm in the chiral limit. All evolutions start from the initial scale $\mu_0 = 0.313$ GeV.

B. DGLAP evolution

In the ILM the partonic distributions are defined at a factorization scale μ_0 which is smaller than the inverse size $1/\rho \sim 630$ MeV of an instanton. To compare our result with the available experiments in [38,65,66], we evolve the PDFs in (99) and (103), starting from say $\mu_0 = 313$ MeV, a nonperturbative scale that is not large enough to resolve the instantons and anti-instantons in the ILM. The PDFs are

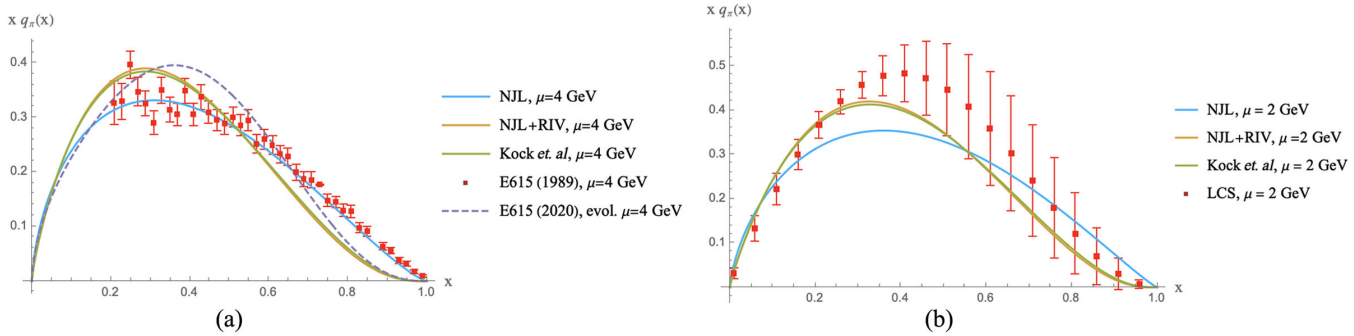

FIG. 7. (a) Pion parton momentum distribution function for zero instanton size (solid blue curve) and finite instanton size of $\rho = 0.317$ fm (solid orange curve), both of which are evolved to $\mu = 4$ GeV with a pion mass $m_\pi = 135$ MeV. The results are compared to the those extracted from the ILM using the LaMET (solid green curve) [54,55] also evolved to $\mu = 4$ GeV. The E615 data from 1989 (red) are from [65], corresponding to a fixed-invariant muon pair mass $m_{\mu^+\mu^-} \geq 4.05$ GeV. The improved E615 data from 2020 (dashed purple curve) are from [66] using the original E615 experimental data from [65]. (b) The same pion parton distribution functions as in (a), but now evolved to $\mu = 2$ GeV, for comparison with the lattice data using cross sections (LCS) (red) from [67].

evolved to 2 GeV for comparison to also lattice data [67]. Since only the valence quark dynamics is retained in our analysis, we will only keep the quark splitting in the DGLAP evolution. The reader may be concerned that at such a low energy scale, an altogether nonperturbative evolution of the type discussed recently in [16] may be required. This point will be addressed in a sequel. Here, we will only implement the perurbative DGLAP evolution for a qualitative comparison.

In Figs. 6(a) and 6(b) we show the DGLAP evolved pion PDF in the zero instanton size approximation, starting from the initial scala $\mu_0 = 313$ MeV up to 4 GeV. In Figs. 6(c) and 6(d) we show the same DGLAP evolution for the results in the ILM, with a finite instanton size $\rho = 0.313$ fm. In both cases, the pion mass is fixed at its physical value $m_\pi = 135$ MeV.

In Fig. 7(a) we compare our DGLAP evolved results with the original E615(1989) data [65] (red) and the subsequent E165(2020) improved analysis [66] (dashed purple curve) at $\mu = 4$ GeV. The data are compiled from measurements of an invariant muon pair mass $m_{\mu^+\mu^-} \geq 4.05$ GeV. Our evolved results are for the zero instanton size (solid blue curve) and finite instanton size in the ILM model (solid orange curve). They are also compared to the extracted pion PDF from the ILM model using LaMET [54,55] (solid green). Our results are evolved from an initial scale $\mu_0 = 313$ MeV below the instanton resolution scale $1/\rho = 631$ MeV to a final scale of 4 GeV. In Fig. 7(b) our evolved results are compared to the LCS lattice results [67] (red) at $\mu = 2$ GeV. All of the theoretical results are also evolved to the same scale.

VIII. $N_f = 2$ INSTANTON-INDUCED INTERACTION WITH UNEQUAL MASSES

To construct the kaon partonic distributions, we need to address the three flavor case with u, d, s quarks. For simplicity, we will consider the reduced mass case with light $m_u = m_d$ and heavier m_s. In this case, the 2-flavor kaon sectors of $SU(3)$ with U spin and V spin are amenable to the same light front effective Lagrangian (23). The only difference is the large difference in the assigned current quark masses. More specifically, we have

$$\mathcal{L} = \bar{\psi}(i\partial\!\!\!/ - M)\psi + \frac{G_K}{2}[\bar{\psi}\psi\hat{D}^{-1}_{K+}\bar{\psi}\psi - \bar{\psi}\tau^a\psi\hat{D}^{-1}_{K-}\bar{\psi}\tau^a\psi - \bar{\psi}i\gamma^5\psi\hat{D}^{-1}_{K+}\bar{\psi}i\gamma^5\psi + \bar{\psi}i\gamma^5\tau^a\psi\hat{D}^{-1}_{K-}\bar{\psi}i\gamma^5\tau^a\psi] \tag{106}$$

with the tadpole resummed vertices

$$\hat{D}^{-1}_{K\pm} = \frac{1}{1 \pm \frac{g_K}{N_c}\left\langle \bar{\psi}\gamma^+ \frac{-i}{\partial_-}\psi \right\rangle}. \tag{107}$$

G_K is the corresponding 't Hooft coupling strength in the Kaon channel. The quark constituent mass is now matrix valued $M = \mathrm{diag}(M_u, M_s)$, where u denotes the lighter quark u or d, and s denotes the heavier strange quark.

A. Gap equation

In the U-spin (V-spin) sector, the effective momentum-dependent form factors $\sqrt{\mathcal{F}_{u/s}(k)}$ for each flavor will also be introduced to the interacting quark fields. Effectively, the quark fields in the 't Hooft interaction terms will be dressed by a form factor,

$$\psi(x) \to \sqrt{\mathcal{F}(i\partial)}\psi(x). \tag{108}$$

The assignment suggested on mass shell in (40) that enforces boost invariance in the two-body state implies that

$$\sqrt{\mathcal{F}(i\partial)} \to \begin{pmatrix} \sqrt{\mathcal{F}_u(i\partial)} & 0 \\ 0 & \sqrt{\mathcal{F}_s(i\partial)} \end{pmatrix}. \tag{109}$$

The nonlocal 't Hooft interaction given by the momentum-dependent form factors yields momentum-dependent gap equations with running constituent masses $M_{u/s}(k^2)$ for each flavor,

$$M_{u/s}(k^2) = M_{u/s}\mathcal{F}_{u/s}(k^2) = M_{u/s}[(zF'(z))^2]\Big|_{z=\frac{k\rho}{2}}. \tag{110}$$

In the low momentum regime ($k\rho \ll 1$), the dynamical constituent masses are constant and a solution to the gap equations in the mean-field approximation reads

$$\frac{M_s - m_s}{M_u} = 2g_K \int \frac{dk^+ d^2k_\perp}{(2\pi)^3}\frac{\epsilon(k^+)}{k^+}\mathcal{F}_u^2(k^2),$$
$$\frac{M_u - m_u}{M_s} = 2g_K \int \frac{dk^+ d^2k_\perp}{(2\pi)^3}\frac{\epsilon(k^+)}{k^+}\mathcal{F}_s^2(k^2). \tag{111}$$

Since the two-flavor quark doublet carries different masses, both $\langle\bar{\psi}\psi\rangle$ and $\langle\bar{\psi}\tau^3\psi\rangle$ receive contributions from the explicit flavor symmetry breaking. In the mean-field approximation, they amount to different scalar condensates

$$\langle\bar{u}u\rangle = -N_c M_u \int \frac{dk^+ d^2k_\perp}{(2\pi)^3}\frac{\epsilon(k^+)}{k^+}\mathcal{F}_u(k^2),$$
$$\langle\bar{s}s\rangle = -N_c M_s \int \frac{dk^+ d^2k_\perp}{(2\pi)^3}\frac{\epsilon(k^+)}{k^+}\mathcal{F}_s(k^2), \tag{112}$$

with

$$\langle \bar{s}s\rangle = \frac{1}{2}(\langle\bar{\psi}\psi\rangle - \langle\bar{\psi}\tau^3\psi\rangle),$$
$$\langle \bar{u}u\rangle = \frac{1}{2}(\langle\bar{\psi}\psi\rangle + \langle\bar{\psi}\tau^3\psi\rangle). \tag{113}$$

To accommodate the effective dynamical mass with the light front formalism, we have to analytically continue the Euclidean momentum dependence k^2 to the Minkowski space. The argument of the form factor will become $2k^+k^-$.

For simplicity, we first analyze the gap equations and quark condensates in the zero instanton size limit. Using the boost-invariant cutoff Λ scheme discussed in Appendix E, we have for the gap equations

$$\frac{M_s - m_s}{M_u} = 2g_K \int \frac{dk^+ d^2k_\perp}{(2\pi)^3}\frac{\epsilon(k^+)}{k^+}\theta(\Lambda/\sqrt{2}-k^+)\theta(\Lambda/\sqrt{2}-k^-)\Big|_{k^-=\frac{k_\perp^2+M_u^2}{2k^+}},$$
$$\frac{M_u - m_u}{M_s} = 2g_K \int \frac{dk^+ d^2k_\perp}{(2\pi)^3}\frac{\epsilon(k^+)}{k^+}\theta(\Lambda/\sqrt{2}-k^+)\theta(\Lambda/\sqrt{2}-k^-)\Big|_{k^-=\frac{k_\perp^2+M_s^2}{2k^+}}. \tag{114}$$

Using the result in (E2), the solutions of the gap equations in zero size limit are

$$\frac{M_s - m_s}{M_u} = \frac{g_K\Lambda^2}{2\pi^2}\left[1 - \frac{M_u^2}{\Lambda^2} + \frac{M_u^2}{\Lambda^2}\ln\frac{M_u^2}{\Lambda^2}\right],$$
$$\frac{M_u - m_u}{M_s} = \frac{g_K\Lambda^2}{2\pi^2}\left[1 - \frac{M_s^2}{\Lambda^2} + \frac{M_s^2}{\Lambda^2}\ln\frac{M_s^2}{\Lambda^2}\right]. \tag{115}$$

In the chiral limit $m_u = m_s = 0$, the constituent masses are equal. The nonzero solution in the chiral limit exists only for sufficiently strong couplings larger than $g_{K,\mathrm{NJL}}^{\mathrm{cr}} = \frac{2\pi^2}{\Lambda^2}$. When g_K is less than $g_{K,\mathrm{NJL}}^{\mathrm{cr}} = \frac{2\pi^2}{\Lambda^2}$, no quark condensate will be formed in the chiral limit. However, as long as the coupling g_K is strong enough, chiral symmetry is dynamically broken, with a nonvanishing scalar quark condensate, in the chiral limit. The constituent mass ratio of two quarks M_s/M_u will be controlled by the coupling g_K and the two current quark mass m_u, m_s. The quark condensates for two flavors are

$$\frac{\langle\bar{u}u\rangle}{\Lambda^3} = -\frac{N_c}{4\pi^2}\left(\frac{M_u}{\Lambda}\right)\left[1 - \frac{M_u^2}{\Lambda^2} + \frac{M_u^2}{\Lambda^2}\ln\frac{M_u^2}{\Lambda^2}\right],$$
$$\frac{\langle\bar{s}s\rangle}{\Lambda^3} = -\frac{N_c}{4\pi^2}\left(\frac{M_s}{\Lambda}\right)\left[1 - \frac{M_s^2}{\Lambda^2} + \frac{M_s^2}{\Lambda^2}\ln\frac{M_s^2}{\Lambda^2}\right]. \tag{116}$$

For a finite instanton size, the integrals in the emergent constituent masses and chiral condensates are naturally regulated by the boost-invariant cutoffs given in (110). More specifically, the mass gaps are given by

$$\frac{M_s - m_s}{M_u} = \frac{4g_K}{\pi^2\rho^2}\int_0^\infty dz z\frac{z^3}{z^2 + \frac{\rho^2 M_u^2}{4}}|z(I_0(z)K_0(z) - I_1(z)K_1(z))'|^4,$$
$$\frac{M_u - m_u}{M_s} = \frac{4g_K}{\pi^2\rho^2}\int_0^\infty dz z\frac{z^3}{z^2 + \frac{\rho^2 M_s^2}{4}}|z(I_0(z)K_0(z) - I_1(z)K_1(z))'|^4, \tag{117}$$

and the scalar condensates are given by

$$\rho^3\langle\bar{u}u\rangle = \frac{2N_c}{\pi^2}\rho M_u\int_0^\infty dz z\frac{z^3}{z^2 + \frac{\rho^2 M_u^2}{4}}|z(I_0(z)K_0(z) - I_1(z)K_1(z))'|^2,$$
$$\rho^3\langle\bar{s}s\rangle = \frac{2N_c}{\pi^2}\rho M_s\int_0^\infty dz z\frac{z^3}{z^2 + \frac{\rho^2 M_s^2}{4}}|z(I_0(z)K_0(z) - I_1(z)K_1(z))'|^2. \tag{118}$$

In Figs. 8(a) and 8(b) we show the change of the constituent u quark mass M_u, and the constituent s quark mass M_s with the strange quark mass m_s, for different multifermion couplings g_K, respectively. The current u quark mass is set to zero. In Fig. 8(c) we show the ratio M_s/M_u for fixed g_K/g_K^{cr} but varying m_u. In Fig. 8(d) we show the ratio M_s/M_u for fixed $m_u = 12.7$ MeV and varying g_K. All Figs. 8(a)–8(d) are for the zero instanton size limit but a finite transverse cutoff Λ. Figures 8(e)–8(h) display the same results for the ILM with a finite instanton size ρ.

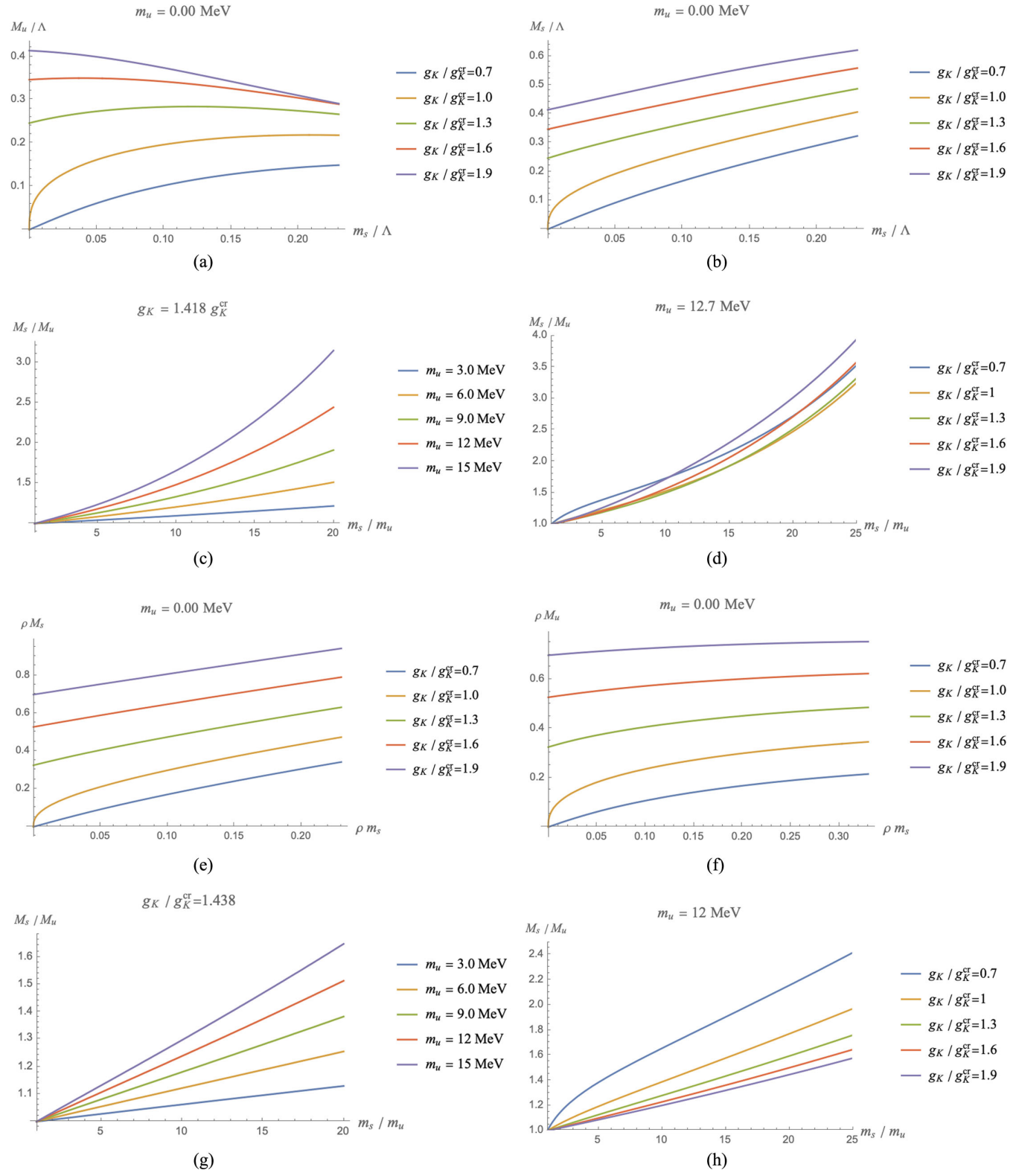

FIG. 8. (a),(b) The constituent masses $M_{u,s}$ versus the strange quark mass m_s for different couplings g_K/g_K^{cr} and fixed $m_u = 0$ in the zero instanton size limit. (c),(d) The constituent mass ratio M_s/M_u versus m_s/m_u, for fixed coupling $g_K/g_K^{cr} = 1.418$ with varying m_u and fixed $m_u = 12.7$ MeV with varying g_K/g_K^{cr} in the zero instanton size limit. (e)–(h) The same constituent masses as in (a)–(d) in the ILM with a finite instanton size.

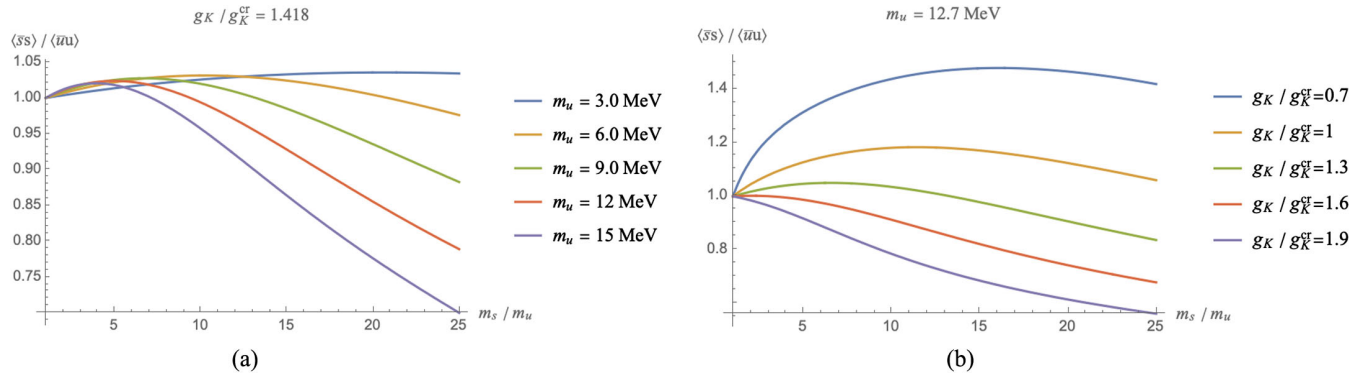

FIG. 9. (a) The ratio of the quark condensates $\langle\bar{s}s\rangle/\langle\bar{u}u\rangle$ versus m_s/m_u for fixed $g_K/g_K^{cr} = 1.418$ and different m_u. (b) The ratio of the quark condensates $\langle\bar{s}s\rangle/\langle\bar{u}u\rangle$ versus m_s/m_u for fixed $m_u = 12.7$ MeV and different g_K/g_K^{cr}.

In Fig. 9(a) we show the change in the ratio of the strange to nonstrange condensates $\langle\bar{s}s\rangle/\langle\bar{u}u\rangle$, with the ratio of the strange to nonstrange current masses m_s/m_u, for different u quark masses but fixed coupling $g_K/g_K^{cr} = 1.418$. In Fig. 9(b) we show the same but now with fixed u quark mass $m_u = 12.7$ MeV and increasing coupling g_K/g_K^{cr}.

IX. KAONS FROM U AND V SPIN: LFWFs AND MASSES

The general light fron state (52) can be readily adapted to kaons with $K^{\pm} = u\bar{s}, s\bar{u}$ in the U-spin sector. In the V-spin sector, we have the pseudoscalars $K^0, \bar{K}^0 = d\bar{s}, s\bar{d}$, with their scalar counterparts K_5^0, $\bar{K}_5^0$. Without loss of generality, we will assume that isospin symmetry still holds. Thus, the result in U spin and V spin will be identical, $\Phi_{K^{\pm}} = \Phi_{K^0} = \Phi_K$. With this in mind, the LFWFs for the pseudoscalar kaons $K^{\pm}$ and their scalar counterparts K_5 are given by

$$\Phi_{K_5}(x,k_\perp,s_1,s_2) = \phi_{K_5}(x,k_\perp)\bar{u}_{s_1}(k)\tau^{\pm}v_{s_2}(P-k),$$
$$\Phi_K(x,k_\perp,s_1,s_2) = \phi_K(x,k_\perp^{\pm})\bar{u}_{s_1}(k)i\gamma^5\tau^{\pm}v_{s_2}(P-k), \tag{119}$$

where $\tau^{\pm} = \frac{1}{2}(\tau^1 \pm i\tau^2)$ are the Pauli matrices for U or V spin. Again, we have separated the spin-independent part of the wave functions and express the spin part in terms of light front Dirac spinors.

A. Bound state equations for kaons

In the kaon channels, there are still two quark species, but their masses are different, compared with the isospin sector. The constituent mass of the s quark is heavier than the u and d quarks. However, we can still assume that isospin symmetry holds for simplicity, i.e. the induced instanton coupling G_K is the same for U-spin and V-spin sectors. With this in mind, we can generalize the light front Hamiltonian in (38) to the U-spin and V-spin sectors. Since the current mass of the s quark is significantly different from that of the u and d quarks, we will treat M as a diagonal matrix $M = \mathrm{diag}(M_u, M_s)$. This will slightly break the U spin in the $K^{\pm}$ channels, or the V-spin symmetry of the K^0 and $\bar{K}^0$ channels.

To be consistent with the boost-invariant light front symmetry requirement in the two-body process, the momentum-dependent cutoff function $\mathcal{F}(k)$ induced from the finite size effect of the instanton ensemble has to be a function of boost-invariant variables $\frac{k_\perp^2+M_u^2}{x}$ and $\frac{k_\perp^2+M_s^2}{\bar{x}}$ related to the quark kinetic energies. In light of the substitution (40), we use

$$\lim_{P^+\to\infty}\sqrt{\mathcal{F}_u(k)\mathcal{F}_s(P-k)} \to \mathcal{F}\left(2P^+P^- = \frac{k_\perp^2+M_u^2}{x} + \frac{k_\perp^2+M_s^2}{\bar{x}}\right). \tag{120}$$

As a result, the bound-state equation for the kaons ($K^{\pm}$) is

$$\begin{aligned} m_K^2\Phi_K(x,k_\perp,s_1,s_2) = &\left[\frac{k_\perp^2+M_u^2}{x} + \frac{k_\perp^2+M_s^2}{\bar{x}}\right]\Phi_K(x,k_\perp,s_1,s_2) \\ &+ \frac{1}{\sqrt{2x\bar{x}}}\sqrt{\mathcal{F}_u(k)\mathcal{F}_s(P-k)}\int_0^1\frac{dy}{\sqrt{2y\bar{y}}}\int\frac{d^2q_\perp}{(2\pi)^3}\sum_{s,s'}\mathcal{V}_{s,s',s_1,s_2}(q,q',k,k')\Phi_K(y,q_\perp,s,s') \\ &\times\sqrt{\mathcal{F}_u(q)\mathcal{F}_s(P-q)}. \end{aligned} \tag{121}$$

The interaction kernel includes the K pseudoscalar meson channel and the K_5 scalar meson channel,

$$\mathcal{V}_{s,s',s_1,s_2}(q,q',k,k') = -g_K[\alpha_{K+}(P^+)\bar{u}_{s_1}(k)\tau^+ i\gamma^5 v_{s_2}(k')\bar{v}_{s'}(q')\tau^- i\gamma^5 u_s(q) - \alpha_{K-}(P^+)\bar{u}_{s_1}(k)\tau^+ v_{s_2}(k')\bar{v}_{s'}(q')\tau^- u_s(q) + \alpha_{K+}(P^+)\bar{u}_{s_1}(k)\tau^- i\gamma^5 v_{s_2}(k')\bar{v}_{s'}(q')\tau^+ i\gamma^5 u_s(q) - \alpha_{K-}(P^+)\bar{u}_{s_1}(k)\tau^- v_{s_2}(k')\bar{v}_{s'}(q')\tau^+ u_s(q)], \quad (122)$$

where

$$\alpha_{K\pm} = \left\{1 \pm g_K \int \frac{dk^+ d^2k_\perp}{(2\pi)^3}\frac{\epsilon(k^+)}{P^+ - k^+}[\mathcal{F}_u(k)\mathcal{F}_s(P-k) + \mathcal{F}_s(k)\mathcal{F}_u(P-k)]\right\}^{-1}. \quad (123)$$

The interaction kernels for K^+ are

$$\sum_{s,s'}\mathcal{V}_{s,s',s_1,s_2}(q,q',k,k')\Phi_{K_5}(y,q_\perp,s,s') = 2\alpha_{K-}(P^+)\mathrm{Tr}[(\not{q}+M_u)(\not{q}'-M_s)]\phi_{K_5}(y,q_\perp)\bar{u}_{s_1}(k)\lambda_U^\pm v_{s_2}(k') = 4\alpha_{K-}(P^+)\left(\frac{q_\perp^2 + y^2M_s^2 - 2y\bar{y}M_uM_s + \bar{y}^2M_u^2}{y\bar{y}}\right)\phi_{K_5}(y,q_\perp)\bar{u}_{s_1}(k)\lambda_U^+ v_{s_2}(k'), \quad (124)$$

$$\sum_{s,s'}\mathcal{V}_{s,s',s_1,s_2}(q,q',k,k')\Phi_K(y,q_\perp,s,s') = -2\alpha_{K+}(P^+)\mathrm{Tr}[(\not{q}+M_u)(\not{q}'+M_s)]\phi_K(y,q_\perp)\bar{u}_{s_1}(k)i\gamma^5\lambda_U^\pm v_{s_2}(k') = -4\alpha_{K+}(P^+)\left(\frac{q_\perp^2 + y^2M_s^2 + 2y\bar{y}M_uM_s + \bar{y}^2M_u^2}{y\bar{y}}\right)\phi_K(y,q_\perp)\bar{u}_{s_1}(k)i\gamma^5\lambda_U^+ v_{s_2}(k'). \quad (125)$$

The kernel for K^- follows similarly from the exchange $u \leftrightarrow s$ and $\tau^+ \leftrightarrow \tau^-$. Hence, the bound state equations

$$\begin{aligned} m^2_{K_5^+}\phi_{K_5^+}(x,k_\perp) &= \left[\frac{k_\perp^2+M_u^2}{x} + \frac{k_\perp^2+M_s^2}{\bar{x}}\right]\phi_{K_5^+}(x,k_\perp) + \frac{2g_K\alpha_{K-}(P^+)}{\sqrt{x\bar{x}}}\sqrt{\mathcal{F}_u(k)\mathcal{F}_s(P-k)}\int_0^1\frac{dy}{\sqrt{y\bar{y}}}\int\frac{d^2q_\perp}{(2\pi)^3} \\ &\times\left(\frac{q_\perp^2 + y^2M_s^2 - 2y\bar{y}M_uM_s + \bar{y}^2M_u^2}{y\bar{y}}\right)\phi_{K_5^+}(y,q_\perp)\sqrt{\mathcal{F}_u(q)\mathcal{F}_s(P-q)}, \\ m^2_{K^+}\phi_{K^+}(x,k_\perp) &= \left[\frac{k_\perp^2+M_u^2}{x} + \frac{k_\perp^2+M_s^2}{\bar{x}}\right]\phi_{K^+}(x,k_\perp) - \frac{2g_K\alpha_{K+}(P^+)}{\sqrt{x\bar{x}}}\sqrt{\mathcal{F}_u(k)\mathcal{F}_s(P-k)}\int_0^1\frac{dy}{\sqrt{y\bar{y}}}\int\frac{d^2q_\perp}{(2\pi)^3}\phi_{K^+}(y,q_\perp) \\ &\times\left(\frac{q_\perp^2 + y^2M_s^2 + 2y\bar{y}M_uM_s + \bar{y}^2M_u^2}{y\bar{y}}\right)\sqrt{\mathcal{F}_u(q)\mathcal{F}_s(P-q)}. \end{aligned} \quad (126)$$

The bound state equations for K^0 and $\bar{K}^0$ follow by interchanging $u \leftrightarrow d$.

B. Kaon spectrum

The bound state masses are solutions to the gaplike equation

$$1 = \int_0^1 dy\int d^2q_\perp\frac{V_X(y,q_\perp)}{y\bar{y}m_X^2 - (q_\perp^2+M^2)}\mathcal{F}_u(q)\mathcal{F}_s(P-q). \quad (127)$$

The contribution of different quark flavors will change as the momentum fraction changes. When $y \sim 0$, most of the hadronic momentum is taken by the s quark. The dynamics of the constituent quark mass will be dominated by the u quark in that region. The mass difference between the two constituents slightly shifts the center of the longitudinal momentum distribution to the lighter constituent, which tends to carry more momentum fraction. The potential for K and K_5 will be

$$V_X = \begin{cases} +\frac{2g_K}{(2\pi)^3}\alpha_{K-}(P^+)\left(\frac{q_\perp^2+y^2M_s^2-2y\bar{y}M_uM_s+\bar{y}^2M_u^2}{y\bar{y}}\right), & \text{scalars } K_5, \\ -\frac{2g_K}{(2\pi)^3}\alpha_{K+}(P^+)\left(\frac{q_\perp^2+y^2M_s^2+2y\bar{y}M_uM_s+\bar{y}^2M_u^2}{y\bar{y}}\right), & \text{pseudo scalars } K. \end{cases} \tag{128}$$

To solve the gap equation (127) for the kaon spectra, we proceed as in the pion case. More specifically, we split the k^+ integral in $\alpha_{K\pm}(P^+)$ to isolate the part carrying the longitudinal momentum fraction x in the bound state with P^+, from the part which is UV dominated by the one-body integral in the gap equation

$$\begin{aligned} \alpha_{K\pm}(P^+)^{-1} &= 1 \pm g_K \int \frac{dk^+d^2k_\perp}{(2\pi)^3}\frac{\epsilon(k^+)}{P^+-k^+}[\mathcal{F}_u(k)\mathcal{F}_s(P-k)+\mathcal{F}_s(k)\mathcal{F}_u(P-k)] \\ &= 1 \pm \frac{g_K}{(2\pi)^3}\int d^2k_\perp\left[\int_0^1 dx\frac{2}{x}-\int_0^\infty dx\frac{1}{x}+\int_{-\infty}^0 dx\frac{1}{x}\right][\mathcal{F}_u(k)\mathcal{F}_s(P-k)+\mathcal{F}_s(k)\mathcal{F}_u(P-k)] \\ &= \begin{cases} \frac{1}{2}\left(\frac{m_s}{M_u}+\frac{m_u}{M_s}\right)-\frac{(M_u-M_s)^2}{2MM_s}+\frac{2g_K}{(2\pi)^3}\int d^2k_\perp\int_0^1 dx\frac{2}{x}[\mathcal{F}_u(k)\mathcal{F}_s(P-k)+\mathcal{F}_s(k)\mathcal{F}_u(P-k)] \\ 2-\frac{1}{2}\left(\frac{m_s}{M_u}+\frac{m_u}{M_s}\right)+\frac{(M_u-M_s)^2}{2MM_s}-\frac{2g_K}{(2\pi)^3}\int d^2k_\perp\int_0^1 dx\frac{2}{x}[\mathcal{F}_u(k)\mathcal{F}_s(P-k)+\mathcal{F}_s(k)\mathcal{F}_u(P-k)]. \end{cases} \end{aligned} \tag{129}$$

In the last split identity, we made use of the solution of the gap equation in (111), namely

$$1-g_K\int_u\frac{dk^+d^2k_\perp}{(2\pi)^3}\frac{\epsilon(k^+)}{k^+}\mathcal{F}_u^2(k)-g_K\int_s\frac{dk^+d^2k_\perp}{(2\pi)^3}\frac{\epsilon(k^+)}{k^+}\mathcal{F}_s^2(k)=\frac{1}{2}\left(\frac{m_s}{M_u}+\frac{m_u}{M_s}\right)-\frac{(M_u-M_s)^2}{2MM_s}. \tag{130}$$

Now we insert (129) for $\alpha_{K\pm}(P^+)$ back into (127) and obtain the mass eigenvalue equation for the kaons

$$\begin{aligned} 0 &= 2-\frac{1}{2}\left(\frac{m_s}{M_u}+\frac{m_u}{M_s}\right)+\frac{(M_u-M_s)^2}{2MM_s} \\ &\quad -\frac{2g_K}{(2\pi)^3}\int_0^1 dy\int d^2q_\perp\left[\frac{2}{y}-\frac{1}{y\bar{y}}+\frac{m_{K_5}^2-(M_u-M_s)^2}{y\bar{y}m_{K_5}^2-(q_\perp^2+yM_s^2+\bar{y}M_u^2)}\right][\mathcal{F}_u(q)\mathcal{F}_s(P-q)+\mathcal{F}_s(q)\mathcal{F}_u(P-q)] \\ &= \frac{(M_u+M_s)^2-M_sm_s-M_um_u}{2M_uM_s} \\ &\quad -\frac{2g_K}{(2\pi)^3}\int_0^1 dy\int d^2q_\perp\left[\frac{m_{K_5}^2-(M_s+M_u)^2}{y\bar{y}m_{K_5}^2-(q_\perp^2+yM_s^2+\bar{y}M_u^2)}\right][\mathcal{F}_u(q)\mathcal{F}_s(P-q)+\mathcal{F}_s(q)\mathcal{F}_u(P-q)] \end{aligned} \tag{131}$$

and

$$\begin{aligned} 0 &= \frac{1}{2}\left(\frac{m_s}{M_u}+\frac{m_u}{M_s}\right)-\frac{(M_u+M_s)^2}{2MM_s} \\ &\quad +\frac{2g_K}{(2\pi)^3}\int dy\int d^2q_\perp\left[\frac{2}{y}-\frac{1}{y\bar{y}}+\frac{m_K^2-(M_s-M_u)^2}{y\bar{y}m_K^2-(q_\perp^2+yM_s^2+\bar{y}M_u^2)}\right][\mathcal{F}_u(q)\mathcal{F}_s(P-q)+\mathcal{F}_s(q)\mathcal{F}_u(P-q)] \\ &= \frac{1}{2}\left(\frac{m_s}{M_u}+\frac{m_u}{M_s}\right)-\frac{(M_u-M_s)^2}{2M_uM_s} \\ &\quad +\frac{2g_K}{(2\pi)^3}\int_0^1 dy\int d^2q_\perp\left[\frac{m_K^2-(M_u-M_s)^2}{y\bar{y}m_K^2-(q_\perp^2+yM_s^2+\bar{y}M_u^2)}\right][\mathcal{F}_u(q)\mathcal{F}_s(P-q)+\mathcal{F}_s(q)\mathcal{F}_u(P-q)]. \end{aligned} \tag{132}$$

The boost-invariant cutoff guarantees the cancellation between the integral $\int_0^1 dy\frac{2}{y}$ and $\int_0^1 dy\frac{1}{y\bar{y}}$. The integral

$$\int_0^1 dx\int d^2k_\perp\frac{1}{x}[\mathcal{F}_u^2(k)+\mathcal{F}_s^2(k)-\mathcal{F}_u(k)\mathcal{F}_s(P-k)-\mathcal{F}_s(k)\mathcal{F}_u(P-k))] \tag{133}$$

in the last line will be dropped, since the difference between these two integrals only depends on the boost-invariant UV cutoff. Indeed, as the cutoff scale $1/\rho$ increases, (133) becomes vanishingly small.

In leading order of the chiral expansion around the small quark mass, we recover to the GOR mass relation as a solution

$$m_K^2 = \frac{m_u + m_s}{f_K^2} |\langle \bar{u}u \rangle + \langle \bar{s}s \rangle| + \mathcal{O}(m_u^2, m_s^2, m_u m_s) \quad (134)$$

with the quark condensate

$$|\langle \bar{u}u \rangle + \langle \bar{s}s \rangle| = \frac{N_c}{2g_K}(M_u + M_s - m_u - m_s)$$

following from the gap equation. The kaon weak decay constant f_K in leading order of the chiral expansion is described by the quark form factor

$$f_K = \frac{\sqrt{N_c}M}{\sqrt{2}\pi}\left[\int_0^1 dy \int_0^\infty dq_\perp^2 \left(\frac{1}{q_\perp^2 + yM_s^2 + \bar{y}M_u^2}\right)[\mathcal{F}_u(k)\mathcal{F}_s(P-k) + \mathcal{F}_s(k)\mathcal{F}_u(P-k)]\right]^{1/2}, \quad (135)$$

where $M = (M_u + M_s)/2$.

In the zero instanton size limit, we can use the transverse cutoff described in Appendix E to analyze the kaon spectra and their dependence on the UV cutoff explicitly. For instance, the eigenvalue equation for the scalar counterpart of the kaon or K_5 is

$$\frac{(M_u + M_s)^2 - M_s m_s - M_u m_u}{2M_u M_s} = \frac{g_K}{4\pi^2}\int_0^1 dy \int_0^{\Lambda^2} dq_\perp^2 \left[\frac{m_{K_5}^2 - (M_s + M_u)^2}{y\bar{y}m_{K_5}^2 - (q_\perp^2 + yM_s^2 + \bar{y}M_u^2)}\right]. \quad (136)$$

The mass of K_5 is above the cutoff scale, $m_{K_5} > \Lambda$, and clearly unbound. In contrast, the pseudoscalar kaons bind. Indeed, the mass eigenvalue m_K is a solution to

$$\begin{aligned}\frac{1}{2}\left(\frac{m_s}{M_u} + \frac{m_u}{M_s}\right) &= \frac{(M_u - M_s)^2}{2M_u M_s} - \frac{g_K}{4\pi^2}\int_0^1 dy \int_0^{\Lambda^2} dq_\perp^2 \left[\frac{m_K^2 - (M_u - M_s)^2}{y\bar{y}m_K^2 - (q_\perp^2 + yM_s^2 + \bar{y}M_u^2)}\right] \\ &= \frac{(M_u - M_s)^2}{2M_u M_s} + \frac{g_K}{4\pi^2}[m_K^2 - (M_u - M_s)^2]\int_0^1 dy \ln\left(1 + \frac{\Lambda^2}{yM_s^2 + \bar{y}M_u^2 - y\bar{y}m_K^2}\right) \end{aligned} \quad (137)$$

with the condition that $(M_s - M_u)^2 \le m_K^2 \le (M_u + M_s)^2$. The last integration can be carried out explicitly, with the final result for the zero instanton size

$$\begin{aligned}\frac{1}{2}\left(\frac{m_s}{M_u} + \frac{m_u}{M_s}\right) = \frac{(M_u - M_s)^2}{2M_u M_s} + \frac{g_K}{4\pi^2}[m_K^2 - (M_u - M_s)^2]\Bigg[&\left(\frac{1}{2} + \frac{M_s^2 - M_u^2}{2m_K^2}\right)\ln\left(1 + \frac{\Lambda^2}{M_s^2}\right) + \left(\frac{1}{2} - \frac{M_s^2 - M_u^2}{2m_K^2}\right)\ln\left(1 + \frac{\Lambda^2}{M_u^2}\right) \\ &- \sqrt{\frac{2(M_s^2 + M_u^2) - m_K^2}{m_K^2} - \frac{(M_s^2 - M_u^2)^2}{m_K^4}}\left(\tan^{-1}\frac{1 + \frac{M_s^2 - M_u^2}{m_K^2}}{\sqrt{\frac{2(M_s^2 + M_u^2) - m_K^2}{m_K^2} - \frac{(M_s^2 - M_u^2)^2}{m_K^4}}} + \tan^{-1}\frac{1 - \frac{M_s^2 - M_u^2}{m_K^2}}{\sqrt{\frac{2(M_s^2 + M_u^2) - m_K^2}{m_K^2} - \frac{(M_s^2 - M_u^2)^2}{m_K^4}}}\right) \\ &+ \sqrt{\frac{4\Lambda^2 + 2(M_s^2 + M_u^2) - m_K^2}{m_K^2} - \frac{(M_s^2 - M_u^2)^2}{m_K^4}} \\ &\times\left(\tan^{-1}\frac{1 + \frac{M_s^2 - M_u^2}{m_K^2}}{\sqrt{\frac{4\Lambda^2 + 2(M_s^2 + M_u^2) - m_K^2}{m_K^2} - \frac{(M_s^2 - M_u^2)^2}{m_K^4}}} + \tan^{-1}\frac{1 - \frac{M_s^2 - M_u^2}{m_K^2}}{\sqrt{\frac{4\Lambda^2 + 2(M_s^2 + M_u^2) - m_K^2}{m_K^2} - \frac{(M_s^2 - M_u^2)^2}{m_K^4}}}\right)\Bigg]. \end{aligned} \quad (138)$$

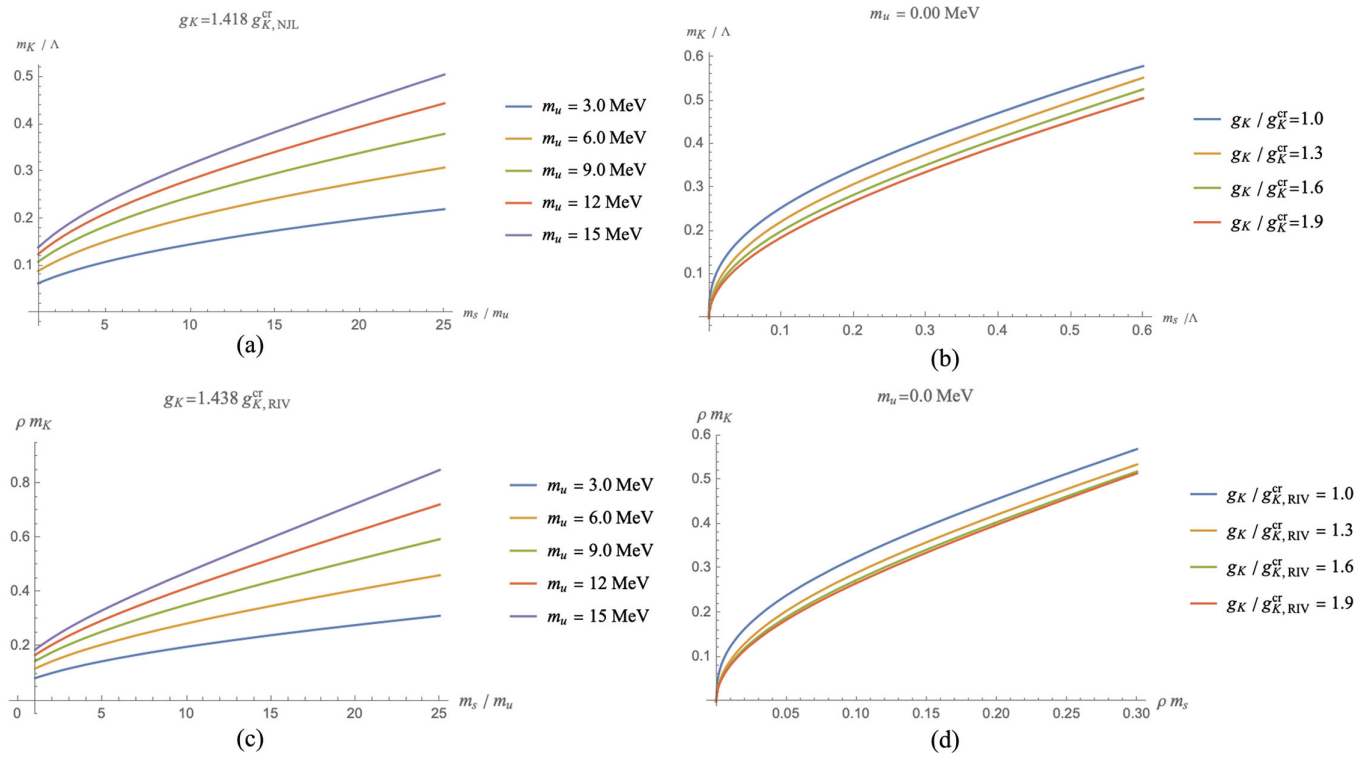

FIG. 10. (a) The change in the kaon mass versus m_s/m_u, for different m_u and fixed $g_K/g_K^{cr} = 1.418$ in the zero instanton size. (b) Same as in (a) for fixed $m_u = 0$ MeV and different g_K/g_K^{cr} in the zero instanton size. (c),(d) Same as in (a),(b) in the ILM with a finite instanton size.

In the second line of (137), the finiteness of the $q_\perp$ integration requires the inequality $y\bar{y}m_K^2 < yM_u^2 + \bar{y}M_s^2$ to hold. This inequality restricts the range of the y integration. To ensure the y integration can run over 0 to 1 smoothly, the kaon mass is constrained as noted.

We show in Fig. 10 the dependence of m_K on the current quark masses m_u, m_s, as well as the multifermion coupling g_K. Although the current quark mass of the strange quark s is substantially larger than that of the u, d quarks, the difference between the two constituent masses M_u and M_s remains small. If we expand Eq. (137) in terms of the current mass difference $\Delta M/M$, where $\Delta M = (M_s - M_u)/2$, the squared kaon mass m_K^2 depends linearly on the quark current masses m_u and m_s at leading order, leading to the expected GOR relation

$$m_K^2 = \frac{m_u + m_s}{f_K^2}|\langle\bar{u}u\rangle + \langle\bar{s}s\rangle| + \mathcal{O}(\Delta M^4), \tag{139}$$

where $M = (M_u + M_s)/2$, $\Delta M = (M_s - M_u)/2$, and

$$|\langle\bar{u}u\rangle + \langle\bar{s}s\rangle| = \frac{N_c}{2g_K}(2M - m_u - m_s). \tag{140}$$

With the first-order correction of the constituent mass difference around the chiral limit, the Kaon decay constant is

$$f_K = \frac{\sqrt{N_c}M}{\sqrt{2}\pi}\ln\left(1 + \frac{\Lambda^2}{M^2}\right)\left[1 - \frac{\Delta M^2}{M^2}\frac{1 + 3\Lambda^2/M^2}{6(1 + \Lambda^2/M^2)^2\ln\left(1 + \frac{\Lambda^2}{M^2}\right)} + \mathcal{O}(\Delta M^4/M^4)\right]. \tag{141}$$

In the zero size approximation, the ILM is NJL-like. We can fix its parameters by fixing the kaon mass, kaon decay constant, and the ratio between the s and u current mass $m_s/m_u = 22.7$. As a result, the transverse cutoff is fixed to $\Lambda = 720.1$ MeV, slightly higher than $\rho = 0.313$ fm in the ILM. The current quark masses are then $m_u = 12.7$ MeV and $m_s = 287.2$ MeV, and the fermionic coupling is fixed to $g_K = 1.418 g^{cr}_{K,\mathrm{NJL}}$. The constituent masses are found to be $M_u = 155.8$ MeV and $M_s = 466.1$ MeV. The quark condensate will thus be $|\langle\bar{u}u\rangle|^{1/3} = 170.7$ MeV and

$|\langle\bar{s}s\rangle|^{1/3}=158.4\,\mathrm{MeV}$. Conversely, by fixing $\Lambda, g_K, m_u/m_s$, the kaon mass and the kaon decay constant are $m_K^{\mathrm{NJL}} = 435$ MeV and $f_K^{\mathrm{NJL}} = 155$ MeV, respectively.

In Fig. 10(a) we show the behavior of the kaon mass m_K/λ versus the ratio of strange to nonstrange current masses m_s/m_u for fixed coupling $g_K/g^{cr}_{K,\mathrm{NJL}}$ and for increasing light quark mass m_u (bottom to top). In Fig. 10(a) we show the same ratio for now fixed $m_u = 0$ but increasing fermionic coupling g_K (top to bottom). Figures 10(a) and 10(b) are for zero size instantons but a fixed cutoff Λ. In Figs. 10(c) and 10(d) we show the same ratios for the ILM with fixed instanton size ρ.

In the ILM, the boost-invariant cutoff for the kaon channels is

$$\sqrt{\mathcal{F}_u(k)\mathcal{F}_s(P-k)} \to \mathcal{F}\left(\frac{2P^+P^-}{\lambda_K^2}\right) = [(zF'(z))^2]\Big|_{z=\frac{\rho}{2\lambda_K}\sqrt{\frac{k_\perp^2+M_u^2}{x}+\frac{k_\perp^2+M_s^2}{\bar{x}}}} \tag{142}$$

with λ_K a parameter of order 1. The mass eigenvalue for K_5 is fixed by

$$\frac{(M_u+M_s)^2 - M_s m_s - M_u m_u}{2M_u M_s} = \frac{g_K}{2\pi^2}\left[(M_u+M_s)^2 - m_K^2\right]\int_0^1 dy \int_{\frac{\rho\sqrt{\bar{y}M_u^2+yM_s^2}}{2\lambda_K\sqrt{y\bar{y}}}}^{\infty} dz \frac{z}{z^2-\frac{\rho^2 m_K^2}{4}}(zF'(z))^4. \tag{143}$$

Regardless of the chiral limit, the scalar kaon state K_5 cannot be formed, due to a repulsive (positive) potential in this channel. The mass eigenvalue for the pseudoscalar kaon is

$$\frac{1}{2}\left(\frac{m_s}{M_u}+\frac{m_u}{M_s}\right) = \frac{(M_u-M_s)^2}{2M_u M_s} + \frac{g_K}{2\pi^2}\left[m_K^2 - (M_u-M_s)^2\right]\int_0^1 dy \int_{\frac{\rho\sqrt{\bar{y}M_u^2+yM_s^2}}{2\lambda_K\sqrt{y\bar{y}}}}^{\infty} dz \frac{z}{z^2-\frac{\rho^2 m_K^2}{4}}(zF'(z))^4. \tag{144}$$

The solution to (144) satisfies the GOR relation in (77). The kaon weak decay constant f_K is fixed by (135) in the chiral limit,

$$f_K \simeq \frac{\sqrt{N_c}}{\pi}\frac{M_u+M_s}{2}\left[\int_0^1 dx \int_{\frac{\rho\sqrt{\bar{x}M_u^2+xM_s^2}}{2\lambda_K\sqrt{x\bar{x}}}}^{\infty} dz z^3 (F'(z))^4\right]^{1/2} \tag{145}$$

With the empirical inputs $f_K = 156.4$ MeV, $m_K = 445.0$ MeV, and $\rho = 630\ \mathrm{MeV}^{-1}$, we fix the ILM parameters in the kaon sector. λ_K is fixed to be 3.970 in the chiral limit. The light current quark mass is $m_u = 12.3$ MeV and $m_s = 296.9$ MeV. The fermionic coupling is $g_K = 1.542 g^{cr}_{K,\mathrm{RIV}}$. The constituent mass with fixed current masses m_u, m_s and fixed coupling is $M_u = 366.1$ MeV and $M_s = 605.8$ MeV. The quark condensate for u and s quarks are $|\langle\bar{u}u\rangle|^{1/3} = 257.2$ MeV and $|\langle\bar{s}s\rangle|^{1/3} = 283.5$ MeV.

C. Kaon DAs and PDFs

The positive kaon LFWFs are generically of the form

$$\phi_{K^+}(x,k_\perp) = \frac{1}{\sqrt{2x\bar{x}}}\frac{C_K}{m_K^2 - \frac{k_\perp^2+xM_s^2+\bar{x}M_u^2}{x\bar{x}}}\sqrt{\mathcal{F}_u(k)\mathcal{F}_s(P-k)}, \tag{146}$$

where C_K is the normalization constant determined by (53). They enter in the definition of the kaon PDFs in the leading twist-2 approximation, as defined by

$$q_K(x) = \int \frac{d\xi^-}{4\pi} e^{-ixP^+\xi^-} \langle K(P)|\bar{\psi}(\xi^-)\gamma^+ W(\xi^-,0)\psi(0)|K(P)\rangle$$
$$= \int \frac{d^2k_\perp}{(2\pi)^3} \sum_{s_1,s_2} |\Phi_K(x,k_\perp,s_1,s_2)|^2, \tag{147}$$

where the gauge link $W(\xi^-,0) = \exp\left[-ig\int_0^{\xi^-} d\eta^- A^+(\eta^-)\right]$ is to 1. In the case of meson PDFs, quark and antiquark distributions are related by the charge symmetry

$$\bar{q}_X(x) = q_{\bar{X}}(x) = q_X(1-x) = \bar{q}_{\bar{X}}(1-x).$$

For charged positive kaons, the u quark PDF is

$$u_{K^+}(x) = \frac{1}{4\pi^2}\int_0^\infty dk_\perp^2 \frac{1}{x\bar{x}} \left| \frac{C_K}{m_K^2 - \frac{k_\perp^2 + xM_s^2 + \bar{x}M_u^2}{x\bar{x}}} \right|^2 \frac{k_\perp^2 + x^2M_s^2 + 2x\bar{x}M_sM_u + \bar{x}^2M_u^2}{x\bar{x}} \mathcal{F}_u(k)\mathcal{F}_s(P-k)$$
$$= \frac{C_K^2}{4\pi^2}\int_0^\infty dk_\perp^2 \frac{k_\perp^2 + x^2M_s^2 + 2x\bar{x}M_sM_u + \bar{x}^2M_u^2}{[x\bar{x}m_K^2 - (k_\perp^2 + xM_s^2 + \bar{x}M_u^2)]^2} \mathcal{F}_u(k)\mathcal{F}_s(P-k). \tag{148}$$

In the ILM, the result is

$$u_{K^+}(x) = \frac{C_K^2}{2\pi^2}\int_{\frac{\rho\sqrt{\bar{x}M_u^2 + xM_s^2}}{2\lambda_K\sqrt{x\bar{x}}}}^\infty dz \frac{z^2 - \frac{\rho^2}{4\lambda_K^2}(M_s - M_u)^2}{\left(\frac{\rho^2 m_K^2}{4\lambda_K^2} - z^2\right)^2} z^5 (F'(z))^4. \tag{149}$$

Note that charge symmetry implies

$$u_{K^+}(x) = \bar{u}_{K^-}(x) = \bar{s}_{K^+}(1-x) = s_{K^-}(1-x).$$

Due to the unequal masses of the u and s quarks, the heavier s quark will carry more momentum fraction inside the kaon. Thus, the positive kaon PDF $u_{K^+}(x)$ will tilt to a small x region.

For comparison, (149) for zero size instantons, and using the transverse cutoff detailed in Appendix F, reduces to

$$u_{K^+}(x) = \frac{C_K^2}{4\pi^2}\theta(x\bar{x})\left[\frac{(m_K^2 - (M_s - M_u)^2)x\bar{x}\Lambda^2}{(xM_s^2 + \bar{x}M_u^2 - x\bar{x}m_K^2)(xM_s^2 + \bar{x}M_u^2 + \Lambda^2 - x\bar{x}m_K^2)} + \ln\left(1 + \frac{\Lambda^2}{xM_s^2 + \bar{x}M_u^2 - x\bar{x}m_K^2}\right)\right]. \tag{150}$$

The normalization constant C_K is related to the effective kaon-quark coupling. In leading order in an expansion using $\Delta M/M$ expansion, we have

$$C_K = -\frac{\sqrt{2N_c}M}{f_K}\left(1 - \frac{m_K^2\Lambda^2}{M^4\left(1+\frac{\Lambda^2}{M^2}\right)\ln\left(1+\frac{\Lambda^2}{M^2}\right)} + \mathcal{O}(\Delta M^2/M^2, m_K^2/M^2)\right). \tag{151}$$

In the chiral limit, C_K satisfies the Goldberger-Treiman relation.

D. Kaon PDF evolution

As we noted earlier for the pion, the PDFs in the ILM are defined at a low renormalization scale μ_0, below the instanton size resolution $1/\rho \sim 631$ MeV. To compare our result with the experiments in [38,65,66], we evolve the PDFs in (99) and (103) starting from $\mu_0 = 313$ MeV. The evolution will be carried to 2 GeV to compare with the available lattice data [67] as well. Since our analysis reduced the PDFs to their valence quark content, only quark splitting will be considered in the DGLAP evolution. A more realistic evolution, starting from this low renormalization, may require the iteration of the instanton interaction as recently suggested in [16]. This point will be considered elsewhere.

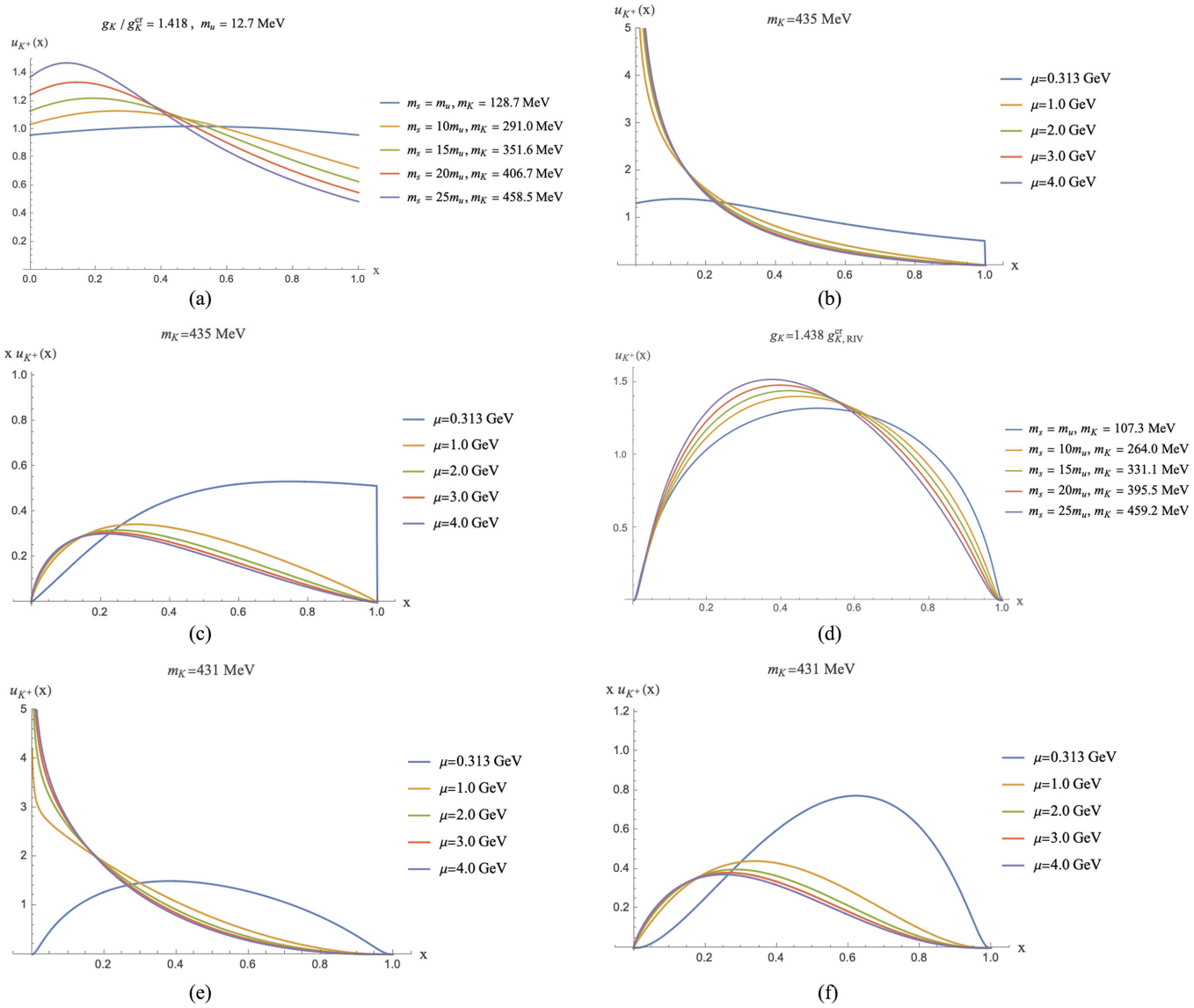

FIG. 11. (a) The kaon charged PDF versus x in the zero instanton size limit for fixed coupling and m_u but varying m_s/m_u. (b) DGLAP evolution from $\mu_0 = 0.313$ GeV to $\mu = 4$ GeV, of the kaon charged PDF versus x in the zero instanton size limit for fixed kaon mass $m_K = 435$ MeV. (c) Same as (b) for the charged kaon momentum distribution. (d)–(f) Same as (a)–(c) for the charged kaon in the ILM with a finite instanton size $\rho = 0.313$ fm.

In Fig. 11(a) we show the kaon PDF at a low renormalization point $\mu_0 = 0.313$ GeV. The displayed results are for fixed fermion coupling g_K and light u quark mass $m_u = 12.7$ MeV, with increasing strange quark mass (bottom to top starting from the left). In Figs. 11(b) and 11(c) we show the DGLAP evolution of the result with $m_K = 435$ MeV from $\mu = \mu_0 = 0.313$ GeV to $\mu = 4$ GeV (bottom to top starting from the left). All Figs. 11(a)–11(c) are carried with zero size instantons but a finite cutoff Λ. The analogous results for the ILM with a finite size instanton $\rho = 0.313$ fm are shown in Figs. 11(d)–11(f). With increasing strange quark mass, the PDF is skewed in favor of $\bar{s}$.

In Fig. 12(a) we show our results for the ratio of the u quark PDF in K^+ to that in π^+ versus parton-x, in comparison to experimental data and lattice measurements. The experimental data are from CERN-NA3 [68] (red dots) which measure the muon pair production within the invariant mass cut between 4.1 and 8.5 GeV to eliminate the meson production on resonance. The lattice measurements are those reported by the MSULAT [69] (purple band) using LaMET at $\mu = 5.2$ GeV. Our DGLAP evolved result from $\mu = \mu_0 = 0.313$ GeV to $\mu = 5.2$ GeV corresponds to the zero instanton size limit (solid blue curve), the ILM with finite instanton size (solid orange curve), and the LaMET in the ILM [54,55] (solid green curve). For additional comparison, we show the results from the Dyson-Schwinger equation with full Bethe-Salpeter wave function from [70] (black dashed curve).

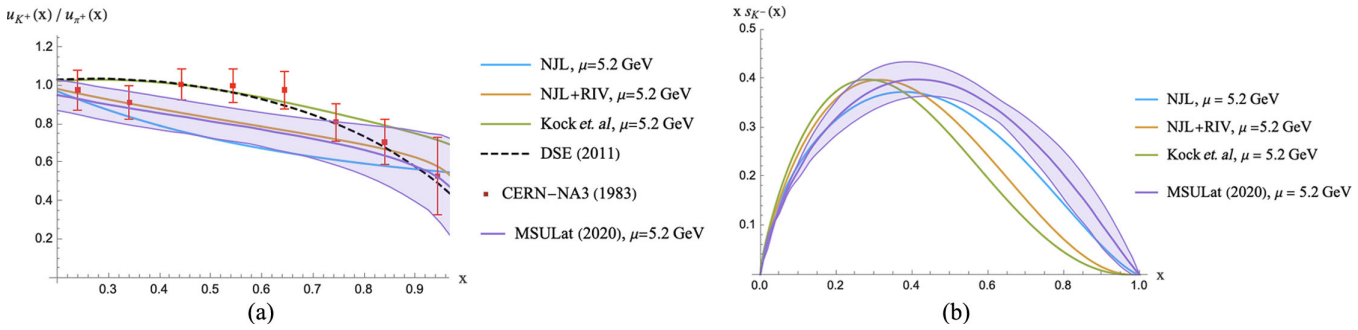

FIG. 12. (a) The ratio of positive charge kaon to pion PDF versus parton x, in the zero instanton size limit, with $m_K = 435$ MeV and evolved to $\mu = 5.2$ GeV (solid blue curve), in the ILM with finite instanton size $\rho = 0.318$ fm with $m_K = 431$ MeV and evolved to $\mu = 5.2$ GeV (solid orange curve). The comparison is to the results of the ILM using the LaMET extraction in [54,55] and evolved to $\mu = 5.2$ GeV (solid green curve) and the results from the Dyson-Schwinger equation with full Bethe-Salpeter wave function [70] (dashed black curve). The data for the measured ratio (red) are from [68] using muon pair production and using the invariant mass cuts between 4.1 and 8.5 GeV to eliminate the meson production on resonance. The recent lattice data MSULAT (purple band) are from [69] using the LaMET construction at $\mu = 5.2$ GeV. (b) The same as in (a) but for the strange quark momentum distribution for the negative kaon $xs_{K^-}(x)$ versus x.

E. ERBL evolution of kaon DA

The kaon DAs are also tied to the kaon LFWFs,

$$\begin{aligned}\phi_K(x) &= -i\int\frac{d\xi^-}{2\pi}e^{ixP^+\xi^-}\langle 0|\bar\psi(0)\gamma^+\gamma^5\frac{\tau^a}{\sqrt{2}}W(0,\xi^-)\psi(\xi^-)|K^a(P)\rangle \\ &= \frac{\sqrt{N_c}}{\sqrt{2}\pi^2}\int dk_\perp^2\frac{\phi_K(x,k_\perp)}{\sqrt{2x\bar x}}[xM_s\mathcal{F}_s(P-k)+\bar xM_u\mathcal{F}_u(k)]\end{aligned} \tag{152}$$

with the standard normalization

$$\langle 0|\bar\psi\gamma^+\gamma^5\frac{\tau^a}{\sqrt{2}}\psi|K^a(P)\rangle = if_KP^+. \tag{153}$$

In the ILM, the kaon DA is

$$\phi_K(x) = \frac{\sqrt{N_c}(xM_s+\bar xM_u)}{2\sqrt{2}\pi^2}\int_0^\infty dk_\perp^2\frac{C_K}{x\bar xm_K^2-(k_\perp^2+xM_s^2+\bar xM_u^2)}\mathcal{F}_u(k)\mathcal{F}_s(P-k). \tag{154}$$

From the normalization condition of the kaon DA, we can extract the kaon mass dependence of the kaon weak decay constant,

$$\begin{aligned}\frac{f_K(m_K)}{f_K} = &\left[\frac{\int_0^1dx\int_0^\infty dk_\perp^2\left(\frac{1}{k_\perp^2+\bar xM_u^2+xM_s^2-x\bar xm_K^2}\right)\mathcal{F}_u(k)\mathcal{F}_s(P-k)}{\left(\int_0^1dx\int_0^\infty dk_\perp^2\frac{(k_\perp^2+\bar xM_u^2+xM_s^2)}{(k_\perp^2+\bar xM_u^2+xM_s^2-x\bar xm_K^2)^2}\mathcal{F}_u(k)\mathcal{F}_s(P-k)\right)^{1/2}}\right] \\ &\times\left[\int_0^1dx\int_0^\infty dk_\perp^2\left(\frac{1}{k_\perp^2+\bar xM_u^2+xM_s^2}\right)\mathcal{F}_u(k)\mathcal{F}_s(P-k)\right]^{-\frac{1}{2}}\end{aligned} \tag{155}$$

with $f_K = f_\pi$ given in (75). In the ILM, the kaon DA is

$$\phi_{K^+}(x) = \frac{\sqrt{N_c}(xM_s+\bar xM_u)}{\sqrt{2}\pi^2}C_K\int_{\rho\frac{\sqrt{\bar xM_u^2+xM_s^2}}{2\lambda_K\sqrt{x\bar x}}}^\infty dz\frac{z^5}{\frac{\rho^2m_K^2}{4\lambda_K^2}-z^2}(F'(z))^4. \tag{156}$$

Its evolution, starting from $\mu_0 = 313$ MeV, will also follow from (C2) in the ERBL regime.

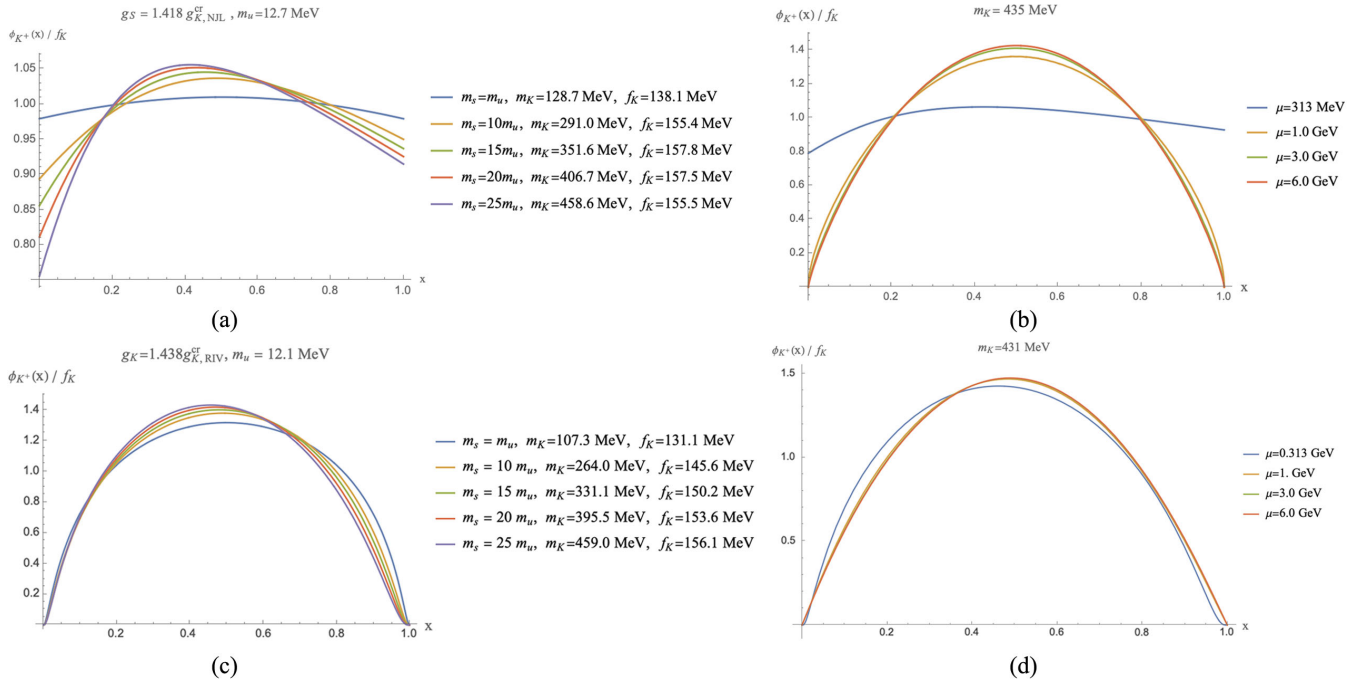

FIG. 13. (a) The positive charged kaon DA versus parton-x for fixed coupling $g_S/g_K^{cr} = 1.418$ and fixed $m_u = 12.7$ MeV but with different ratios m_s/m_u in the zero instanton size limit. (b) The positive charged kaon DA versus parton-x for fixed $m_K = 435$ MeV using the ERBL evolution from the initial $\mu = 0.313$ GeV to $\mu = 6$ GeV. (c),(d) Same as (a),(b) but in the ILM for a fixed instanton size $\rho = 0.313$ fm.

For completeness, we note that in the zero instanton size limit, the form factor will reduce to the transverse cutoff discussed in Appendix F, with the result for the kaon DA as

$$\begin{aligned}\phi_{K^+}(x) &= \frac{\sqrt{N_c}(xM_s + \bar{x}M_u)}{2\sqrt{2}\pi^2}\theta(x\bar{x})\int_0^{\Lambda^2} dk_\perp^2 \frac{C_K}{x\bar{x}m_K^2 - (k_\perp^2 + xM_s^2 + \bar{x}M_u^2)} \\ &= -\frac{\sqrt{N_c}(xM_s + \bar{x}M_u)C_K}{2\sqrt{2}\pi^2}\theta(x\bar{x})\ln\left(1 + \frac{\Lambda^2}{xM_s^2 + \bar{x}M_u^2 - x\bar{x}m_K^2}\right)\end{aligned} \tag{157}$$

with $\phi_{K^-}(x) = \phi_{K^+}(1-x)$. The kaon decay constant f_K simplifies to

$$f_K = C_K\frac{\sqrt{N_c}M}{2\sqrt{2}\pi^2}\int_0^1 dx \frac{xM_s + \bar{x}M_u}{M}\ln\left(1 + \frac{\Lambda^2}{xM_s^2 + \bar{x}M_u^2 - x\bar{x}m_K^2}\right). \tag{158}$$

In Fig. 13(a) we show the kaon DA at the low renormalization point $\mu_0 = 0.313$ MeV with increasing quark mass (top to bottom from the left). The results are for instantons of zero size, a fixed cutoff Λ, a fixed fermion coupling g_S, and a light quark mass $m_u = 12.7$ MeV. In Fig. 13(b) the same results for $m_K = 435$ MeV are evolved from $\mu = \mu_0 = 0.313$ GeV to $\mu = 6$ GeV (top to bottom from the left). Figures 13(c) and 13(d) are the results for the ILM with a finite instanton size, with a slight difference in the input parameters.

In Fig. 14 our results for the kaon DA are compared to the recent lattice results MSULAT [60] using LaMET (purple band). Our results are for instantons of zero size evolved to $\mu = 2$ GeV (blue solid curve), the ILM with finite size instantons (orange solid curve), and the ILM using the LaMET construction [54,55] (solid green curve). For further comparison, we show the asymptotic QCD result of $6x\bar{x}$ [56] (dashed red curve) and the results from the Dyson-Schwinger equation with Bethe-Salpeter wave functions [59] (dashed black curve).

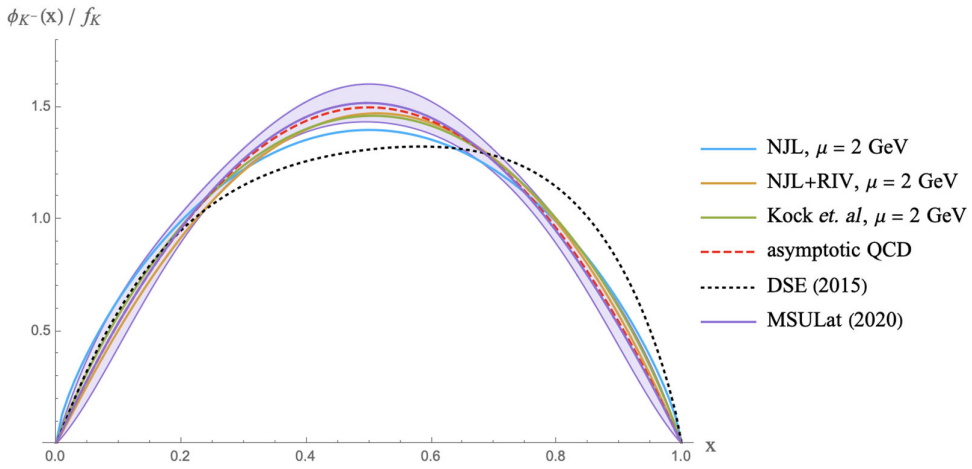

FIG. 14. Evolution of the negative kaon DA in (157) with $m_K = 435$ MeV from $\mu = 0.313$ GeV to $\mu = 2$ GeV in the zero instanton size limit (solid blue curve) and in the ILM with a finite instanton size in (156) with $m_K = 431$ MeV (solid orange curve). The results are compared to those obtained also from the ILM (solid green curve) using the LaMET construction in [54,55], also evolved to $\mu = 2$ GeV. The results using the Dyson-Schwinger equation with Bethe-Salpeter wave functions (dashed black curve) are from [59]. The QCD asymptotic result of $6x\bar{x}$ (dashed red curve) is from [56]. The recent lattice data MSULAT (purple band) are from [60] using the LaMET construction.

X. CONCLUSIONS

We presented a comprehensive analysis of the spontaneous breaking of chiral symmetry on the light front in the context of the ILM with induced nonlocal multifermion interactions. The new element in the light front analysis is the splitting of the effective fermion fields into good plus bad components, with the latter nonpropagating in the light front direction. It is a constraint that, once eliminated, generates additional multifermion interactions between solely the good fermionic components in the emergent multiflavor and nonlocal 't Hooft interaction. This construction generalizes the original arguments presented in [39–41] using local NJL interactions. The nonlocality is important in the characterization of the partonic distributions.

In the mean-field approximation (leading contribution in $1/N_c$), the spontaneous breaking of chiral symmetry parallels that in the rest frame. A running constituent mass and chiral condensates are generated, that are identical to the ones derived in the rest frame, thanks to boost invariance. More importantly, we have shown that the pion and kaon DAs and PDFs derived on the light front in the mean-field approximation are all in agreement with those established in the ILM using the LaMET construction.

The results we presented for the pion and kaon partonic distributions are all evaluated at a low factorization scale $\mu_0 < 1/\rho \sim 630$ MeV. A comparison with experimental data and lattice results at larger scales requires evolution. For simplicity, we assumed that factorization holds at this relatively low scale and used perturbative QCD evolution. Good agreements with the existing data for the pion and kaon were found.

The present analysis of the pion and kaon parton distributions relies on the mean-field approximation in the ILM. It is the leading contribution in a $1/N_c$ bookkeeping analysis, that can be improved *a priori*. Clearly, the present analysis can be extended to study the formation of light diquarks on the light front, as well the nucleon and delta baryons.

A major goal of the upcoming physics at the electron ion collider (EIC) is to understand the partonic composition of nucleons and nuclei as they enter in their composition of mass and spin. The present analysis shows that for pions and kaons, most of their composition follows from the QCD vacuum. At low resolution, it is mostly due to the emerging multifermion 't Hooft interactions induced by the light quark zero modes as captured by the ILM. The pion and kaon longitudinal parton distributions are sensitive to the nature of the quark zero modes in the vacuum.

Contrary to common lore, on the light front the vacuum is anything but trivial. Its main effect is to induce the spontaneous breaking of chiral symmetry with a running constituent quark mass for the valence partons. It also, induces nonperturbative multifermion interactions among the flying leading partons and a scalar chiral condensate much like in the rest frame. How this analysis in the context of the ILM squares with the recently suggested superfluid at zero x-parton [52] would be of future interest.

ACKNOWLEDGMENTS

This work is supported by the Office of Science, U.S. Department of Energy, under Contract No. DE-FG-88ER40388.

APPENDIX A: CONVENTIONS USED ON THE LF

Throughout this paper, our conventions of the light front frame follows Kogut-Soper convention based on the Weyl chiral basis of the gamma matrices,

$$\gamma^0 = \begin{pmatrix} 0 & \mathbb{1} \\ \mathbb{1} & 0 \end{pmatrix}, \qquad \gamma^i = \begin{pmatrix} 0 & \sigma^i \\ -\sigma^i & 0 \end{pmatrix}. \tag{A1}$$

The light front components are normalized to be

$$\gamma^{\pm} = \frac{\gamma^0 \pm \gamma^3}{\sqrt{2}} \tag{A2}$$

with light front projection defined by

$$\mathcal{P}_+ = \frac{1}{2}\gamma^-\gamma^+ = \begin{pmatrix} 1 & 0 & 0 & 0 \\ 0 & 0 & 0 & 0 \\ 0 & 0 & 0 & 0 \\ 0 & 0 & 0 & 1 \end{pmatrix} \tag{A3}$$

and $\mathcal{P}_- = 1 - \mathcal{P}_+$. The free LF spinors for the quarks and antiquarks are

$$u_s(p) = \frac{1}{\sqrt{\sqrt{2}p^+}}(\not{p} + M)\begin{pmatrix} \chi_s \\ \chi_s \end{pmatrix} \tag{A4}$$

and

$$v_s(p) = \frac{1}{\sqrt{\sqrt{2}p^+}}(\not{p} - M)\begin{pmatrix} 2s\chi_s \\ -2s\chi_s \end{pmatrix}, \tag{A5}$$

respectively, with χ_s a 2-spinor with a spin pointing in the z direction and M the constituent quark mass.

To denote the spin states in the creation of a quark-antiquark pair, the matrix elements with different spin states can be written as a matrix with $[s_1 s_2]$ entries,

$$\bar{u}_{s_1}(k)v_{s_2}(P-k) = \frac{1}{\sqrt{x\bar{x}}}\begin{pmatrix} k_L & M(\bar{x}-x) \\ M(\bar{x}-x) & -k_R \end{pmatrix} \tag{A6}$$

for the scalar, and

$$\bar{u}_{s_1}(k)i\gamma^5 v_{s_2}(P-k) = \frac{i}{\sqrt{x\bar{x}}}\begin{pmatrix} -k_L & M \\ -M & -k_R \end{pmatrix} \tag{A7}$$

for the pseudoscalar, with $k_{L/R} = k^1 \mp ik^2$ and $x = k^+/P^+$ the quark momentum fraction on the LF. Similarly, for the quark-quark pair, the spin matrix elements with entries $[s's]$ are

$$\bar{u}_{s'}(p)u_s(k) = \sqrt{p^+k^+}\begin{pmatrix} M\left(\frac{1}{p^+}+\frac{1}{k^+}\right) & \frac{p_L}{p^+}-\frac{k_L}{k^+} \\ \frac{k_R}{k^+}-\frac{p_R}{p^+} & M\left(\frac{1}{p^+}+\frac{1}{k^+}\right) \end{pmatrix}, \tag{A8}$$

$$\bar{u}_{s'}(p)\gamma^5 u_s(k) = \sqrt{p^+k^+}\begin{pmatrix} M\left(\frac{1}{p^+}-\frac{1}{k^+}\right) & \frac{k_L}{k^+}-\frac{p_L}{p^+} \\ \frac{k_R}{k^+}-\frac{p_R}{p^+} & -M\left(\frac{1}{p^+}-\frac{1}{k^+}\right) \end{pmatrix}, \tag{A9}$$

$$\bar{v}_s(k)v_{s'}(p) = \sqrt{p^+k^+}\begin{pmatrix} -M\left(\frac{1}{p^+}+\frac{1}{k^+}\right) & \frac{k_L}{k^+}-\frac{p_L}{p^+} \\ \frac{p_R}{p^+}-\frac{k_R}{k^+} & -M\left(\frac{1}{p^+}+\frac{1}{k^+}\right) \end{pmatrix}, \tag{A10}$$

$$\bar{v}_s(k)\gamma^5 v_{s'}(p) = \sqrt{p^+k^+}\begin{pmatrix} -M\left(\frac{1}{p^+}-\frac{1}{k^+}\right) & \frac{p_L}{p^+}-\frac{k_L}{k^+} \\ \frac{p_R}{p^+}-\frac{k_R}{k^+} & M\left(\frac{1}{p^+}-\frac{1}{k^+}\right) \end{pmatrix}. \tag{A11}$$

The lowest Fock states for the scalar σ and pseudoscalar π are explicitly

$$|\sigma, P\rangle = \frac{1}{\sqrt{N_c}}\int_0^1 \frac{dx}{\sqrt{2x\bar{x}}}\int \frac{d^2k_\perp}{(2\pi)^3}\{\phi_\sigma^0(x,k_\perp)[b_\uparrow^\dagger(k)c_\downarrow^\dagger(P-k) + b_\downarrow^\dagger(k)c_\uparrow^\dagger(P-k)] + \phi_\sigma^{+1}(x,k_\perp)b_\uparrow^\dagger(k)c_\uparrow^\dagger(P-k) + \phi_\sigma^{-1}(x,k_\perp)b_\downarrow^\dagger(k)c_\downarrow^\dagger(P-k)\}|0\rangle, \tag{A12}$$

$$|\pi, P\rangle = \frac{1}{\sqrt{N_c}}\int_0^1 \frac{dx}{\sqrt{2x\bar{x}}}\int \frac{d^2k_\perp}{(2\pi)^3}\{\phi_\pi^0(x,k_\perp)[b_\uparrow^\dagger(k)c_\downarrow^\dagger(P-k) - b_\downarrow^\dagger(k)c_\uparrow^\dagger(P-k)] + \phi_\pi^{+1}(x,k_\perp)b_\uparrow^\dagger(k)c_\uparrow^\dagger(P-k) + \phi_\pi^{-1}(x,k_\perp)b_\downarrow^\dagger(k)c_\downarrow^\dagger(P-k)\}|0\rangle, \tag{A13}$$

with the light front normalizations subsumed, provided that

$$\int_0^1 dx \int \frac{d^2k_\perp}{(2\pi)^3} |\phi_\sigma^0|^2 + |\phi_\sigma^{+1}|^2 + |\phi_\sigma^{-1}|^2 = 1 \tag{A14}$$

and

$$\int_0^1 dx \int \frac{d^2k_\perp}{(2\pi)^3} |\phi_\pi^0|^2 + |\phi_\pi^{+1}|^2 + |\phi_\pi^{-1}|^2 = 1. \tag{A15}$$

Each spin-wave function can also be redefined to extract out the corresponding normalization of their spin state with

$$\phi_\sigma^0 = \frac{M(\bar{x}-x)}{\sqrt{x\bar{x}}}\phi_\sigma; \qquad \phi_\sigma^{+1} = \frac{k_L}{\sqrt{x\bar{x}}}\phi_\sigma; \qquad \phi_\sigma^{-1} = \frac{-k_R}{\sqrt{x\bar{x}}}\phi_\sigma \tag{A16}$$

and

$$\phi_\pi^0 = \frac{iM}{\sqrt{x\bar{x}}}\phi_\pi; \qquad \phi_\pi^{+1} = \frac{-ik_L}{\sqrt{x\bar{x}}}\phi_\pi; \qquad \phi_\pi^{-1} = \frac{-ik_R}{\sqrt{x\bar{x}}}\phi_\pi. \tag{A17}$$

APPENDIX B: TWO-BODY 'T HOOFT HAMILTONIAN ON THE LIGHT FRONT

The general form of the two-body bound state equation can be written as

$$\int \frac{dq^+ d^2q_\perp}{(2\pi)^3} \hat{H}_{s_1 s_2 s_1' s_2'}(k, P-k, q, P-q)\Phi_X(q, P-q, s_1', s_2') = m_X^2 \Phi_X(k, P-k, s_1, s_2), \tag{B1}$$

where the light front Hamiltonian in the momentum space is

$$\hat{H}_{s_1 s_2 s_1' s_2'}(k, P-k, k', P-k') = \left[\frac{k_\perp^2 + M^2}{x} + \frac{k_\perp^2 + M^2}{\bar{x}}\right](2\pi)^3 \delta_+^3(k-k') + \frac{1}{\sqrt{2x\bar{x}}}\mathcal{V}_{s_1, s_2, s_1', s_2'}(k, P-k, k', P-k')\frac{1}{\sqrt{2y\bar{y}}P^+} \tag{B2}$$

for a pair of identical constituents. The labels 1, 2 refer to the two constituents. To address the s-channel and t-channel on equal footing, we use the Fierze rearranged instanton induced 't Hooft interaction,

$$\begin{aligned}\mathcal{L}_{\prime\text{tHooft}} = \frac{G}{8(N_c^2-1)}\Bigg(&\frac{N_c^2-1}{N_c^2}[(\bar{\psi}\psi)^2 - (\bar{\psi}i\gamma^5\psi)^2 - (\bar{\psi}\tau^a\psi)^2 + (\bar{\psi}i\gamma^5\tau^a\psi)^2] \\ &+ \frac{N_c-2}{4N_c}[(\bar{\psi}\lambda^\alpha\psi)^2 - (\bar{\psi}i\gamma^5\lambda^\alpha\psi)^2 - (\bar{\psi}\lambda^\alpha\tau^a\psi)^2 + (\bar{\psi}i\gamma^5\tau^a\lambda^\alpha\psi)^2] + \frac{1}{8}(\bar{\psi}\sigma^{\mu\nu}\lambda^\alpha\psi)^2 - \frac{1}{8}(\bar{\psi}\sigma^{\mu\nu}\lambda^\alpha\tau^a\psi)^2\Bigg).\end{aligned} \tag{B3}$$

1. s-channel

The interaction in the s-channel follows solely from the first contribution in (B3) through the substitution $(\bar{\psi}\psi)^2 \to \bar{u}_{1'}v_{2'}\bar{v}_2 u_1$,

$$\begin{aligned}\mathcal{V}^S_{s_1, s_2, s_1', s_2'}(k_1, k_2, k_1', k_2') = -\frac{G}{4(N_c^2-1)}&[\alpha_+(P^+)\bar{u}_{s_1'}(k_1')v_{s_2'}(k_2')\bar{v}_{s_2}(k_2)u_{s_1}(k_1) - \alpha_-(P^+)\bar{u}_{s_1'}(k_1')\tau^a v_{s_2'}(k_2')\bar{v}_{s_2}(k_2)\tau^a u_{s_1}(k_1) \\ &- \alpha_-(P^+)\bar{u}_{s_1}(k_1)i\gamma^5 v_{s_2}(k_2)\bar{v}_{s_2'}(k_2')i\gamma^5 u_{s_1'}(k_1') + \alpha_+(P^+)\bar{u}_{s_1}(k_1)i\gamma^5\tau^a v_{s_2}(k_2)\bar{v}_{s_2'}(k_2')i\gamma^5 u_{s_1'}(k_1')]\end{aligned} \tag{B4}$$

in leading order in $1/N_c$. The colored vertices in (B3) do not contribute in the s-channel to this order, since the bound two-body eigenstate is colorless. The extra vertex factors of $\alpha_\pm(P^+)$ resum the tadpoles.

2. t-channel

The interaction in the t-channel follows from the second and third contributions in (B3), through the substitution $(\bar{\psi}\psi)^2 \to -\bar{u}_{1'}u_1\bar{v}_2 v_{2'}$,

$$\mathcal{V}^T_{s_1,s_2,s_1',s_2'}(k_1,k_2,k_1',k_2') = \frac{G}{4(N_c^2-1)}(1-\tau_1^a\tau_2^a)\left[\frac{N_c^2-1}{2N_c}(\bar{u}_{s_1}(k_1)u_{s_1'}(k_1')\bar{v}_{s_2'}(k_2')v_{s_2}(k_2) - \bar{u}_{s_1'}(k_1')i\gamma^5 u_{s_1}(k_1)\bar{v}_{s_2}(k_2)i\gamma^5 v_{s_2'}(k_2')) + \frac{N_c^2-1}{4N_c}\bar{u}_{s_1'}(k_1')\sigma^{\mu\nu}u_{s_1}(k_1)\bar{v}_{s_2}(k_2)\sigma_{\mu\nu}v_{s_2'}(k_2')\right] \tag{B5}$$

also in leading order in $1/N_c$. The minus sign arises from Fermi statistics. We made use of the color averaging $\langle\lambda_1^\alpha\cdot\lambda_2^\alpha\rangle = 2\frac{N_c^2-1}{N_c}$ in the t-channel, since the interaction kernel acts on a color-singlet two-body eigenstate.

3. Eikonal approximation

In the eikonal or large momentum limit, $k_1^+ \approx k_1'^+$ and $k_2^+ \approx k_2'^+$ as the in-out particles fly on straight trajectories. The bound state equation simplifies by replacing the y dependence in the interaction kernel by x, with the result

$$m_X^2\Phi_X(x,k_\perp,s_1,s_2) = \frac{k_\perp^2+M^2}{x\bar{x}}\Phi_X(x,k_\perp,s_1,s_2) - \frac{1}{2x\bar{x}}\sqrt{\mathcal{F}(k)\mathcal{F}(P-k)}\int_0^1 dy \times \int\frac{d^2q_\perp}{(2\pi)^3}\sum_{s,s'}\left[\mathcal{V}^{S/T}_{s_1,s_2,s,s'}(k,P-k,q,P-q)\sqrt{\mathcal{F}(q)\mathcal{F}(P-q)}\right]\Big|_{x=y}\Phi_X(y,q_\perp,s,s'). \tag{B6}$$

In coordinate space, the LFWF is defined as

$$\Phi(\xi^-,b_\perp) = \int\frac{dxd^2k_\perp}{(2\pi)^3}\Phi(x,k_\perp)e^{-ixP^+\xi^- + ik_\perp\cdot b_\perp} \tag{B7}$$

and the bound state equation is now a standard Schrödinger equation,

$$\left[\frac{-\nabla_\perp^2+M^2}{x\bar{x}}\delta_{s_1s_1'}\delta_{s_2s_2'} + \hat{V}_{s_1s_2,s_1's_2'}(\xi^-,b_\perp)\right]\Phi_X(\xi^-,b_\perp,s_1',s_2') = m_X^2\Phi_X(\xi^-,b_\perp,s_1,s_2) \tag{B8}$$

with the spin-flavor-dependent potential

$$\hat{V}(\xi^-,b_\perp) = -2g_S(1-\tau_1^a\tau_2^a)\frac{1}{2x\bar{x}}\mathcal{F}^2\left(\frac{-\nabla_\perp^2+M^2}{x\bar{x}}\right)V(1,2). \tag{B9}$$

The momentum fraction in coordinate space is $\frac{1}{x} = \frac{-i}{\partial_-}$ with $\partial_- = \frac{1}{P^+}\frac{\partial}{\partial\xi^-}$. In the large N_c limit, the interaction kernel in (B9) simplifies to

$$
\begin{aligned}
V(1,2) = &\left[M\mathbb{1}_1 M\mathbb{1}_2 - \frac{1}{2}(\sigma_{1\perp}\times\nabla_\perp)(M\mathbb{1}_2) + \frac{1}{2}(M\mathbb{1}_1)(\sigma_{2\perp}\times\nabla_\perp)\right.\\
&\left. - \frac{1}{4}(\sigma_{1\perp}\times\nabla_\perp)(\sigma_{2\perp}\times\nabla_\perp) - \frac{1}{4}(i\sigma_{1\perp}\cdot\nabla_\perp)(i\sigma_{2\perp}\cdot\nabla_\perp)\right]\delta^2(b_\perp)\\
&- \left[M\sigma_{1z}M\sigma_{2z} + \frac{1}{2}(i\sigma_{1\perp}\cdot\nabla_\perp)(M\sigma_{2z}) - \frac{1}{2}(M\sigma_{1z})(i\sigma_{2\perp}\cdot\nabla_\perp)\right.\\
&\left. - \frac{1}{4}(i\sigma_{1\perp}\cdot\nabla_\perp)(i\sigma_{2\perp}\cdot\nabla_\perp) - \frac{1}{4}(\sigma_{1\perp}\times\nabla_\perp)(\sigma_{2\perp}\times\nabla_\perp)\right]\delta^2(b_\perp)\\
&+ [(M\sigma_{1\perp}\sigma_{2z} - M\sigma_{1z}\sigma_{2\perp})\cdot i\nabla_\perp + (\sigma_{1\perp}\cdot\nabla_\perp)(\sigma_{2\perp}\cdot\nabla_\perp) - (\sigma_{1\perp}\times\nabla_\perp)(\sigma_{2\perp}\times\nabla_\perp)]\delta^2(b_\perp)\\
&+ \frac{1}{2}[(\sigma_{1\perp}\cdot\nabla_\perp\delta^2(b_\perp))(\sigma_{2\perp}\cdot\nabla_\perp) + (\sigma_{1\perp}\cdot\nabla_\perp)(\sigma_{2\perp}\cdot\nabla_\perp\delta^2(b_\perp))]\\
&- \frac{1}{2}[(\sigma_{1\perp}\times\nabla_\perp\delta^2(b_\perp))(\sigma_{2\perp}\times\nabla_\perp) + (\sigma_{1\perp}\times\nabla_\perp)(\sigma_{2\perp}\times\nabla_\perp\delta^2(b_\perp))]. \qquad \text{(B10)}
\end{aligned}
$$

The first two lines in (B10) stem from the nontensor parts in (B3), in agreement with [14]. The remaining contributions in (B3) are from the tensor part in (B3). Note that the minus sign from the Fermi statistics is compensated by the minus sign from the antispinor contraction $\bar{v}v$, with net attraction in the t-channel for the pion and sigma.

APPENDIX C: DGLAP EVOLUTION AND ERBL EVOLUTION

Dokshitzer-Gribov-Lipatov-Altarelli-Parisi (DGLAP) evolution is governed by

$$
\mu\frac{d}{d\mu}\begin{pmatrix} q(x,\mu)\\ g(x,\mu)\end{pmatrix} = \sum_{q'}\frac{\alpha_s(\mu)}{\pi}\int_x^1\frac{dy}{y}\begin{pmatrix} P_{qq'}(x/y) & P_{qg}(x/y)\\ P_{gq'}(x/y) & P_{gg}(x/y)\end{pmatrix}\begin{pmatrix} q'(y,\mu)\\ g(y,\mu)\end{pmatrix} \qquad \text{(C1)}
$$

with the splitting functions defined as follows:

$$
P_{qq}(x) = C_F\left[\frac{1+x^2}{(1-x)_+} + \frac{3}{2}\delta(1-x)\right],
$$

$$
P_{qg}(x) = \frac{1}{2}[x^2 + (1-x)^2],
$$

$$
P_{gq}(x) = C_F\left[\frac{1+(1-x)^2}{x}\right],
$$

$$
P_{gg}(x) = 2C_A\left[\frac{x}{(1-x)_+} + \frac{1-x}{x} + x(1-x)\right] + \frac{\beta_0}{2}\delta(1-x),
$$

where $C_F = \frac{N_c^2-1}{2N_c}$, $C_A = N_c$, and the one loop running coupling $\beta_0 = \frac{11}{3}N_c - \frac{2}{3}n_f$.

The full evolution of the quark parton distribution inside a hadron is described by the DGLAP equations. At low energy, where the valence degrees of freedom dominate, the valence quark distribution is sufficient to describe the hadronic structure. Only the quark-to-quark splitting process denoted by $P_{qq}(x)$, has to be taken into account. As the energy scale increases, the sea quark and gluon production spreads the momentum distribution on more partons, effectively shifting the momentum valence quark distribution to small x, and eventually softening the $x = 1$ tail behavior.

On the other hand, the evolution of the light front wave function and its associated distribution amplitudes is governed by the Efremov-Radyushkin-Brodsky-Lepage (ERBL) equation, which expands the LFWF and DA from the asymptotic form $6x(1-x)$, in a complete basis of Gegenbauer polynomials,

$$
\phi(x,Q) = 6x\bar{x}\sum_{n=0}^{\infty}a_n(Q_0)\left(\frac{\alpha_s(Q^2)}{\alpha_s(Q_0^2)}\right)^{\gamma_n/\beta_0}C_n^{3/2}(x-\bar{x}). \qquad \text{(C2)}
$$

The anomalous dimension associated with the evolution is defined as

$$
\gamma_n = C_F\left[-3 + 4\sum_{j=1}^{n+1}\frac{1}{j} - \frac{2}{(n+1)(n+2)}\right], \qquad \text{(C3)}
$$

where

$$\alpha_s(Q) = \frac{4\pi}{\beta_0 \ln\left(\frac{Q^2}{\Lambda^2_{\rm QCD}}\right)}$$

and $\Lambda_{\rm QCD} = 226$ MeV. $C_n^m(z)$ are Gegenbauer polynomials. Due to the orthogonality of the Gegenbauer polynomials, the initial coefficients can be evaluated by

$$a_n(Q_0) = \frac{2(2n+3)}{3(n+1)(n+2)} \int_0^1 dy C_n^{3/2}(y-\bar{y})\phi(y,Q_0). \tag{C4}$$

APPENDIX D: RANDOM INSTANTON VACUUM

Here we briefly review the emergence of the running constituent quark mass $M(k)$ in the ILM by resummation of the leading $1/N_c$ contributions [7,9]. The analysis is in the rest frame in Euclidean signature. For a sufficiently dilute vacuum composed of instantons and anti-instantons, the gauge fields are

$$A(x) = \sum_{I=1}^{N_-} A_I(x) + \sum_{\bar{I}}^{N_+} A_{\bar{I}}(x), \tag{D1}$$

where $I, \bar{I}$ refer to the instanton and anti-instanton moduli. More specifically, each instanton is localized at z_I, with size ρ_I and color orientation U_I

$$A_I(x) = U_I A(x - z_I, \rho_I) U_I^\dagger. \tag{D2}$$

For a topologically neutral vacuum, the mean number of instantons match that of the anti-instantons $N_+ = N_-$.

Light quarks in the ILM scatter randomly at each instanton and anti-instanton site, with the light quark propagator

$$S(x,y) = \left\langle \langle x| \frac{1}{-i\partial\!\!\!/ - A\!\!\!/ - im} |y\rangle \right\rangle_A \tag{D3}$$

averaged over (D1) with $N = N_+ + N_-$ fixed in an Euclidean 4-volume V. The average runs the entire instanton ensemble with equal sampling. The planar rescattering contributions to the light quark propagator in leading order in $1/N_c$ counting gives [7,71]

$$S^{-1} - S_0^{-1} = \frac{N}{2N_c V} \langle x| \left[\sum_I \int d^4 z_I dU_I \frac{1}{S - A\!\!\!/_I^{-1}} + \sum_{\bar{I}} \int d^4 z_{\bar{I}} dU_{\bar{I}} \frac{1}{S - A\!\!\!/_{\bar{I}}^{-1}} \right] |y\rangle \tag{D4}$$

with the apparent diluteness factor $\rho^4 N/N_c V \sim \kappa_{I+\bar{I}}/N_c$. The dominant contribution to (D4) stems from the quark zero modes with a running constituent quark mass [54]

$$M(k,m) = m + \frac{M(0,0)}{(1+\xi^2)^{1/2} + \xi} \times [z(I_0(z)K_0(z) - I_1(z)K_1(z))']^2 \Big|_{z=\frac{k\rho}{2}} \tag{D5}$$

with

$$\xi = \frac{N_c m M(0,0)}{4\pi^2 \rho^2 N/V}.$$

If we define $M = M(0,m)$ and $M(k^2) = M(k,m)$, then

$$M(k^2) = M(zF'(z))^2 + m[1 - (zF'(z))^2]\Big|_{z=\frac{k\rho}{2}} \tag{D6}$$

with

$$F(z) = I_0(z)K_0(z) - I_1(z)K_1(z)$$

the profile of the quark zero mode in singular gauge. The running quark mass asymptotes the current mass m for $k\rho \gg 1$, and reduces to the constant mass M for $k\rho \ll 1$.

APPENDIX E: GAP EQUATION FOR ZERO INSTANTON SIZE

In the zero instanton size limit, the induced form factor from the quark zero modes $\mathcal{F}(k^2) \to 1$ and the induced 't Hooft effective interactions become local in Euclidean space. While their continuation to Minkowski space is straightforward, they lead to diverging results both in the IR and UV in the mean-field treatment. This situation is familiar for local fermionic or NJL type interactions in the rest frame, and therefore carry to the light front.

For virtual loops with running momenta k in Euclidean space, the cutoff choice should preserve $O(4)$ symmetry, which naturally means $\sqrt{k^2} < \Lambda_E$. For virtual loops in Minkowski space, the cutoff should preserve boost invariance on the light front, which translates to $\sqrt{2}k^\pm < \Lambda$ or equivalently [40,41]

$$\frac{k_\perp^2 + M^2}{\sqrt{2}\Lambda} < k^+ < \frac{\Lambda}{\sqrt{2}}. \tag{E1}$$

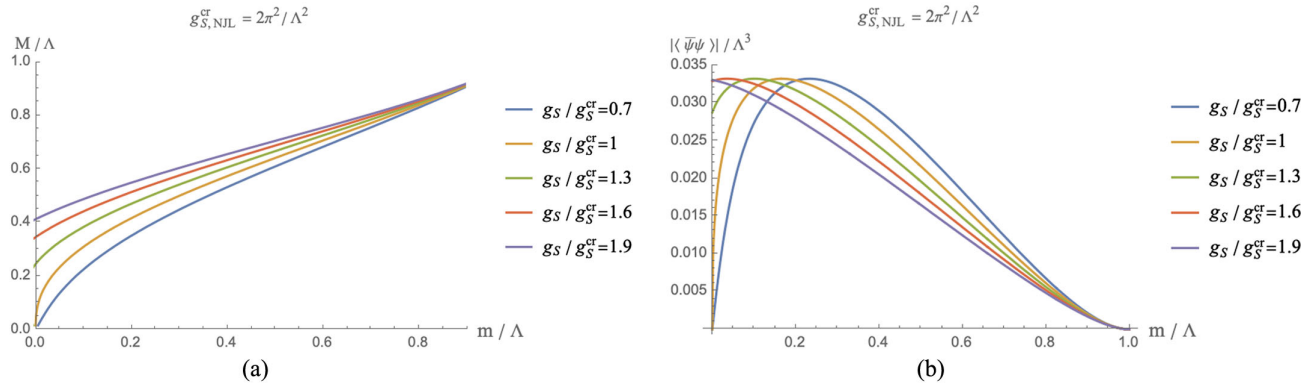

FIG. 15. (a) The change of the constituent mass M versus the current mass m, for different couplings g_S/g_S^{cr} with $g_S^{cr} = 2\pi^2/\Lambda^2$ in the zero instanton size limit. (b) Same as in (a) for the chiral condensate.

The lower bound follows from the on-shell condition $k^2 = 2k^+k^- - k_\perp^2 = M^2$.

With this in mind, the diverging integrals in (45) and (47) after the boost-invariant regularization yield

$$\int \frac{dk^+ d^2k_\perp}{(2\pi)^3}\frac{\epsilon(k^+)}{k^+}\theta(\Lambda/\sqrt{2}-k^+)\theta(\Lambda/\sqrt{2}-k^-)\Big|_{k^-=\frac{k_\perp^2+M^2}{2k^+}} = \frac{\Lambda^2}{4\pi^2}\left[1-\frac{M^2}{\Lambda^2}+\frac{M^2}{\Lambda^2}\ln\frac{M^2}{\Lambda^2}\right]. \tag{E2}$$

As a result, the gap equation in the zero instanton size limit is

$$\frac{m}{M} = 1-\frac{g_S\Lambda^2}{2\pi^2}\left[1-\frac{M^2}{\Lambda^2}+\frac{M^2}{\Lambda^2}\ln\frac{M^2}{\Lambda^2}\right] \tag{E3}$$

and the quark condensate $\langle\bar{\psi}\psi\rangle$ is

$$\frac{\langle\bar{\psi}\psi\rangle}{\Lambda^3} = -\frac{N_c}{2\pi^2}\left(\frac{M}{\Lambda}\right)\left[1-\frac{M^2}{\Lambda^2}+\frac{M^2}{\Lambda^2}\ln\frac{M^2}{\Lambda^2}\right]. \tag{E4}$$

A nonzero constituent quark mass M develops whenever the fermionic interaction is sufficiently attraCtive with $g_S > g^{cr}_{S,NJL} = \frac{2\pi^2}{\Lambda^2}$.

In Fig. 15(a) we show the dependence of the constituent quark mass M/Λ versus the current quark mass m/Λ, with increasing fermionic coupling g_S (bottom to top from left) for a fixed cutoff Λ and a critical coupling $g^{cr}_{S,NJL} = 2\pi^2/\Lambda^2$. The same display for the chiral condensate is shown in In Fig. 15(b).

APPENDIX F: BOUND STATES FOR ZERO INSTANTON SIZE

In the zero instanton size limit, the emergent form factor from the quark zero modes reduces to 1, $\mathcal{F} \to 1$. To regulate the vacuum or zero-body integrals to one loop, we use the parity-even and boost-invariant sharp cutoff discussed in Appendix E. In an n-body state on the light front, the natural cutoff from time ordered perturbation theory relates to the light front energy $K^- = \sum_i k_i^-$ of free valence quarks [51],

$$K^- = \sum_{i=1}^{n}\frac{k_{\perp i}^2 + M_i^2}{x_i K^+} < 2\Lambda^2. \tag{F1}$$

Here $k_{\perp i}$ and x_i, are the transverse momentum and the longitudinal momentum fraction of the valence parton-i, respectively. This cutoff is boost invariant and parity even. For two-body bound states with unequal masses, it translates to

$$\frac{k_\perp^2 + M_u^2}{x} + \frac{k_\perp^2 + M_s^2}{\bar{x}} < 2\Lambda^2 \sim \frac{1}{\rho^2}. \tag{F2}$$

A similar cutoff was used in [40] for equal quark masses and independently argued in the context of the LaMET analysis of the ILM in [54].

1. σ meson

$$\begin{aligned}\frac{m}{M} &= -\frac{g_s}{4\pi^2}\int_0^1 dy\int_0^{\Lambda^2} dq_\perp^2\left[\frac{m_\sigma^2-4M^2}{y\bar{y}m_\sigma^2-(q_\perp^2+M^2)}\right]\\ &= -\frac{g_s}{4\pi^2}(4M^2-m_\sigma^2)\int_0^1 dy\ln\left(1+\frac{\Lambda^2}{M^2-y\bar{y}m_\sigma^2}\right), \qquad m_\sigma^2<4M^2\\ &= -\frac{g_s}{2\pi^2}(4M^2-m_\sigma^2)\\ &\quad\times\left[\frac{1}{2}\ln\left(1+\frac{\Lambda^2}{M^2}\right)-\sqrt{\frac{4M^2-m_\sigma^2}{m_\sigma^2}}\left(\tan^{-1}\frac{1}{\sqrt{\frac{4M^2-m_\sigma^2}{m_\sigma^2}}}-\sqrt{\frac{4(M^2+\Lambda^2)-m_\sigma^2}{4M^2-m_\sigma^2}}\tan^{-1}\frac{1}{\sqrt{\frac{4(M^2+\Lambda^2)-m_\sigma^2}{m_\sigma^2}}}\right)\right].\end{aligned} \tag{F3}$$

The sigma is a threshold state with a mass $m_\sigma = 2M$ in the chiral limit but otherwise unbound in ILM with a sharp or a smooth cutoff on the light front.

2. π_5 meson

$$\begin{aligned}2-\frac{m}{M} &= \frac{g_s}{4\pi^2}\int_0^1 dy\int_0^{\Lambda^2} dq_\perp^2\left[\frac{m_{\pi_5}^2-4M^2}{y\bar{y}m_{\pi_5}^2-(q_\perp^2+M^2)}\right]\\ &= \frac{g_s}{4\pi^2}(4M^2-m_{\pi_5}^2)\int_0^1 dy\ln\left(1+\frac{\Lambda^2}{M^2-y\bar{y}m_{\pi_5}^2}\right), \qquad m_{\pi_5}^2<4M^2\\ &= \frac{g_s}{2\pi^2}(4M^2-m_{\pi_5}^2)\\ &\quad\times\left[\frac{1}{2}\ln\left(1+\frac{\Lambda^2}{M^2}\right)-\sqrt{\frac{4M^2-m_{\pi_5}^2}{m_{\pi_5}^2}}\tan^{-1}\frac{1}{\sqrt{\frac{4M^2-m_{\pi_5}^2}{m_{\pi_5}^2}}}+\sqrt{\frac{4(M^2+\Lambda^2)-m_{\pi_5}^2}{m_{\pi_5}^2}}\tan^{-1}\frac{1}{\sqrt{\frac{4(M^2+\Lambda^2)-m_{\pi_5}^2}{m_{\pi_5}^2}}}\right].\end{aligned} \tag{F4}$$

3. σ_5 meson

$$\begin{aligned}2-\frac{m}{M} &= \frac{g_s}{4\pi^2}\int_0^1 dy\int_0^{\Lambda^2} dq_\perp^2\left[\frac{m_{\sigma_5}^2}{y\bar{y}m_{\sigma_5}^2-(q_\perp^2+M^2)}\right]\\ &= -\frac{g_s}{2\pi^2}m_{\sigma_5}^2\\ &\quad\times\left[\frac{1}{2}\ln\left(1+\frac{\Lambda^2}{M^2}\right)-\sqrt{\frac{4M^2-m_{\sigma_5}^2}{m_{\sigma_5}^2}}\left(\tan^{-1}\frac{1}{\sqrt{\frac{4M^2-m_{\sigma_5}^2}{m_{\sigma_5}^2}}}-\sqrt{\frac{4(M^2+\Lambda^2)-m_{\sigma_5}^2}{4M^2-m_{\sigma_5}^2}}\tan^{-1}\frac{1}{\sqrt{\frac{4(M^2+\Lambda^2)-m_{\sigma_5}^2}{m_{\sigma_5}^2}}}\right)\right].\end{aligned} \tag{F5}$$

The instanton induced interactions are repulsive in both of the σ_5, π_5 channels on the light front. There are no bound states in this channel in the chiral limit or otherwise.

4. π meson

$$\frac{m}{M} = -\frac{g_s}{4\pi^2}\int_0^1 dy \int_0^{\Lambda^2} dq_\perp^2 \left[\frac{m_\pi^2}{y\bar{y}m_\pi^2 - (q_\perp^2 + M^2)}\right]$$
$$= \frac{g_s}{4\pi^2} m_\pi^2 \int_0^1 dy \ln\left(1 + \frac{\Lambda^2}{M^2 - y\bar{y}m_\pi^2}\right), \qquad m_\pi^2 < 4M^2$$
$$= \frac{g_s}{2\pi^2} m_\pi^2 \left[\frac{1}{2}\ln\left(1+\frac{\Lambda^2}{M^2}\right) - \sqrt{\frac{4M^2 - m_\pi^2}{m_\pi^2}}\tan^{-1}\frac{1}{\sqrt{\frac{4M^2-m_\pi^2}{m_\pi^2}}} + \sqrt{\frac{4(M^2+\Lambda^2) - m_\pi^2}{m_\pi^2}}\tan^{-1}\frac{1}{\sqrt{\frac{4(M^2+\Lambda^2)-m_\pi^2}{m_\pi^2}}}\right]. \quad \text{(F6)}$$

This is by far the strongest channel in the ILM with a strongly bound π state. The dependence of the pion m_π on the current mass m for fixed Λ is shown in Fig. 16. The pion mass m_π increases as m increases to eventually reach the 2-constituent quark threshold $2M$. It is a true Goldstone mode, with the mass vanishing in the chiral limit

$$m_\pi^2 = \frac{m/M}{\frac{g_s}{4\pi^2}\ln(1+\frac{\Lambda^2}{M^2})} = \frac{2m}{f_\pi^2}|\langle\bar{\psi}\psi\rangle| + \mathcal{O}(m^2) \quad \text{(F7)}$$

which is the expected Gell-Mann-Oakes-Renner relation. In the chiral limit, the pion decay constant is

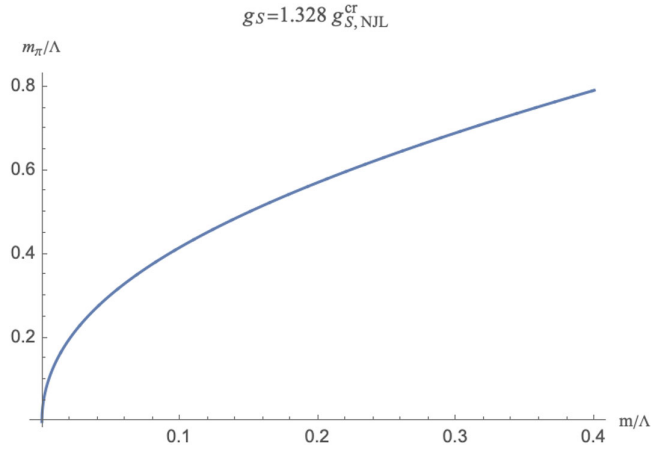

FIG. 16. Pion mass versus the current quark mass with fixed cutoff Λ and a fermion coupling g_S in the zero instanton size limit.

$$f_\pi = \frac{\sqrt{N_c}M}{\sqrt{2}\pi}\left[\ln\left(1+\frac{\Lambda^2}{M^2}\right)\right]^{1/2}. \quad \text{(F8)}$$

With the physical input of the pion decay constant and pion mass, we can fix the best parameters for our NJL-type model. The transverse cutoff is fixed to be $\Lambda = 729$ MeV, roughly higher than inverse instanton size $\rho = 0.313$ fm. The current quark mass we obtained is $m = 12.4$ MeV and the coupling will be fixed to be $g_S = 1.314 g^{cr}_{S,\mathrm{NJL}}$. The constituent mass with the given current mass and fixed coupling will be $M = 207.7$ MeV. The quark condensate will thus be $|\langle\bar{\psi}\psi\rangle|^{1/3} = 228.9$ MeV. The pion mass and the pion decay constant with the given parameters will be $m_\pi^{\mathrm{NJL}} = 135.0$ MeV and $f_\pi^{\mathrm{NJL}} = 130.3$ MeV, respectively, which is very consistent with the physical values.

APPENDIX G: FERMIONIC CONSTRAINT IN THE OPERATOR FORM

One of the key features of the light front approach is the elimination of the fermionic constraint on the bad component of the fermionic field. In the main text, we have used an auxiliary field approach and the mean-field approximation to eliminate the bad component in leading order in $1/N_c$. Here, we briefly show that the elimination can be enforced solely at the operator level, without recourse to auxiliary fields, using power counting in $1/N_c$.

The multifermion interactions generated in the ILM are essentially determinantal, owing to the induced $U_A(1)$ flavor symmetry breaking by instantons. By Fierzing, they consist of combinations of only twist-3 operators, $\sigma = \bar{\psi}\psi$, $\pi = \bar{\psi}i\gamma^5\psi$, $\sigma^a = \bar{\psi}\tau^a\psi$, and $\pi^a = \bar{\psi}i\tau^a\gamma^5\psi$, which form a closed set. The elimination of the bad component ψ_- in favor of the good component ψ_+ amounts to the closed hierarchy in $1/N_c$,

$$\sigma(x) = \sigma^{(0)}(x) - \frac{g_S}{2N_c}[\hat{V}(x)\sigma(x) - \hat{A}(x)\pi(x) - \hat{V}^a(x)\sigma^a(x) + \hat{A}^a(x)\pi^a(x)], \tag{G1}$$

$$\pi(x) = \pi^{(0)}(x) - \frac{g_S}{2N_c}[-\hat{A}(x)\sigma(x) - \hat{V}(x)\pi(x) + \hat{A}^a(x)\sigma^a(x) + \hat{V}^a(x)\pi^a(x)], \tag{G2}$$

$$\sigma^a(x) = \sigma^{a(0)}(x) - \frac{g_S}{2N_c}[\hat{V}^a(x)\sigma(x) - \hat{A}^a(x)\pi(x) - \hat{V}^{ab}(x)\sigma^b(x) + \hat{A}^{ab}(x)\pi^b(x)], \tag{G3}$$

$$\pi^a(x) = \pi^{a(0)}(x) - \frac{g_S}{2N_c}[-\hat{A}^a(x)\sigma(x) - \hat{V}^a(x)\pi(x) + \hat{A}^{ab}(x)\sigma^b(x) + \hat{V}^{ab}(x)\pi^b(x)], \tag{G4}$$

with $g_S = G_S N_c$ assumed of fixed order in N_c, and

$$\sigma^{(0)}(x) = \bar{\psi}_+(x)\frac{1}{2}(i\gamma^i_\perp \overrightarrow{\partial_i} + m)\gamma^+\left(\frac{-i}{\partial_-}\psi_+(x)\right) + \left(\frac{i}{\partial_-}\bar{\psi}_+(x)\right)\frac{1}{2}(i\gamma^i_\perp \overleftarrow{\partial}_i + m)\gamma^+\psi_+(x), \tag{G5}$$

$$\pi^{(0)}(x) = \bar{\psi}_+(x)\frac{1}{2}(-i\gamma^i_\perp \overrightarrow{\partial_i} + m)i\gamma^5\gamma^+\left(\frac{-i}{\partial_-}\psi_+(x)\right) - \left(\frac{i}{\partial_-}\bar{\psi}_+(x)\right)\frac{1}{2}(i\gamma^i_\perp \overleftarrow{\partial}_i + m)i\gamma^5\gamma^+\psi_+(x), \tag{G6}$$

$$\sigma^{a(0)}(x) = \bar{\psi}_+(x)\frac{1}{2}(-i\gamma^i_\perp \overrightarrow{\partial_i} + m)\gamma^+\tau^a\left(\frac{-i}{\partial_-}\psi_+(x)\right) + \left(\frac{i}{\partial_-}\bar{\psi}_+(x)\right)\frac{1}{2}(i\gamma^i_\perp \overleftarrow{\partial}_i + m)\gamma^+\tau^a\psi_+(x), \tag{G7}$$

$$\pi^{a(0)}(x) = \bar{\psi}_+(x)\frac{1}{2}(-i\gamma^i_\perp \overrightarrow{\partial_i} + m)i\gamma^5\gamma^+\tau^a\left(\frac{-i}{\partial_-}\psi_+(x)\right) - \left(\frac{i}{\partial_-}\bar{\psi}_+(x)\right)\frac{1}{2}(i\gamma^i_\perp \overleftarrow{\partial}_i + m)i\gamma^5\gamma^+\tau^a\psi_+(x). \tag{G8}$$

In this hierarchy, the active operators generate

$$\hat{V}(x)[\cdot] = \bar{\psi}_+(x)\gamma^+\frac{-i}{\partial_-}(\psi_+(x)[\cdot]) + \frac{i}{\partial_-}(\bar{\psi}_+(x)[\cdot])\gamma^+\psi_+(x), \tag{G9}$$

$$\hat{A}(x)[\cdot] = \bar{\psi}_+(x)i\gamma^+\gamma^5\frac{-i}{\partial_-}(\psi_+(x)[\cdot]) - \frac{i}{\partial_-}(\bar{\psi}_+(x)[\cdot])i\gamma^+\gamma^5\psi_+(x), \tag{G10}$$

$$\hat{V}^a(x)[\cdot] = \bar{\psi}_+(x)\gamma^+\tau^a\frac{-i}{\partial_-}(\psi_+(x)[\cdot]) + \frac{i}{\partial_-}(\bar{\psi}_+(x)[\cdot])\gamma^+\tau^a\psi_+(x), \tag{G11}$$

$$\hat{A}^a(x)[\cdot] = \bar{\psi}_+(x)i\gamma^+\gamma^5\tau^a\frac{-i}{\partial_-}(\psi_+(x)[\cdot]) - \frac{i}{\partial_-}(\bar{\psi}_+(x)[\cdot])i\gamma^+\gamma^5\tau^a\psi_+(x), \tag{G12}$$

$$\hat{V}^{ab}(x)[\cdot] = \bar{\psi}_+(x)\gamma^+\tau^a\tau^b\frac{-i}{\partial_-}(\psi_+(x)[\cdot]) + \frac{i}{\partial_-}(\bar{\psi}_+(x)[\cdot])\gamma^+\tau^b\tau^a\psi_+(x), \tag{G13}$$

$$\hat{A}^{ab}(x)[\cdot] = \bar{\psi}_+(x)i\gamma^+\gamma^5\tau^a\tau^b\frac{-i}{\partial_-}(\psi_+(x)[\cdot]) - \frac{i}{\partial_-}(\bar{\psi}_+(x)[\cdot])i\gamma^+\gamma^5\tau^b\tau^a\psi_+(x). \tag{G14}$$

In the light front vacuum $|0\rangle$ empty of valence particles and anitparticles, these operators can develop a vev. Parity and isospin symmetry (chiral limit) restrict these vevs,

$$\langle\sigma^{(0)}(x)\rangle = -2N_c m\int\frac{d^4k}{(2\pi)^4}\frac{4ik^+}{(k^2-M^2)k^+} = -2N_c m\int\frac{dk^+d^2k_\perp}{(2\pi)^3}\frac{\epsilon(k^+)}{k^+}, \tag{G15}$$

$$\langle\hat{V}(x)\rangle = -4N_c\int\frac{dk^+d^2k_\perp}{(2\pi)^3}\frac{\epsilon(k^+)}{k^+}, \tag{G16}$$

$$\langle\hat{V}^{ab}(x)\rangle = \langle\hat{V}(x)\rangle\delta^{ab}, \tag{G17}$$

$$\langle \hat{A}(x)\rangle = \langle \hat{V}^a(x)\rangle = \langle \hat{A}^a(x)\rangle = \langle \hat{A}^{ab}(x)\rangle = 0. \quad \text{(G18)}$$

Here $\epsilon(k^+) = \mathrm{sgn}(k^+)$ is the signum function. A nonvanishing vev for the scalar operator in (G15) reflects on the spontaneous breaking of chiral symmetry and is mainly driven by the accumulation of the $k^+ = 0$ zero modes on the light front. With this in mind, the vev of the scalar $\sigma = \bar{\psi}\psi$ operator can be unwound to all orders in $1/N_c$,

$$\langle \sigma(x)\rangle = \langle \sigma^{(0)}\rangle \left[1 + 2g_s \int \frac{dk^+ d^2k_\perp}{(2\pi)^3} \frac{\epsilon(k^+)}{k^+} + 4g_s^2 \left(\int \frac{dk^+ d^2k_\perp}{(2\pi)^3} \frac{\epsilon(k^+)}{k^+}\right)^2 + \cdots\right] \quad \text{(G19)}$$

which is a resummation of all the tadpole diagrams in leading order in $1/N_c$. The elimination of the bad component of the fermionic field on the light front amounts to a mass renormalization.

To characterize the operator hierarchy (G1)–(G4) in different Fock sectors, it is best to shift to momentum space:

$$\sigma(P) = \int dx^- d^2x_\perp \sigma(x) e^{iP^+x^- - P_\perp \cdot x_\perp}, \quad \text{(G20)}$$

$$\pi(P) = \int dx^- d^2x_\perp \sigma_5(x) e^{iP^+x^- - P_\perp \cdot x_\perp}, \quad \text{(G21)}$$

$$\sigma^a(P) = \int dx^- d^2x_\perp \pi_5^a(x) e^{iP^+x^- - P_\perp \cdot x_\perp}, \quad \text{(G22)}$$

$$\pi^a(P) = \int dx^- d^2x_\perp \pi^a(x) e^{iP^+x^- - P_\perp \cdot x_\perp}, \quad \text{(G23)}$$

with the expectation values

$$\langle \hat{V}(x)[e^{-iPx}]\rangle = 4N_c \int \frac{dk^+ d^2k_\perp}{(2\pi)^3} \frac{\epsilon(k^+)}{P^+ - k^+} e^{-iPx},$$
$$\langle \hat{V}^{ab}(x)[e^{-iPx}]\rangle = \delta^{ab} \langle \hat{V}(x)[e^{-iPx}]\rangle.$$

In the two-body Fock space, with P the total momentum of the pair, we have

$$\sigma(P) = \sigma^{(0)}(P) - 2g_s \int \frac{dk^+ d^2k_\perp}{(2\pi)^3} \frac{\epsilon(k^+)}{P^+ - k^+} \sigma(P), \quad \text{(G24)}$$

$$\pi(P) = \pi^{(0)}(P) + 2g_s \int \frac{dk^+ d^2k_\perp}{(2\pi)^3} \frac{\epsilon(k^+)}{P^+ - k^+} \pi(x), \quad \text{(G25)}$$

$$\sigma^a(P) = \sigma^{a(0)}(P) + 2g_s \int \frac{dk^+ d^2k_\perp}{(2\pi)^3} \frac{\epsilon(k^+)}{P^+ - k^+} \sigma^a(P), \quad \text{(G26)}$$

$$\pi^a(P) = \pi^{a(0)}(P) - 2g_s \int \frac{dk^+ d^2k_\perp}{(2\pi)^3} \frac{\epsilon(k^+)}{P^+ - k^+} \pi^a(P). \quad \text{(G27)}$$

Again, the elimination of the bad component of the fermionic field amounts to a resummation of the tadpole contributions, which is equivalent to a vertex renormalization of the multifermion interaction by the factor

$$\alpha^{\pm}(P^+) = \left[1 \pm 2g_s \int \frac{dk^+ d^2k_\perp}{(2\pi)^3} \frac{\epsilon(k^+)}{P^+ - k^+}\right]^{-1}.$$

More specifically, we have

$$\sigma(P) = \sigma^{(0)}(P)\left[1 - 2g_s \int \frac{dk^+ d^2k_\perp}{(2\pi)^3} \frac{\epsilon(k^+)}{P^+ - k^+} + 4g_s^2 \left(\int \frac{dk^+ d^2k_\perp}{(2\pi)^3} \frac{\epsilon(k^+)}{P^+ - k^+}\right)^2 + \cdots\right], \quad \text{(G28)}$$

$$\pi(P) = \pi^{(0)}(P)\left[1 + 2g_s \int \frac{dk^+ d^2k_\perp}{(2\pi)^3} \frac{\epsilon(k^+)}{P^+ - k^+} + 4g_s^2 \left(\int \frac{dk^+ d^2k_\perp}{(2\pi)^3} \frac{\epsilon(k^+)}{P^+ - k^+}\right)^2 + \cdots\right], \quad \text{(G29)}$$

$$\sigma^a(P) = \sigma^{a(0)}(P)\left[1 + 2g_s \int \frac{dk^+ d^2k_\perp}{(2\pi)^3} \frac{\epsilon(k^+)}{P^+ - k^+} + 4g_s^2 \left(\int \frac{dk^+ d^2k_\perp}{(2\pi)^3} \frac{\epsilon(k^+)}{P^+ - k^+}\right)^2 + \cdots\right], \quad \text{(G30)}$$

$$\pi^a(P) = \pi^{a(0)}(P)\left[1 - 2g_s \int \frac{dk^+ d^2k_\perp}{(2\pi)^3} \frac{\epsilon(k^+)}{P^+ - k^+} + 4g_s^2 \left(\int \frac{dk^+ d^2k_\perp}{(2\pi)^3} \frac{\epsilon(k^+)}{P^+ - k^+}\right)^2 + \cdots\right]. \quad \text{(G31)}$$

The zeroth order operators in $1/N_c$ in momentum space are

$$\sigma^{(0)}(P)=\int[d^3k]_+\int[d^3q]_+\bar{\psi}_+(k)\left[\frac{\gamma^+(\vec{\gamma}_\perp\cdot\vec{q}+m)}{2q^+}+\frac{(\vec{\gamma}_\perp\cdot\vec{k}+m)\gamma^+}{2k^+}\right]\psi_+(q)(2\pi)^3\delta^3_+(P+k-q), \tag{G32}$$

$$\pi^{(0)}(P)=\int[d^3k]_+\int[d^3q]_+\bar{\psi}_+(k)\left[\frac{i\gamma^5\gamma^+(\vec{\gamma}_\perp\cdot\vec{q}+m)}{2q^+}-\frac{i\gamma^5\gamma^+(\vec{\gamma}_\perp\cdot\vec{k}+m)}{2k^+}\right]\psi_+(q)(2\pi)^3\delta^3_+(P+k-q), \tag{G33}$$

$$\sigma^{a(0)}(P)=\int[d^3k]_+\int[d^3q]_+\bar{\psi}_+(k)\left[\frac{\gamma^+\tau^a(\vec{\gamma}_\perp\cdot\vec{q}+m)}{2q^+}+\frac{(\vec{\gamma}_\perp\cdot\vec{k}+m)\gamma^+\tau^a}{2k^+}\right]\psi_+(q)(2\pi)^3\delta^3_+(P+k-q), \tag{G34}$$

$$\pi^{a(0)}(P)=\int[d^3k]_+\int[d^3q]_+\bar{\psi}_+(k)\left[\frac{i\gamma^5\gamma^+\tau^a(\vec{\gamma}_\perp\cdot\vec{q}+m)}{2q^+}-\frac{i\gamma^5\gamma^+\tau^a(\vec{\gamma}_\perp\cdot\vec{k}+m)}{2k^+}\right]\psi_+(q)(2\pi)^3\delta^3_+(P+k-q), \tag{G35}$$

with $[d^3k]_+=\frac{dk^+d^2k_\perp}{2k^+(2\pi)^3}\epsilon(k^+)$.

APPENDIX H: LIGHT FRONT ZERO MODES

In the ILM, the spontaneous breaking of chiral symmetry and the emergence of a scalar quark condensate are due to the instanton and anti-instanton fermionic zero modes as we noted above. In the rest frame and in Euclidean signature, this is manifest in (42) with the $k^2=0$ pole for $M\to m$. In Minkowski signature on the light front, this is manifest in (45) with the $k^+=0$ pole. Technically, there is a subtlety in trying to relate (42)–(45) by analytical continuation since

$$I(M^2)=\int\frac{d^2k_\perp dk^+dk^-}{(2\pi)^4}\frac{4i}{2k^+k^--k_\perp^2-M^2+i\epsilon}\mathcal{F}^2(k)\to\int\frac{dk^+d^2k_\perp}{(2\pi)^3}\frac{\epsilon(k^+)}{k^+}\mathcal{F}^2(k) \tag{H1}$$

assumes that the pole $k^-=\frac{k_\perp^2+M^2}{2k^+}$ remains within the closing contour. However, as $k^+\to 0$, the pole pinches the contour, hence the subtlety [72]. Another way to see this is to rewrite (H1) using the Schwinger trick.

In the zero instanton size limit,

$$I(M^2)\to\int\frac{d^2k_\perp dk^+dk^-}{(2\pi)^4}\int_0^\infty d\alpha 4e^{i\alpha(2k^+k^--k_\perp^2-M^2+i\epsilon)}, \tag{H2}$$

the k^- integration yields a singular delta function,

$$\int_{-\infty}^{\infty}\frac{dk^-}{2\pi}e^{i\alpha 2k^+k^-}\to\frac{1}{2\alpha}\delta(k^+). \tag{H3}$$

The spontaneous breaking of chiral symmetry on the light front stems from the accumulation of the $k^+=0$ fermionic modes in the gap equation. The singularity can be regulated by the covariant Bogoliubov-Parasiuk-Hepp-Zimmermann (BPHZ) subtraction scheme

$$\frac{\partial I(M^2)}{\partial M^2}\to-\int\frac{d^2k_\perp}{(2\pi)^3}\frac{2}{k_\perp^2+M^2}, \tag{H4}$$

hence

$$\int\frac{dk^+d^2k_\perp}{(2\pi)^3}\frac{\epsilon(k^+)}{k^+}=2\int\frac{d^2k_\perp}{(2\pi)^3}\ln\left(\frac{\Lambda^2}{k_\perp^2+M^2}\right) \tag{H5}$$

with Λ a dimensionful scale left over by the substraction.

[1] G. R. Farrar and D. R. Jackson, Phys. Rev. Lett. **43**, 246 (1979).
[2] J.-H. Zhang, J.-W. Chen, X. Ji, L. Jin, and H.-W. Lin, Phys. Rev. D **95**, 094514 (2017).
[3] X. Ji, Phys. Rev. Lett. **110**, 262002 (2013).
[4] A. V. Radyushkin, Phys. Rev. D **95**, 056020 (2017).
[5] S.-i. Nam, Mod. Phys. Lett. A **32**, 1750218 (2017).
[6] M. C. Chu, J. M. Grandy, S. Huang, and J. W. Negele, Phys. Rev. D **49**, 6039 (1994).
[7] D. Diakonov and V. Y. Petrov, Nucl. Phys. **B272**, 457 (1986).
[8] E. V. Shuryak, Nucl. Phys. **B319**, 541 (1989).
[9] M. A. Nowak, J. J. M. Verbaarschot, and I. Zahed, Nucl. Phys. **B325**, 581 (1989).
[10] M. Kacir, M. Prakash, and I. Zahed, Acta Phys. Pol. B **30**, 287 (1999).
[11] T. Schäfer and E. V. Shuryak, Rev. Mod. Phys. **70**, 323 (1998).
[12] E. Shuryak and I. Zahed, Phys. Rev. D **107**, 034023 (2023).
[13] E. Shuryak and I. Zahed, Phys. Rev. D **107**, 034024 (2023).
[14] E. Shuryak and I. Zahed, Phys. Rev. D **107**, 034025 (2023).
[15] E. Shuryak and I. Zahed, Phys. Rev. D **107**, 034026 (2023).
[16] E. Shuryak and I. Zahed, Phys. Rev. D **107**, 034027 (2023).
[17] E. Shuryak and I. Zahed, Phys. Rev. D **107**, 094005 (2023).
[18] L. Chang, I. C. Cloet, J. J. Cobos-Martinez, C. D. Roberts, S. M. Schmidt, and P. C. Tandy, Phys. Rev. Lett. **110**, 132001 (2013).
[19] C. Chen, L. Chang, C. D. Roberts, S. Wan, and H.-S. Zong, Phys. Rev. D **93**, 074021 (2016).
[20] M. Ding, K. Raya, D. Binosi, L. Chang, C. D. Roberts, and S. M. Schmidt, Phys. Rev. D **101**, 054014 (2020).
[21] E. Ruiz Arriola and W. Broniowski, Phys. Rev. D **66**, 094016 (2002).
[22] A. E. Dorokhov, W. Broniowski, and E. Ruiz Arriola, Phys. Rev. D **84**, 074015 (2011).
[23] W. Broniowski and E. Ruiz Arriola, Phys. Lett. B **773**, 385 (2017).
[24] W. Broniowski and E. Ruiz Arriola, Proc. Sci. Hadron2017 (**2018**) 174 [arXiv:1711.09355].
[25] M. Praszalowicz and A. Rostworowski, arXiv:hep-ph/0205177.
[26] D. G. Dumm, S. Noguera, N. N. Scoccola, and S. Scopetta, Phys. Rev. D **89**, 054031 (2014).
[27] V. Y. Petrov and P. V. Pobylitsa, arXiv:hep-ph/9712203.
[28] V. Y. Petrov, M. V. Polyakov, R. Ruskov, C. Weiss, and K. Goeke, Phys. Rev. D **59**, 114018 (1999).
[29] A. E. Dorokhov, Nuovo Cimento A **109**, 391 (1996).
[30] A. E. Dorokhov and L. Tomio, arXiv:hep-ph/9803329.
[31] I. V. Anikin, A. E. Dorokhov, and L. Tomio, Phys. At. Nucl. **64**, 1329 (2001).
[32] A. E. Dorokhov and L. Tomio, Phys. Rev. D **62**, 014016 (2000).
[33] S.-i. Nam, H.-C. Kim, A. Hosaka, and M. M. Musakhanov, Phys. Rev. D **74**, 014019 (2006).
[34] A. V. Radyushkin, arXiv:hep-ph/9406237.
[35] S. J. Brodsky, F.-G. Cao, and G. F. de Teramond, Phys. Rev. D **84**, 033001 (2011).
[36] S. J. Brodsky, G. F. de Teramond, H. G. Dosch, and J. Erlich, Phys. Rep. **584**, 1 (2015).
[37] S. Jia and J. P. Vary, Phys. Rev. C **99**, 035206 (2019).
[38] J. Lan, C. Mondal, S. Jia, X. Zhao, and J. P. Vary, Phys. Rev. Lett. **122**, 172001 (2019).
[39] W. Bentz, T. Hama, T. Matsuki, and K. Yazaki, Nucl. Phys. **A651**, 143 (1999).
[40] K. Itakura and S. Maedan, Phys. Rev. D **62**, 105016 (2000).
[41] K. Naito, S. Maedan, and K. Itakura, Phys. Rev. D **70**, 096008 (2004).
[42] D. B. Leinweber, arXiv:hep-lat/0004025.
[43] J. C. Biddle, W. Kamleh, and D. B. Leinweber, Phys. Rev. D **102**, 034504 (2020).
[44] J. C. Biddle, W. Kamleh, and D. B. Leinweber, EPJ Web Conf. **245**, 06010 (2020).
[45] E. V. Shuryak, Nucl. Phys. **B198**, 83 (1982).
[46] T. Banks and A. Casher, Nucl. Phys. **B169**, 103 (1980).
[47] J. J. M. Verbaarschot and I. Zahed, Phys. Rev. Lett. **70**, 3852 (1993).
[48] G. 't Hooft, Phys. Rev. D **14**, 3432 (1976); **18**, 2199(E) (1978).
[49] S. Chernyshev, M. A. Nowak, and I. Zahed, Phys. Rev. D **53**, 5176 (1996).
[50] Y. Nambu and G. Jona-Lasinio, Phys. Rev. **122**, 345 (1961).
[51] G. P. Lepage and S. J. Brodsky, Phys. Rev. D **22**, 2157 (1980).
[52] X. Ji, Nucl. Phys. **B960**, 115181 (2020).
[53] X. Ji, Y. Liu, and I. Zahed, Phys. Rev. D **103**, 074002 (2021).
[54] A. Kock, Y. Liu, and I. Zahed, Phys. Rev. D **102**, 014039 (2020).
[55] A. Kock and I. Zahed, Phys. Rev. D **104**, 116028 (2021).
[56] A. Efremov and A. Radyushkin, Phys. Lett. **94B**, 245 (1980).
[57] E. M. Aitala *et al.* (E791 Collaboration), Phys. Rev. Lett. **86**, 4768 (2001).
[58] W. Broniowski, E. R. Arriola, and K. Golec-Biernat, Phys. Rev. D **77**, 034023 (2008).
[59] C. Shi, C. Chen, L. Chang, C. D. Roberts, S. M. Schmidt, and H.-S. Zong, Phys. Rev. D **92**, 014035 (2015).
[60] R. Zhang, C. Honkala, H.-W. Lin, and J.-W. Chen, Phys. Rev. D **102**, 094519 (2020).
[61] S. D. Drell and T.-M. Yan, Phys. Rev. Lett. **24**, 181 (1970).
[62] G. B. West, Phys. Rev. Lett. **24**, 1206 (1970).
[63] R. Bowler and M. Birse, Nucl. Phys. **A582**, 655 (1995).
[64] T. Hell, S. Rößner, M. Cristoforetti, and W. Weise, Phys. Rev. D **79**, 014022 (2009).
[65] J. S. Conway *et al.*, Phys. Rev. D **39**, 92 (1989).

[66] M. Aicher, A. Schafer, and W. Vogelsang, Phys. Rev. Lett. **105**, 252003 (2010).
[67] R. S. Sufian, C. Egerer, J. Karpie, R. G. Edwards, B. Joó, Y.-Q. Ma, K. Orginos, J.-W. Qiu, and D. G. Richards, Phys. Rev. D **102**, 054508 (2020).
[68] J. Badier *et al.*, Phys. Lett. **93B**, 354 (1980).
[69] H.-W. Lin, J.-W. Chen, Z. Fan, J.-H. Zhang, and R. Zhang, Phys. Rev. D **103**, 014516 (2021).
[70] T. Nguyen, A. Bashir, C. D. Roberts, and P. C. Tandy, Phys. Rev. C **83**, 062201 (2011).
[71] P. V. Pobylitsa, Phys. Lett. B **226**, 387 (1989).
[72] T.-M. Yan, Phys. Rev. D **7**, 1780 (1973).